Escola de Camins
Escola Tècnica Superior d'Enginyeria de Camins, Canals i Ports
UPC BARCELONATECH

Analysis of the effects of friction on tuned mass dampers.

Application to slender tower structures

TREBALL FINAL DE GRAU

Treball realitzat per:
Arnau Sabat Bayarri

Dirigit per:
Jesús Miguel Bairan García

Grau en:
Enginyeria Civil

Barcelona, 22/09/2017

Departament d'enginyeria de la construcció

Contents

1. Introduction

1.1. Background and motivation

Offshore wind power, which involves the installation of wind turbines at sea, is a technology that was first explored in the 1990s, but that only recently started being feasible in terms of cost. Higher wind speeds in the oceans and the "not in my backyard" effect have increased the interest in offshore wind facilities. The last 10 years, numerous offshore wind farms have been commissioned, especially in the UK, Denmark, Germany and China.

Many studies have been conducted on the dynamic behavior of fully-built wind turbines, but there is also interest in researching the response of offshore wind towers that are in the process of building. Since offshore conditions cause the construction of wind towers to be a slower and more delicate procedure, the combination of strong waves and gusts of wind (like those of figure 1.1) could cause harmonic oscillation that may result in heavy damage to the structure. Tuned mass dampers (shortened TMD) are widely used and researched devices that can aid in the vibration control of these types of structures.

With this in mind, the Department of Structures and Materials of UPC Civil Engineering carried out several experiments in order to study the behavior of unfinished offshore wind turbine towers in unfavorable conditions such as stormy weather, and how it could be improved with tuned mass dampers. These experiments began with the design and building of a wind tower replica at a reduced scale (modern wind towers reach heights upwards of $100m$) and a new tuned mass damper prototype. A sinusoidal force, exciting the tower into harmonic oscillation, was applied, and the displacement of the tower at various heights was recorded.

The results were then compared with a MATLAB-coded dynamic model of the tower and TMD. Some discrepancies between the experimental and the theoretical models were found, which were mostly attributed to the internal friction of the TMD, which hadn't been accounted for in the code.

These discrepancies motivated the search of a better model to suit these experiments, which in turn needed more insight into the impact of friction in tuned mass dampers.

Figure 1.1.: Heavy seas engulf offshore wind turbines that are part of the Block Island wind farm, located 6.1km from the shore of New Shoreham, US. Taken with permission from the U.S. Department of Energy

1.2. Scope

The broad focus of the thesis will be the analysis of the effects of internal friction on the operation of a tuned mass damper. In the replica wind tower experiments, the presence of friction in the TMD resulted in a inferior performance than the models predicted, which meant that TMD wasn't operating at its expected capacity. A better understanding of TMD friction can help in improving not only their performance in wind towers, but in numerous other applications as well.

Tuned mass dampers, as their name implies, need a certain tuning of their structural parameters in order to maximize their effectiveness. This tuning is usually carried out with Den Hartog's procedure, first introduced in 1928, which assumes that the main system has no damping and at the same time doesn't take into account any friction. Since the parameters obtained with this method will be fairly inaccurate, an analytic search for a better way of determining these parameters will be conducted.

When a set of equations that can theoretically improve the quality of these parameters is found, intensive testing will be carried out with a new coded dynamic model that can process the non-linear nature of frictional forces. A series of conclusions will be derived from the results of this testing, hoping to answer the following questions:

→ How does friction influence the performance of a TMD?

→ Can we develop better suited formulas to design (or at the very least pre-design) TMD

with friction?

→ Do these formulas withstand testing against a dynamic model?

→ In what way are the various design and environmental parameters interacting?

This project will simplify many geometric characteristics of the wind tower, as well as properties of the used material, in order to achieve an overarching conclusion that can be applied to slender tower structures as a whole, as well as improve the computation times of the code.

1.3. Methodology

A big part of this thesis hinges on having a reliable model in which a main system (for example, a tower) and a TMD with friction can be studied. Such a piece of code can be developed in most of the modern programming languages, but MATLAB was chosen because (i) it's easy to read and write thanks to its integrated suite, (ii) it's very flexible and filled with built-in functions that simplify the matter at hand, (iii) it includes various tools to debug and speed up the code, (iv) it has a fast and complete plotting library, (v) it has considerable support and available literature, and (vi) it transitions well into the parametric study that will also be conducted in the thesis.

This numerical model needs to:

→ Be able to solve (integrate) dynamic equations of the form $M\ddot{d} + C\dot{d} + Kd = P(t)$, of at least two degrees of freedom. M, C, K are mass, damping and stiffness matrices, d, $\dot{d}$, $\ddot{d}$ are the displacement, velocity and acceleration vectors and $P(t)$ a vector with the applied force at a certain time t. This is the general equation that will govern the model of the structure.

→ Be capable of handling non-linear dynamic properties. Since friction is a highly non-linear phenomenon, this is an important prerequisite and the biggest change from the previous model. The non-linear portion of the dynamic equation will be the stiffness matrix: the friction model will share similarities with the response of idealized elastoplastic materials to external loads.

→ Be fast enough to carry out multiple non-linear simulations in succession while taking assumable amounts of time. The evaluation of the TMD design will take several iterations to make sure the optimum parameters are being used: having a lightweight model will ease the execution of this process. Appropriate time steps and specific parameters will be researched for the chosen numerical integration method, and a simplified geometric model is going to be used to greatly improve times.

Then, some new design equations will be derived to fit the TMD friction model. These equations will stem from the similarities between the elastoplastic model and the behavior of frictional forces. Their main scope will be the optimization of the design properties of the TMD subsystem, according to the present conditions.

Finally, the validation of these new design equations will be carried out with a parametric study, using the developed MATLAB numeric model. Initially, the system's mass, stiffness and damping will be fixed according to the physical wind tower replica. Then, the strength of the disturbing force and the TMD's friction coefficient and its mass, stiffness, damping, and maximum accepted displacement will be adjusted in order to find the validity of the found equations and their sensibility to the parameters. Significant parametric interactions will be of great interest.

This parametric study will be carried out in MATLAB as well, allowing a practical handle on the already developed numerical model, while at the same time taking advantage of MATLAB's advanced plotting capabilities.

2. State of the art

In this chapter, several relevant topics are researched with the intent of having a wide understanding on the topic of vibrations, numerical methods and the devices that will be used in the parametric study.

2.1. Structural dynamics

2.1.1. Equations of motion

Equations of motion permit the description of a physical system over a period of time. They can easily be derived from Newton's laws of motion, first published in 1687. Newton's second law, as interpreted by Kelvin and Tait (1867), states:

> Change of motion is proportional to the impressed force, and takes place in the direction of the straight line in which the force acts.

For the mass portrayed in figure 2.1, this means that the resultant of the forces is equal to:

$$P(t) - F_D - F_S = M\ddot{d}$$

Where $P(t)$ is the externally applied force, and $F_D,\ F_S$ are, respectively, the internal *damping* and *stiffness* forces, which work in the opposite direction of movement. The equation explicitly includes the acceleration of the system $\ddot{d} = \ddot{d}(t)$, while the velocity $\dot{d} = \dot{d}(t)$ and the displacement $d = d(t)$ can be obtained via integration. For an elastic object with linear damping this equation can be further developed to get:

$$\begin{aligned} P(t) - C\dot{d} - Kd &= M\ddot{d} \\ M\ddot{d} + C\dot{d} + Kd &= P(t) \end{aligned} \tag{2.1}$$

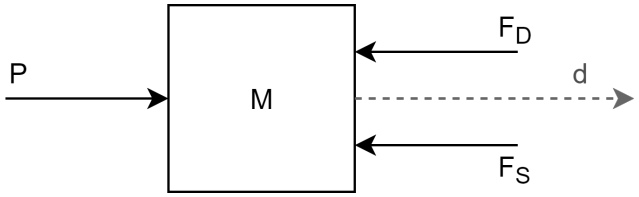

Figure 2.1.: Simple mass M under the action of forces $P,\ F_D,\ F_S$

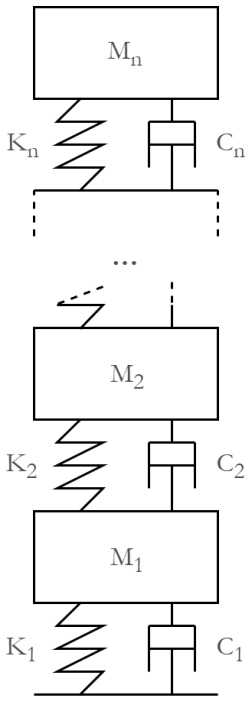

Figure 2.2.: Representation of an elastic system of n masses with linear damping

Where K, C are, respectively, the characteristic stiffness and damping of the system. Equation 2.1 is an implicit second-order linear ordinary differential equation. If the stiffness of the material is non-linear (as in the case of a plastic material), the equation takes the following form:

$$M\ddot{d} + C\dot{d} + F_S(d) = P(t)$$

This can be extended to multiple degrees-of-freedom (MDOF) systems, in which a new equation is introduced for every new mass in the system. Assuming the existence of n masses in a MDOF system, the resulting system of equations would look like:

$$M_i\ddot{d}_i + C_i\dot{d}_i + F_{S,i}(d_i) = P_i(t)$$
$$i = 1, 2, ..., n$$

And this set of n equations can be written much more comfortably in matrix form:

$$\mathbf{M}\ddot{d} + \mathbf{C}\dot{d} + \mathbf{F}_S(d) = \mathbf{P}(t) \tag{2.2}$$

Where $\mathbf{M}$, $\mathbf{C}$ are known as the mass and damping matrices of the system. If the material is elastic, $\mathbf{F}_S(d) = \mathbf{K}d$ and then $\mathbf{K}$ is known as the stiffness matrix of the system:

$$\mathbf{M}\ddot{d} + \mathbf{C}\dot{d} + \mathbf{K}d = \mathbf{P}(t) \tag{2.3}$$

The vectors containing the displacements, velocities and accelerations of the system at a given time are, respectively, d, $\dot{d}$, $\ddot{d}$. $\mathbf{P}(t)$ is a vector that contains the force applied on each mass.

$$d = \begin{bmatrix} d_1 \\ d_2 \\ ... \\ d_n \end{bmatrix}, \dot{d} = \begin{bmatrix} \dot{d}_1 \\ \dot{d}_2 \\ ... \\ \dot{d}_n \end{bmatrix}, \ddot{d} = \begin{bmatrix} \ddot{d}_1 \\ \ddot{d}_2 \\ ... \\ \ddot{d}_n \end{bmatrix}, \mathbf{P}(t) = \begin{bmatrix} P_1(t) \\ P_2(t) \\ ... \\ P_n(t) \end{bmatrix}$$

$$\mathbf{M} = \begin{bmatrix} M_1 & 0 & 0 & 0 \\ 0 & M_2 & 0 & 0 \\ 0 & 0 & ... & ... \\ 0 & 0 & ... & M_n \end{bmatrix}, \mathbf{C} = \begin{bmatrix} C_1 + C_2 & -C_2 & ... & 0 \\ -C_2 & C_2 + C_3 & ... & 0 \\ ... & ... & ... & ... \\ 0 & 0 & ... & C_n \end{bmatrix} \tag{2.4}$$

$$\mathbf{K} = \begin{bmatrix} K_1 + K_2 & -K_2 & ... & 0 \\ -K_2 & K_2 + K_3 & ... & 0 \\ ... & ... & ... & ... \\ 0 & 0 & ... & K_n \end{bmatrix}$$

An analytical solution can be found under the following assumptions:

→ The system is SDOF (single degree-of-freedom): it has a single mass that can move in one dimension.

→ The mass acts with perfect elasticity: the stiffness force scales linearly ($F_S = Kd$).

→ The damping is viscous: the damping force scales linearly with respect to the velocity ($F_D = C\dot{d}$).

→ The applied force is modeled as a function that has continuity in the studied time frame, such as $P(t) = P_1 \sin(\omega t)$.

The model developed for this thesis will need to support multiple degrees of freedom and non-linearity, for reasons that will be discussed in the following chapters. As a consequence, an analytical, closed-form solution is not going to be possible, and numerical methods will be researched and employed.

2.1.2. Vibration and resonance

Ultimately, the goal of this thesis is to reduce the negative effects that resonance can cause on a given structure, so a comprehensive understanding of vibration theory is necessary.

In this section, time will be devoted to gradually build up the theory of vibration and introduce new concepts until the case of the thesis can be tackled.

2.1.2.1. Free vibration

A structure is under free vibration when it suffers a disturbance from its static equilibrium state and then is allowed to vibrate without further external forces taking place.

Free vibration without damping

When a system is undamped, any vibration caused by a disturbance will persist until a new external force is placed onto the structure. In the case of free vibration, that means the system will display a harmonic response that will be repeated indefinitely.

The homogeneous differential equation for an undamped and linear SDOF system is:

$$m\ddot{d} + kd = 0 \tag{2.5}$$

The disturbance that starts the vibration is introduced by setting initial values for the displacement and the velocity:

$$d(0) = d_0$$
$$\dot{d}(0) = \dot{d}_0$$

And a possible solution for the differential equation 2.5 could be:

$$d(t) = a\sin(\omega t) + b\cos(\omega t)$$

Where $a,\ b$ are integration constants. Applying to this solution the initial values of displacement and velocity previously defined, the following values for the $a,\ b$ constants are found:

$$a = \dot{d}_0/\omega$$
$$b = d_0$$

Which results in the following updated formulation of the solution:

$$d(t) = \frac{\dot{d}_0}{\omega}\sin(\omega t) + d_0\cos(\omega t) \tag{2.6}$$

The angular frequency ω of the system can be obtained by setting the initial velocity $\dot{d}_0 = 0$, then substituting the solution 2.6 back into equation 2.5, and finally solving for the frequency:

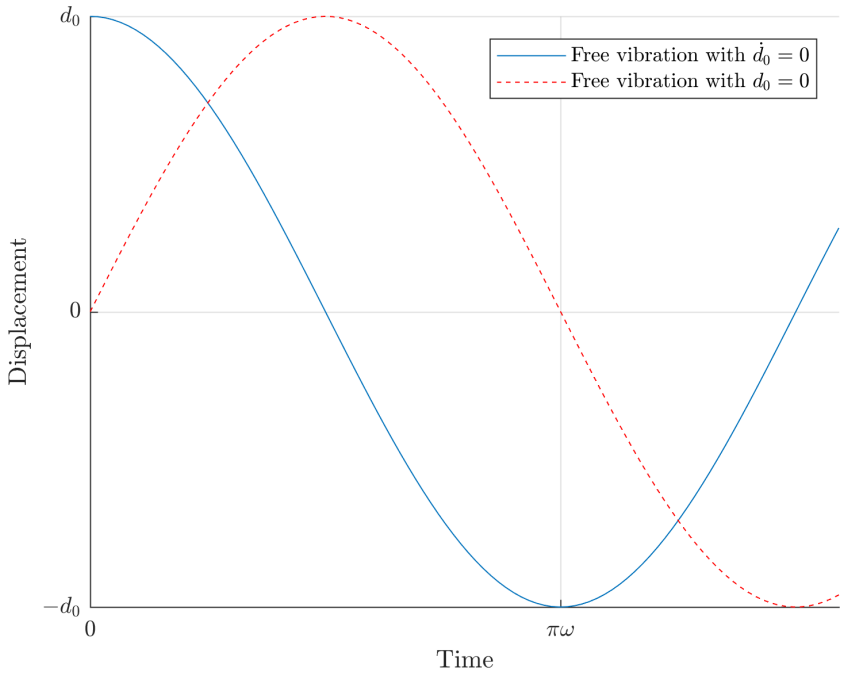

Figure 2.3.: Free vibration of an undamped single-degree-of-freedom system with different initial states

$$-m\omega^2 d_0 \cos(\omega t) + k d_0 \cos(\omega t) = 0$$
$$\omega^2 m = k$$
$$\omega = \sqrt{k/m}$$

An example of an undamped single-DOF structure structure in free vibration can be seen in figure 2.3.

The time a system needs to complete a full cycle of free vibration is the natural period, formally defined as:

$$T = \frac{2\pi}{\omega}$$

And the frequency of vibration is defined as the inverse of the natural period:

$$f = \frac{1}{T}$$

Free vibration with damping

If the system has viscous damping, the governing equation of motion becomes:

$$m\ddot{d} + c\dot{d} + kd = 0 \tag{2.7}$$

The amount of damping (c) controls the number of cycles the structure completes before

Table 2.1.: Representative damping ratios of assorted materials and systems. Adapted from Adams and Askenazi (1999)

System	Damping ratio (ξ)
Metals (in elastic range)	< 0.01
Metal structures with joints	~ 0.03
Aluminum	~ 0.0004
Shock absorbers	~ 0.3
Rubber	~ 0.05
Buildings during earthquake	$0.01 - 0.05$

returning to a static state. Here, it is useful to introduce the concept of *critical damping*, which can be calculated as:

$$c_{cr} = 2m\omega = \frac{2k}{\omega} \tag{2.8}$$

If the actual damping of the system is less than the critical damping ($c < c_{cr}$) the system is said to be underdamped, and it will oscillate around its equilibrium while gradually losing amplitude, until the equilibrium is finally reached.

If the system's damping is more than the critical ($c > c_{cr}$) the system is said to be overdamped, and it will return to equilibrium position without oscillating. The minimum value of damping for which this occurs is the critical damping ($c = c_{cr}$).

Taking this into account, the *damping ratio* is a dimensionless variable that can be defined as:

$$\xi = \frac{c}{c_{cr}}$$

Values for the damping ratio on most materials and structures range around $0.01 - 0.05$, as it can be seen in table 2.1.

Introducing these parameters into the equation of motion with damping (2.7) results in the following:

$$\ddot{d} + 2\xi\omega\dot{d} + \omega^2 d = 0 \tag{2.9}$$

The value that the damping ratio takes in structural dynamics is usually $\xi \ll 1/2$, so the study of underdamped systems is much more interesting due to their wider, real-world implications. The analytical solution of an underdamped system governed by equation 2.9 can be derived (Chopra (2001)) as:

$$d(t) = e^{-\xi\omega t}\left[d_0\cos(\omega t) + \left(\frac{d_0 + \xi\omega u_0}{\omega_D}\right)\sin(\omega_D t)\right] \tag{2.10}$$

Where ω_D, known as the *damped frequency*, is defined as:

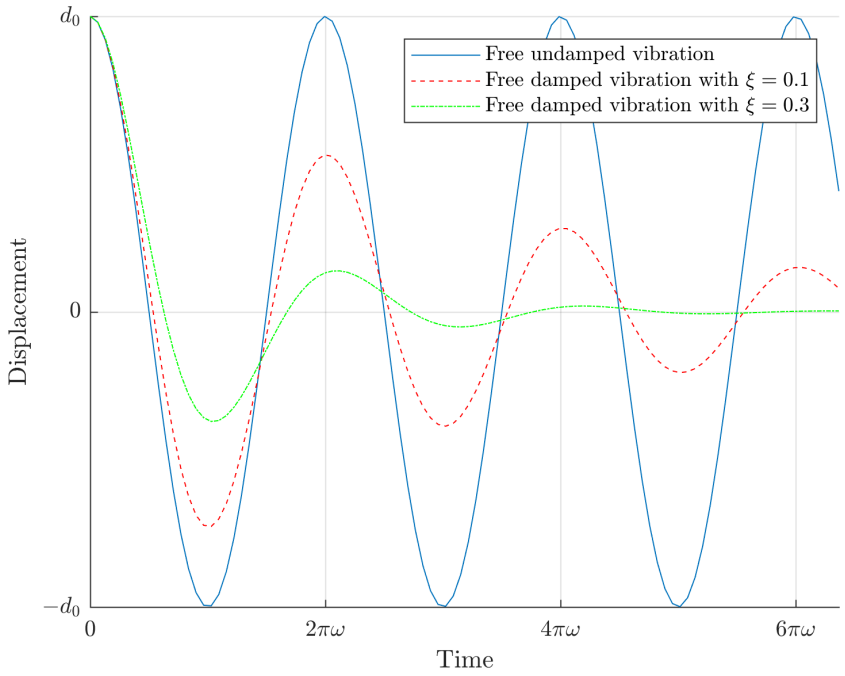

Figure 2.4.: Comparison of free vibration with and without damping, and the effect of the critical damping ratio ξ

$$\omega_D = \omega\sqrt{1-\xi^2}$$

A graphic comparison of the displacements of an undamped system versus two underdamped systems with different damping ratios can be examined in figure 2.4.

The amplitude of the displacement of a damped system in free vibration is modified by the exponential $e^{-\xi\omega t}$, so if the natural period ($T = \frac{2\pi}{\omega}n$) is substituted in, the following value can be obtained:

$$\lambda_n = e^{-2\pi\xi n}$$

Each successive peak n of the damped system will have an amplitude of λ_n times the initial, so the impact of the damping can be known beforehand.

2.1.2.2. Harmonic excitation

Harmonic forces can be modeled by either a sine $p(t) = p_0 \sin(\omega_p t)$ or a cosine $p(t) = p_0 \cos(\omega_p t)$, where ω_p is the angular frequency and p_0 is the amplitude (the maximum value) of the force.

Harmonic excitation without damping

The equation of motion for an undamped single-DOF system in harmonic excitation is:

$$m\ddot{d} + k\dot{d} = p_0 \sin(\omega_p t) \tag{2.11}$$

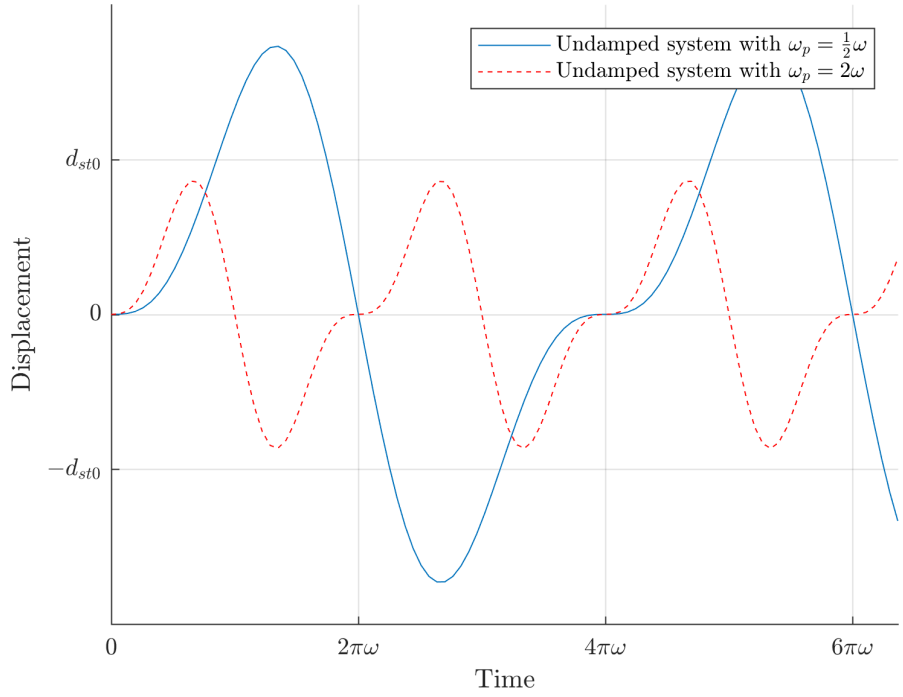

Figure 2.5.: Vibration of two undamped systems excited by a sinusoidal force of identical amplitude but different frequency

Setting the initial values $d(0) = d_0$ and $\dot{d}(0) = \dot{d}_0$ and dealing with the particular and homogeneous solution of the differential equation 2.11 leads to the equation:

$$d(t) = d_0 \cos(\omega t) + \left[\frac{d_0}{\omega} - \frac{p_0}{k} \cdot \frac{\omega_p/\omega}{1 - (\omega_p/\omega)^2}\right] \sin(\omega t) + \frac{p_0}{k} \cdot \frac{1}{1 - (\omega_p/\omega)^2} \sin(\omega_p t) \tag{2.12}$$

The first part of this equation is governed by the angular frequency of the system (ω) and is called the *transient vibration*, because it depends on the initial displacement and velocity. The second part is governed by the angular frequency of the excitation force (ω_p) and is called the *steady-state vibration*, because it is caused by the excitation force itself.

If the initial conditions are zero ($d_0 = \dot{d}_0 = 0$), equation 2.12 can be simplified to:

$$d(t) = \frac{p_0}{k} \cdot \frac{1}{1 - (\omega_p/\omega)^2} \left(\sin(\omega_p t) - \omega_p/\omega \cdot \sin(\omega t)\right) \tag{2.13}$$

An example of this equation can be seen in figure 2.5. The constant d_{st0} is used to describe the maximum static displacement that the force $p(t)$ can cause to the system, and it's known as the *static deformation*. It is calculated as:

$$d_{st0} = p_0/k$$

The ratio between the maximum displacement that the system experiences at any time and the static deformation is called the *dynamic magnification factor* (DMF):

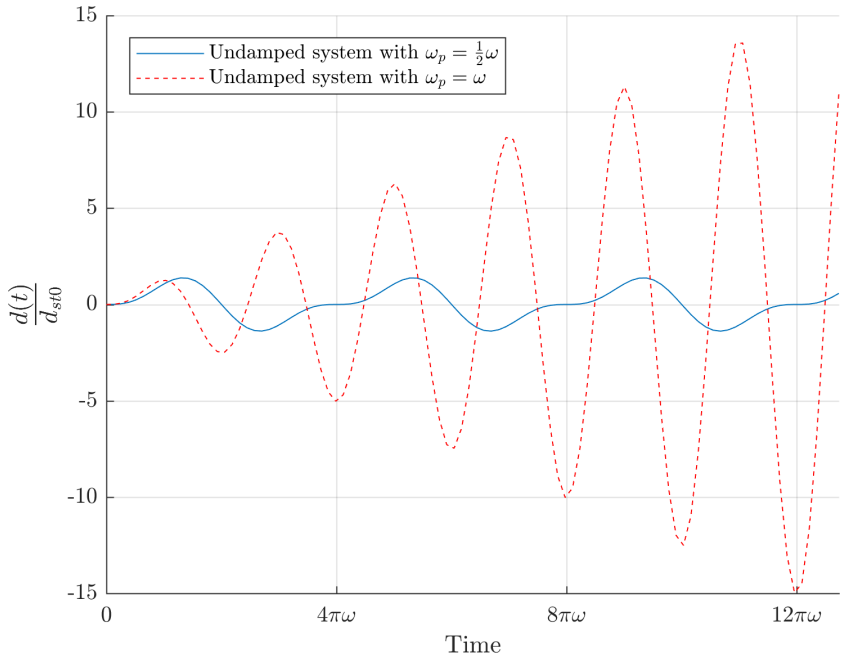

Figure 2.6.: Excited vibration of two undamped system, one of which has entered harmonic resonance

$$DMF = \frac{\max\{|d(t)|\}}{d_{st0}} \tag{2.14}$$

Where $|d(t)|$ is the absolute value of all the displacements that occur over time.

The *resonant frequency* (also known as natural frequency) is the forcing force frequency for which the DMF is maximized. In the undamped system case, this happens when $\omega_p = \omega$, and it is then said that the system has entered *resonance,* or that *harmonic oscillation* is occurring. In that case, equation 2.13 is no longer valid, and the solution becomes:

$$d(t) = -\frac{1}{2} \cdot \frac{p_0}{2k}(\omega t \cdot \cos(\omega t) - \sin(\omega t)) \tag{2.15}$$

For an undamped system that has entered resonance, the growth of the amplitude of the displacement is unbounded and increases indefinitely. In figure 2.6, an example of how resonance affects an undamped system is presented.

Real structures, however, always have a certain degree of damping, and their limit is set by the resistance of the materials and the build.

Harmonic excitation with damping

Finally, the equation that describes a harmonically-excited SDOF system with damping is the following:

$$m\ddot{d} + c\dot{d} + kd = p_0 \sin(\omega_p t) \tag{2.16}$$

The solution of this system, obtained with an analogous procedure to that of the previous

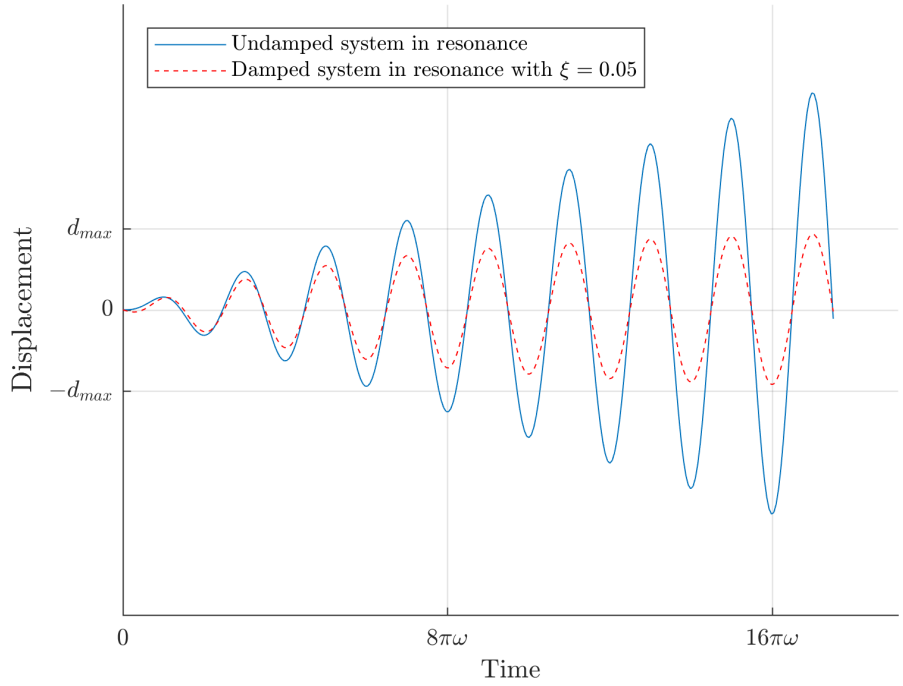

Figure 2.7.: Comparison of a damped versus an undamped system that enter resonance. The value d_{max} is a property of the damped system

cases, has the following condensed aspect:

$$d(t) = e^{-\xi\omega t}\left(\mathcal{A}\cos(\omega_D t) + \mathcal{B}\sin(\omega_D t)\right) + \mathcal{C}\sin(\omega_p t) + \mathcal{D}\cos(\omega_p t) \tag{2.17}$$

Where $\mathcal{A}$, $\mathcal{B}$, $\mathcal{C}$, $\mathcal{D}$ are lengthy constants that depend on the properties of the system and the acting force.

In lightly damped systems that have entered resonance ($\omega_p = \omega$), equation 2.17 can be approximated to:

$$d(t) \approx \frac{d_{st0}}{2\xi}\left(e^{-\xi\omega t} - 1\right)\cos(\omega t)$$

In this equation, it can be appreciated that damping effectively limits the maximum value of $d(t)$ when the system has entered resonance to $d_{max} \leq \frac{d_{st0}}{2\xi}$. This fact can be observed in the comparison of figure 2.7.

For damped systems, the resonant frequency is slightly lower than for undamped systems. Its value is the previously defined damped frequency:

$$\omega_D = \omega\sqrt{1-\xi^2}$$

For real systems ($\xi \ll 1/2$) this value stays very close to the system's natural frequency ω, as it can be seen in figure 2.8.

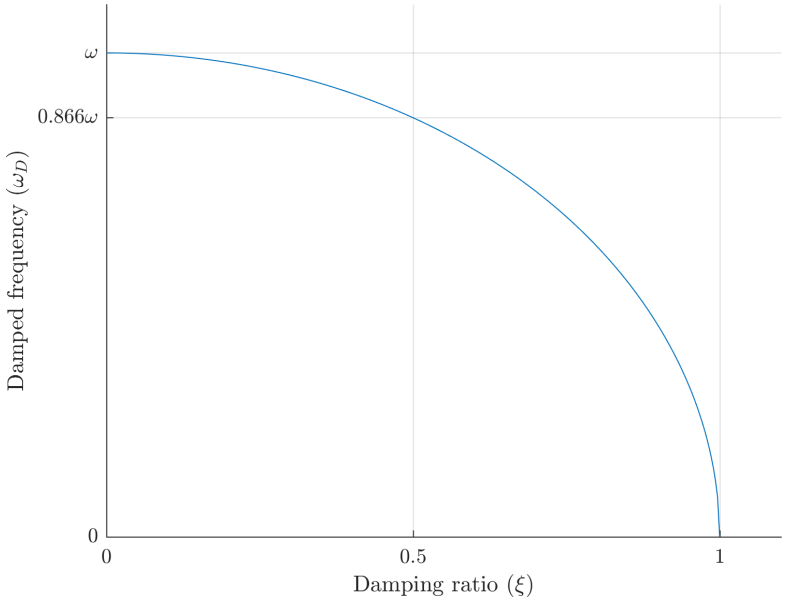

Figure 2.8.: Relation between the damped frequency (which produces resonance) and the damping ratio. Note that real systems usually have a ratio far lower than $1/2$

2.1.2.3. Extension to MDOF systems

The concept of natural frequency can be extended to multiple degrees-of-freedom systems. Starting with the matrix form of the undamped free vibration equation of motion (2.5) $\mathbf{M}\ddot{d} + \mathbf{K}d = 0$, and the solution in equation 2.6, it can readily be extended to multiple dimensions:

$$d(t) = \bar{a} \cdot \sin(\omega t) + \bar{b} \cdot \cos(\omega t)$$

Where two arrays of constants have been introduced:

$$\bar{a} = \begin{bmatrix} a_1 \\ a_2 \\ \dots \\ a_n \end{bmatrix}, \bar{b} = \begin{bmatrix} b_1 \\ b_2 \\ \dots \\ b_n \end{bmatrix}$$

The acceleration of the system is therefore:

$$\ddot{d}(t) = -\bar{a}\omega^2 \cdot \sin(\omega t) - \bar{b}\omega^2 \cdot \cos(\omega t) = -\omega^2 \cdot d(t)$$

Applying this solution to the undamped equation of motion results in:

$$\begin{aligned} \mathbf{M}(-\omega^2 \cdot d) + \mathbf{K}d &= 0 \\ \left[\mathbf{K} - \omega^2\mathbf{M}\right] d &= 0 \end{aligned} \tag{2.18}$$

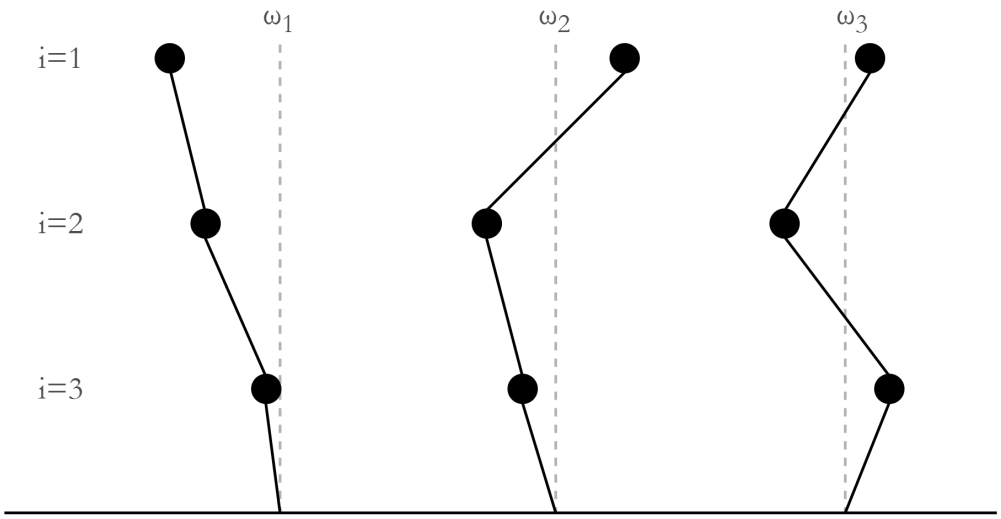

Figure 2.9.: Graphic visualization of the natural modes for a given 3-DOF structure

Which is the classical formulation of the eigenvalues problem. To solve it, the determinant (which is also called the eigenproblem's *characteristic equation*) has to be equal to zero $\left|\mathbf{K} - \omega^2\mathbf{M}\right| = 0$, condition that n (different or not) values of ω^2 can fulfill. If the characteristic equation is solved, all the values for the natural frequencies of the system are obtained. Frequency ω_1 will be the natural frequency of mass m_1, frequency ω_2 will be the natural frequency of mass m_2 and so forth.

As it has been already stated, in undamped systems the resonant frequency equals the natural frequency, but in damped systems the resonant frequency is a slightly lower $\omega_D = \omega\sqrt{1-\xi^2}$. Since the damping ratios contemplated in this thesis are lower than $\xi < 0.2$, which results in a modifier of $\sqrt{1-(0.2)^2} \approx 0.980$, the resonant frequency of a damped system will be approximated to that of an undamped system (that is, its natural frequency).

After solving the eigenproblem in equation 2.18, an eigenvector is obtained for each natural frequency. These vectors are called the *natural modes* of the structure and they indicate the shape (see figure 2.9) in which the structure responds to harmonic excitations of frequency equal to the corresponding natural frequency of the mode.

In structural dynamics, the lowest frequency is associated to the fundamental (or first) mode, since it is often the easiest frequency to excite with real-world forces, like for instance wind loads or cyclic mechanical loads. The rest of the modes are called the *harmonics*. The first harmonic corresponds to ω_2, the second harmonic to ω_3, and so on. See figure 2.10 for an example of the response of a multiple-DOF system when its fundamental frequencies are excited.

In linear theory, the response of a system is given by the superposition of the response of each mode to the exciting frequency.

Lumped mass model

One of the possibilities when analyzing the response of continuous structures is to idealize it by using a *lumped mass* model. These models agglomerate a portion of the structure into a

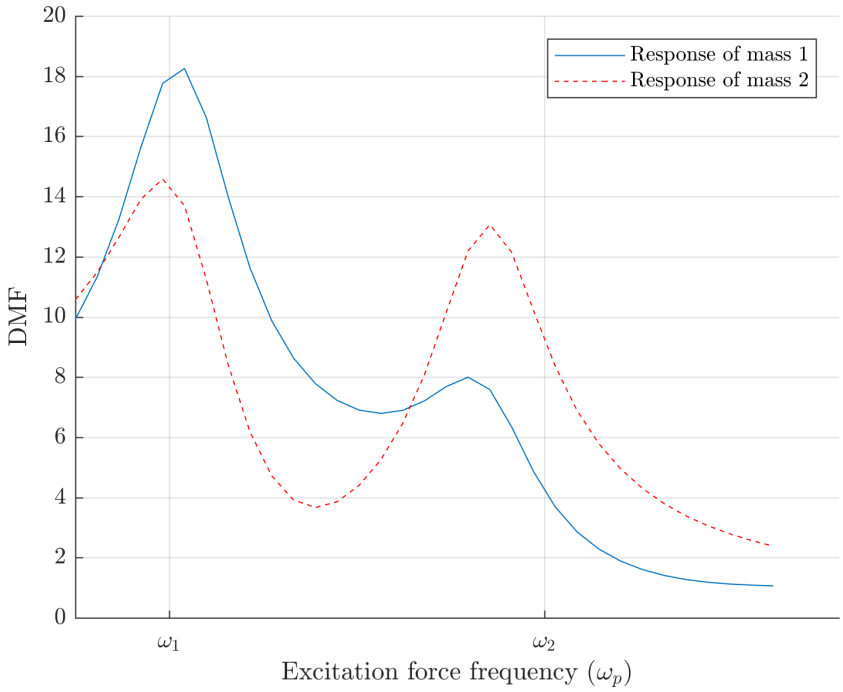

Figure 2.10.: Response of two masses that are part of a 2-DOF damped system according to different values of the exciting force's frequency

single mass of equivalent properties.

In the construction of multi-story buildings, lumped mass models are called *shear buildings*, and they reduce each story into a single mass with stiffness that depends on the anchoring and material of the columns. This allows for a convenient way of finding the approximated fundamental frequency of said structure without engaging in finite element analysis.

To obtain an approximation of a structure's damping, Rayleigh's method is usually applied.

This method assumes that damping is proportional to both mass and stiffness, resulting in the equation:

$$\mathbf{C} = \eta\mathbf{M} + \delta\mathbf{K} \tag{2.19}$$

Where η and δ are the proportional constants, which can be retrieved by solving the following system:

$$\begin{bmatrix} \xi_i \\ \xi_j \end{bmatrix} = \frac{1}{2} \begin{bmatrix} 1/\omega_i & \omega_i \\ 1/\omega_j & \omega_j \end{bmatrix} \begin{bmatrix} \eta \\ \delta \end{bmatrix} \tag{2.20}$$

Here, i, j are the indexes that correspond to the frequencies for which Rayleigh damping is going to be modeled. Usually, $i = 1$, $j = 2$. If the selected damping for both frequencies is the same, then:

$$\delta = \frac{2\xi}{\omega_1 + \omega_2}$$
$$\eta = \omega_1 \omega_2 \delta$$

As Wilson (1998) and Zareian and Medina (2010) argue, Rayleigh damping is not a good choice when conducting strict earthquake analysis, since the damping of higher modes is overestimated. However, when analyzing the response of lower modes, it serves as a good approximation.

2.1.3. Vibration control

The basic principle behind vibration control mechanisms is the conservation of energy: if a structure is considered a closed system, any energy transmitted by the disturbing forces that cannot be dissipated through heat, friction, or structural transmission, is going to end up as additional deformations on the system:

$$E_{in} = E_{deformations} + E_{dissipated}$$

Two main categories of vibration control exist at present: the *active control* and the *passive control*.

Passive control covers all the methods that cannot adapt to the characteristics of the acting force or the current status of the structure. Active control methods, on the other hand, include sensors that can draw up-to-date information of the acting forces and the state of the structure, processing units that can evaluate the best action in a given situation, and actuators that conduct the physical actions determined by the processing. Active control have enhanced adaptability and a relative insensitivity to the site conditions, but require external energy sources and a bigger expenditure. Some examples of these kind of devices are the active mass dampers (AMD) or the pulse generators.

For instance, the pulse generator of figure 2.11 expels bursts of compressed air through the nozzles installed on each story to cancel out the excitation forces. A computer is in charge of figuring out which nozzles go off at adequate times.

According to Soong and Costantinou (1994), passive control methods include two subcategories: seismic isolation and supplemental damping systems.

Seismic isolation is accomplished by having a foundation that is both highly flexible and also able to absorb great quantities of energy. This effectively decreases the total energy that is assimilated by the system, and detaches the rest of the structure in order to isolate it from earth movements. A practical seismic isolation system needs the follow elements:

→ High flexibility[1] in order to produce the isolation of the structure.

→ High energy dissipation capacity, to reduce the structure's displacements.

[1] High flexibility is equivalent to low stiffness

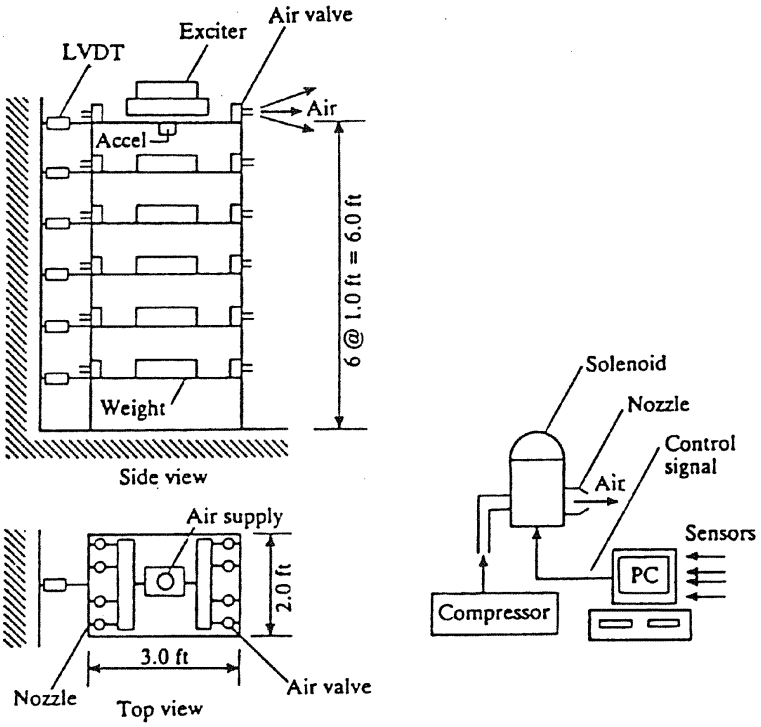

Figure 2.11.: Pulse generator system. Retrieved from Soong and Costantinou (1994)

→ The means to still provide enough stiffness so that the structure can withstand service loads.

Elastomeric bearings are the most common seismic isolation device in use in construction. They are often seen in bridges, as a laminated composite of mild steel and rubber that rests between the abutments and the columns. Some other forms of seismic isolation are the sliding bearings with friction and the fluid viscous dampers.

Conversely, supplemental damping systems are added mechanical devices that work in association with the structure in order to dissipate energy. Some of these systems are the tuned mass damper (TMD) and the tuned liquid damper (TLD).

Tuned liquid dampers (figure 2.12), which are widely used in ships, dissipate energy by displacing a mass of water (or other liquids) that rests inside a container. The vibration frequency is adjusted by changing the container size and the depth of the liquid, and the damping capacity is adjusted by placing rods or other elements in the liquid.

In section 2.3, tuned mass dampers will be discussed in detail.

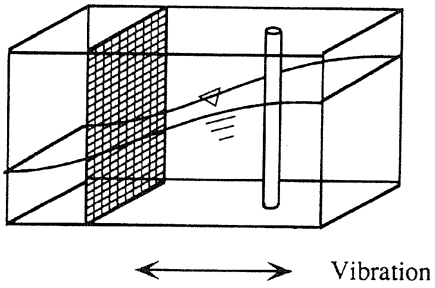

Figure 2.12.: Design of an sloshing tuned liquid damper. Retrieved from Soong and Costantinou (1994)

2.2. Numerical analysis of the equations of motion

Numerical methods can be categorized as either explicit or implicit depending on the way in which the state of the system is computed each time step.

In *explicit methods*, the state of system can be directly calculated with closed-form expressions that rely upon the system's state at previous times. For example, given a system $\mathbb{S}$ at different time steps t_{i-1}, t_i, t_{i+1}, there is a function $\mathcal{F}$ such that the following expression is valid:

$$\mathbb{S}(t_{i+1}) = \mathcal{F}(\mathbb{S}(t_i), \mathbb{S}(t_{i-1}))$$

For *implicit methods*, the state of the system can only be calculated with a system of equations that relies on the state of the system at previous times and at the current time. Following the previous example, a function $\mathcal{G}$ can now be found such that the following expression is valid:

$$\mathcal{G}(\mathbb{S}(t_{i+1}), \mathbb{S}(t_i), \mathbb{S}(t_{i-1})) = 0$$

Implicit methods are slower at computing each time step and are harder to implement and code, but they are convenient when handling stiff equations. Stiff equations often require very small time steps in order to converge if explicit methods are used, while implicit methods can work with bigger time steps and are unconditionally stable. Furthermore, some explicit methods can add numeric damping into the computed solutions. Positive numeric damping underestimates the response of a given system, while negative numeric damping amplifies it.

The equation of motion 2.2, discussed previously, is a second-order system of differential equations. A couple of numerical methods that deal with such equations are discussed below.

2.2.1. Central difference method

The central difference method (Whittaker et al. (1924)) is an explicit method able to solve the linear version of the equation of motion (equation 2.3).

The central difference approximation can be derived from the first Taylor expansion of any function $f(x)$ evaluated at $x = (a - h)$ and $x = (a + h)$:

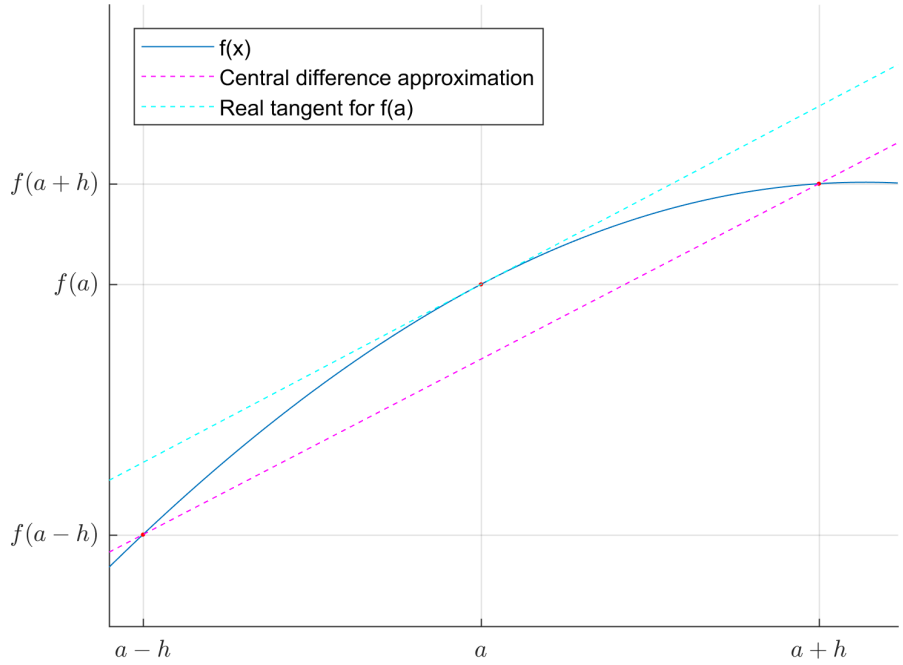

Figure 2.13.: The differential approximation of the slope $f'(a)$ of the function is the basis of the central difference method

$$f(a+h) = f(a) + \frac{f'(a)}{1!}(a+h-a) = f(a) + f'(a) \cdot h \tag{2.21}$$

$$f(a-h) = f(a) + \frac{f'(a)}{1!}(a-h-a) = f(a) - f'(a) \cdot h \tag{2.22}$$

Where $h \ll a$. Subtracting equation 2.22 from 2.21 and solving for $f'(a)$:

$$f'(a) = \frac{f(a+h) - f(a-h)}{2h} \tag{2.23}$$

A visual interpretation of this principle is shown in picture 2.13.

If the equation of the central difference 2.23 is adapted into the equations-of-motion nomenclature, it can be written as:

$$\dot{d}(t) = \frac{d(t+h) - d(t-h)}{2h} \tag{2.24}$$

Where h is the chosen time step. A similar procedure can be repeated again, now with the second derivative Taylor expansion:

$$\begin{aligned} f(a+h) &= f(a) + f'(a) \cdot h + \frac{f''(a) \cdot h^2}{2} \\ f(a-h) &= f(a) - f'(a) \cdot h + \frac{f''(a) \cdot h^2}{2} \end{aligned}$$

Adding these equations up and solving for $f''(a)$:

Algorithm 2.1 The central difference method

1. Input the mass, damping and stiffness matrices of the system.
2. Initialize the state of the system $d_0,\ \dot{d}_0,\ \ddot{d}_0$ and compute $d_1 = d_0 - h \cdot \dot{d}_0 + \frac{h^2}{2}\ddot{d}_0$.
3. Calculate the $\mathbf{A}_1,\ \mathbf{A}_2,\ \mathbf{A}_2$ matrices.
4. For each time step:
   a) Solve $\mathbf{A}_1 d_{i+1} = \mathbf{A}_2 d_i + \mathbf{A}_3 d_{i-1} + \mathbf{P}_i$ for d_{i+1} with Gaussian elimination and back-substitution.
   b) Compute velocity $\dot{d}_{i+1}$ and acceleration $\ddot{d}_{i+1}$ at step $i+1$ with equations 2.24 and 2.25.

$$f''(a) = \frac{f(a+h) - 2f(a) + f(a-h)}{h^2}$$

And in the appropriate nomenclature:

$$\ddot{d}(t) = \frac{d(t+h) - 2d(t) + d(t-h)}{h^2} \tag{2.25}$$

Inserting equations 2.24 and 2.25 into 2.2 results in:

$$\left\{\frac{\mathbf{M}}{h^2} + \frac{\mathbf{C}}{2h}\right\} d_{i+1} = \left\{\frac{2\mathbf{M}}{h^2} - \mathbf{K}\right\} d_i + \left\{\frac{\mathbf{C}}{2h} - \frac{\mathbf{M}}{h^2}\right\} d_{i-1} + \mathbf{P}_i$$

Where $d_{i+1} = d(t+h)$, $d_i = d(t)$, $d_{i-1} = d(t-h)$, $\mathbf{P}(t) = \mathbf{P}_i$ are all $n \times 1$ vectors, and n is the size of the system. After grouping matrices operations, this equation can be compactly written as:

$$\mathbf{A}_1 d_{i+1} = \mathbf{A}_2 d_i + \mathbf{A}_3 d_{i-1} + \mathbf{P}_i$$

Where $\mathbf{A}_1,\ \mathbf{A}_2,\ \mathbf{A}_2$ will remain constant given a linear system a fixed time step. Factorization of these matrices allows faster computing times during the central differences algorithm loop (2.1).

The central difference method is usually stable for time steps that verify:

$$h < \frac{T}{\pi}$$

Where T is the shortest natural period of the studied structure.

2.2.2. The Wilson-Θ method

The Wilson-Θ method (Bathe and Wilson (1976)) assumes that acceleration is linear between time t and $t + \theta h$ (see figure 2.14 for a visual interpretation), where θ is a chosen parameter that affects the stability of the system. If $\theta \geq 1.37$ the method is unconditionally stable, and thus $\theta = 1.4$ is usually the employed value.

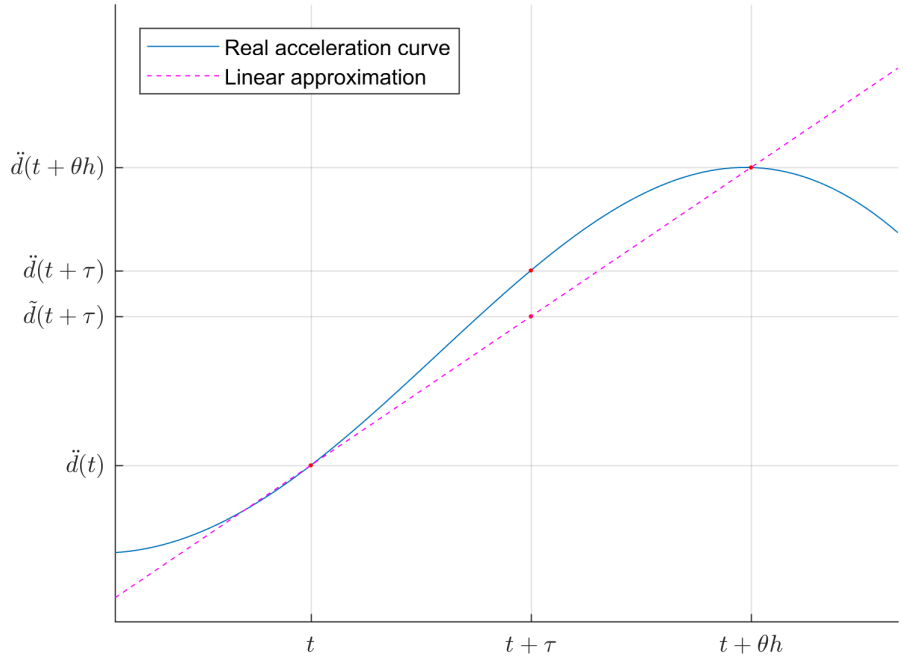

Figure 2.14.: Depiction of a linear approximation $\tilde{d}(t+\tau)$ to the real acceleration curve $\ddot{d}(t)$, which serves as the basis of the Wilson-Θ method

For a certain time increase τ such that $0 < \tau < \theta h$, acceleration scales linearly:

$$\ddot{d}_{t+\tau} = \ddot{d}_t + \frac{\tau}{\theta h}\left(\ddot{d}_{t+\theta h} - \ddot{d}_t\right) \tag{2.26}$$

If this expression is integrated for $\int_0^\tau \ddot{d}_{t+\tau} d\tau$ then:

$$\dot{d}_{t+\tau} - \dot{d}_t = \tau \dot{d}_t + \frac{\tau^2}{2\theta h}\left(\ddot{d}_{t+\theta h} - \ddot{d}_t\right)$$

Clearing up:

$$\dot{d}_{t+\tau} = \dot{d}_t + \tau \ddot{d}_t + \frac{\tau^2}{2\theta h}\left(\ddot{d}_{t+\theta h} - \ddot{d}_t\right) \tag{2.27}$$

Integrating again ends up in:

$$d_{t+\tau} = d_t + \tau \dot{d}_t + \frac{\tau^2}{2}\ddot{d}_t + \frac{\tau^3}{6\theta h}\left(\ddot{d}_{t+\theta h} - \ddot{d}_t\right) \tag{2.28}$$

Solving for $\tau = \theta h$ in equations 2.27 and 2.28 gives the following:

$$\dot{d}_{t+\theta h} = \dot{d}_t + \frac{\theta h}{2}\left(\ddot{d}_{t+\theta h} + \ddot{d}_t\right)$$
$$d_{t+\theta h} = d_t + \theta h \dot{d}_t + \frac{\theta^2 h^2}{6}\left(\ddot{d}_{t+\theta h} + 2\ddot{d}_t\right)$$

And these can be solved for $\ddot{d}_{t+\theta h}$ and $\dot{d}_{t+\theta h}$ in terms of $d_{t+\theta h}$:

Algorithm 2.2 The Wilson-Θ method

1. Input the mass, damping and stiffness matrices of the system.
2. Initialize the state of the system d_0, $\dot{d}_0$, $\ddot{d}_0$ and choose the θ constant and time step.
3. For each time step:
   a) Solve $d_{t+\theta h}$ with equation 2.32.
   b) Solve d_{t+h}, $\dot{d}_{t+h}$ and $\ddot{d}_{t+h}$ evaluating equations 2.26, 2.27 and 2.28 respectively, with the output from 2.32 and 2.29.

$$\ddot{d}_{t+\theta h} = \frac{6}{\theta^2 h^2}\left(d_{t+\theta h} - d_t\right) - \frac{6}{\theta h}\dot{d}_t - 2\ddot{d}_t \tag{2.29}$$

$$\dot{d}_{t+\theta h} = \frac{3}{\theta h}\left(d_{t+\theta h} - d_t\right) - 2\dot{d}_t - \frac{\theta h}{2}\ddot{d}_t \tag{2.30}$$

Now, back to the linear equation of motion for a time $t + \theta h$:

$$\mathbf{M}\ddot{d}_{t+\theta h} + \mathbf{C}\dot{d}_{t+\theta h} + \mathbf{K}d_{t+\theta h} = \mathbf{P}_{t+\theta h} \tag{2.31}$$

Substituting 2.29 and 2.30 into 2.31 results in an explicit equation from which $d_{t+\theta h}$ can be made explicit:

$$\begin{aligned}\left\{\frac{6}{\theta^2 h^2}\mathbf{M} + \frac{3}{\theta h}\mathbf{C} + \mathbf{K}\right\} d_{t+\theta h} = \left\{\frac{6}{\theta^2 h^2}\mathbf{M} + \frac{3}{\theta h}\mathbf{C}\right\} d_t \\ + \left\{\frac{6}{\theta h}\mathbf{M} + 2\mathbf{C}\right\}\dot{d}_t + \left\{2\mathbf{M} + \frac{\theta h}{2}\mathbf{C}\right\}\ddot{d}_t + \mathbf{P}_{t+\theta h}\end{aligned} \tag{2.32}$$

And this can be simplified with precomputed $\mathbf{A}_i$ matrices.

$$\mathbf{A}_1 d_{t+\theta h} = \mathbf{A}_2 d_t + \mathbf{A}_3\dot{d}_t + \mathbf{A}_4\ddot{d}_t + \mathbf{P}_{t+\theta h}$$

Then, substituting $d_{t+\theta h}$ into 2.29, the acceleration $\ddot{d}_{t+\theta h}$ can be obtained. Evaluating equations 2.26, 2.27 and 2.28 with $\tau = h$ will finally provide the values for $\ddot{d}_{t+h}$, $\dot{d}_{t+h}$, d_{t+h}.

The Wilson-Θ method can be adapted for non-linear use by introducing the concept of the tangent stiffness matrix $\mathbf{K}_t$, which has to be computed every time step based on the displacement history:

$$\mathbf{F}_S(d_{t+h}) = \mathbf{K}_t d_t$$

A one-dimensional interpretation of tangent stiffness can be seen in figure 2.15.

As it was already discussed that the Wilson-Θ method is unconditionally stable for $\theta \geq 1.37$. Otherwise, stability is only achieved if $h < 0.551T$.

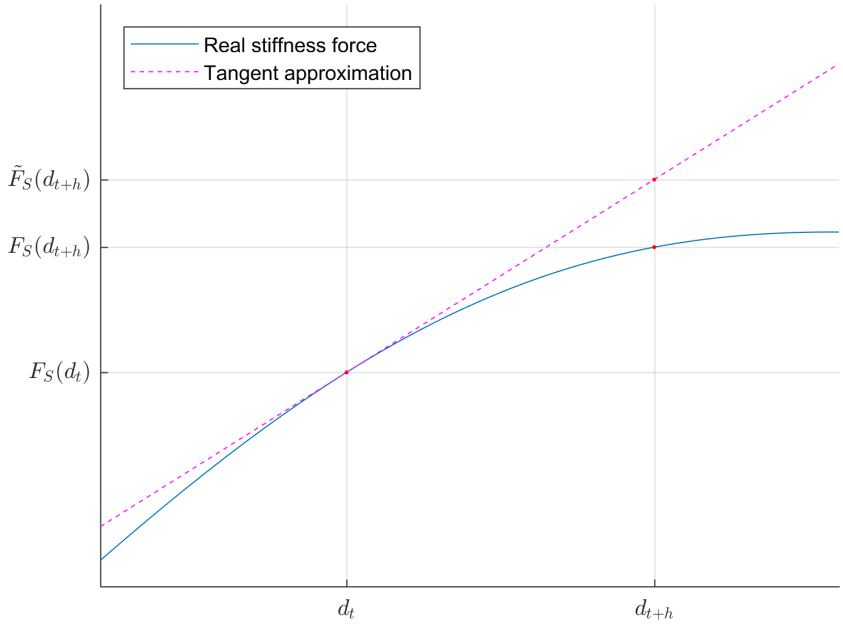

Figure 2.15.: Stiffness force function $F_D(d)$ with a tangent approximation $\tilde{F}_D(d_{t+h})$: the slope at each time is the tangent stiffness (K_t), which is usually used to compute the stiffness force at the next time step

2.2.3. The Newmark family of methods

The Newmark family of methods (Newmark (1959)) is derived from the Taylor series expansion:

$$f(t_i + h) = f(t_i) + hf'(t_i) + \frac{h^2}{2}f''(t_i) + ... + R_s$$

Where R_s is the remainder:

$$R_s = \frac{1}{s!}\int_{t_i}^{t_i+h} f^{(s+1)}(\tau)\,[t_i + h - \tau]^s\,d\tau$$

Newmark applied the truncated series to the displacement and velocity of the system, and added the γ and β parameters, resulting in:

$$\dot{d}_{i+1} = \dot{d}_i + (1-\gamma)\ddot{d}_i h + \gamma\ddot{d}_{i+1}h \tag{2.33}$$

$$d_{i+1} = d_i + \dot{d}_i h + (1/2 - \beta)\ddot{d}_i h^2 + \beta\ddot{d}_{i+1}h^2 \tag{2.34}$$

Substituting equations 2.33 and 2.34 into the linear equation of motion (2.3) results in the following:

$$\left\{\mathbf{M} + \gamma h\mathbf{C} + \beta h^2\mathbf{K}\right\} d_{i+1} = \mathbf{P}_{i+1} - \{\mathbf{K}\}\, d_i - \{\mathbf{C} + h\mathbf{K}\}\,\dot{d}_i - \left\{(1-\gamma)h\mathbf{C} + (1/2-\beta)h^2\mathbf{K}\right\}\ddot{d}_i$$

Which can be simplified to:

Table 2.2.: Various characteristics for the family of Newmark methods. Adapted from Géradin and Rixen (2014)

Algorithm	γ	β	Stability limit ωh	Numerical damping ratio	Periodicity error
Purely explicit	0	0	0	$-\frac{\omega h}{4}$	–
Central difference	$\frac{1}{2}$	0	2	0	$-\frac{\omega^2 h^2}{24}$
Linear acceleration	$\frac{1}{2}$	$\frac{1}{6}$	3.46	0	$\frac{\omega^2 h^2}{24}$
Average constant acceleration	$\frac{1}{2}$	$\frac{1}{4}$	∞	0	$\frac{\omega^2 h^2}{12}$

$$\hat{\mathbf{K}} d_{i+1} = \hat{\mathbf{P}}_{i+1}$$

Where $\hat{\mathbf{K}} = \left\{\mathbf{M} + \gamma h \mathbf{C} + \beta h^2 \mathbf{K}\right\}$ can be precomputed before the iteration loop, but $\hat{\mathbf{P}}_{i+1}$ has to be computed at each time step.

If $\gamma = 1/2$, the Newmark method has no numerical damping whatsoever. For $\gamma = 0$, negative numerical damping is introduced, which causes highly unstable behavior. Any other value of γ introduces positive numerical damping. Newmark settled on $\gamma = 1/2$, which is why the original method is also called Newmark-β.

Giving different values to these parameters gives the algorithm varied properties. An example of what some of these values accomplish can be seen in table 2.2.

The Newmark method, as presented in algorithm 2.3, is only capable of solving linear problems. In order to handle non-linear systems, a modification to the algorithm has to be made to account for the changing stiffness. This modification will be discussed in section 3.4, devoted to the building of the model.

Algorithm 2.3 The linear Newmark method

1. Input the mass, damping and stiffness matrices of the system.
2. Initialize the state of the system (d_0, $\dot{d}_0$, $\ddot{d}_0$) and choose the γ, β parameters and the time step.
3. Precompute the $\hat{\mathbf{K}}$ matrix.
4. For each time step:
   a) Compute $\Delta\hat{\mathbf{P}}_i = \Delta\mathbf{P}_i + \left[\frac{1}{\beta h}\mathbf{M} + \frac{\gamma}{\beta}\mathbf{C}\right]\dot{d}_i + \left[\frac{1}{2\beta}\mathbf{M} + h\left(\frac{\gamma}{2\beta} - 1\right)\mathbf{C}\right]\ddot{d}_i$.
   b) Solve for Δd_i in $\hat{\mathbf{K}}\Delta d_i = \Delta\hat{\mathbf{P}}_{i+1}$.
   c) Then, $d_{i+1} = d_i + \Delta d_i$.
   d) Compute the new velocity and acceleration vectors with equations:
      i. $\Delta\dot{d}_i = \frac{\gamma}{\beta h}\Delta d_i - \frac{\gamma}{\beta}\dot{d}_i + h\left(1 - \frac{\gamma}{2\beta}\right)\ddot{d}_i$
      ii. $\Delta\ddot{d}_i = \frac{1}{\beta h^2}\Delta d_i - \frac{\gamma}{\beta h}\dot{d}_i - \frac{1}{2\beta}\ddot{d}_i$

2.3. Tuned mass dampers

Tuned mass dampers (TMD), also known as *absorbers*, are a type of supplemental damping system comprised of a mass, a spring and a viscous damper, properly tuned in order to attenuate undesired frequencies in a given structure.

By and large, TMD are optimized to filter out the effect of external forces that excite the fundamental mode of the structure, since it is the one that produces the most damaging effects.

The invention of the tuned mass damper is attributed to German shipbuilder Hermann Frahm, back in 1909. The patent (figure 2.16) described it as a "device for damping vibrations of bodies", and proposed different mechanisms to achieve the desired effect.

TMD are usually installed at the top of structures. When the structure starts vibrating, the TMD is excited accordingly. In this way, kinetic energy is relieved from the system and transferred to the device.

To maximize dissipation, the natural frequency of the TMD is tuned to a value that is close to the natural frequency of the structure. TMD are low on maintenance and highly reliable, in addition to not needing any external power source to function.

An important aspect of tuned mass dampers is that each of these devices can only counter one specific frequency. A way around this limitation is the use of multiple tuned mass dampers (MTMD) in order to attack several frequencies of interest at once. Jangid (1999), for instance, used numerical search techniques to find the optimum parameters of such a system, and found moderate success in providing a smoother response curve (see figure 2.17).

Furthermore, adding a TMD to a structure clearly increases the total mass of the system, which results in a downwards shift of the fundamental frequency, and a worse system response to the surrounding frequencies. This can be seen in figure 2.18.

Tuned mass dampers specialize in softening the worst-case scenarios that harmonic oscillation cause on structures.

Tuned mass dampers are governed by the equation of motion of damped systems under forced vibration:

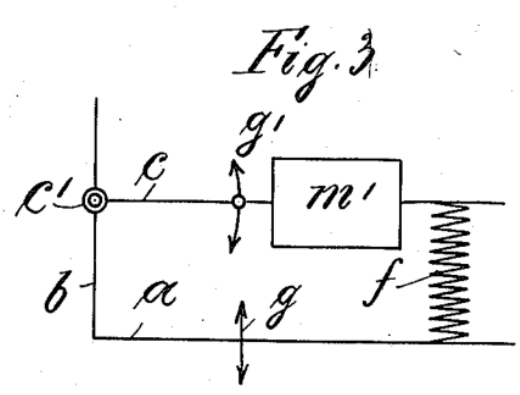

Figure 2.16.: Figure of the original 1911 Hermann Frahm patent. Retrieved from U.S. Patent No. 989,958

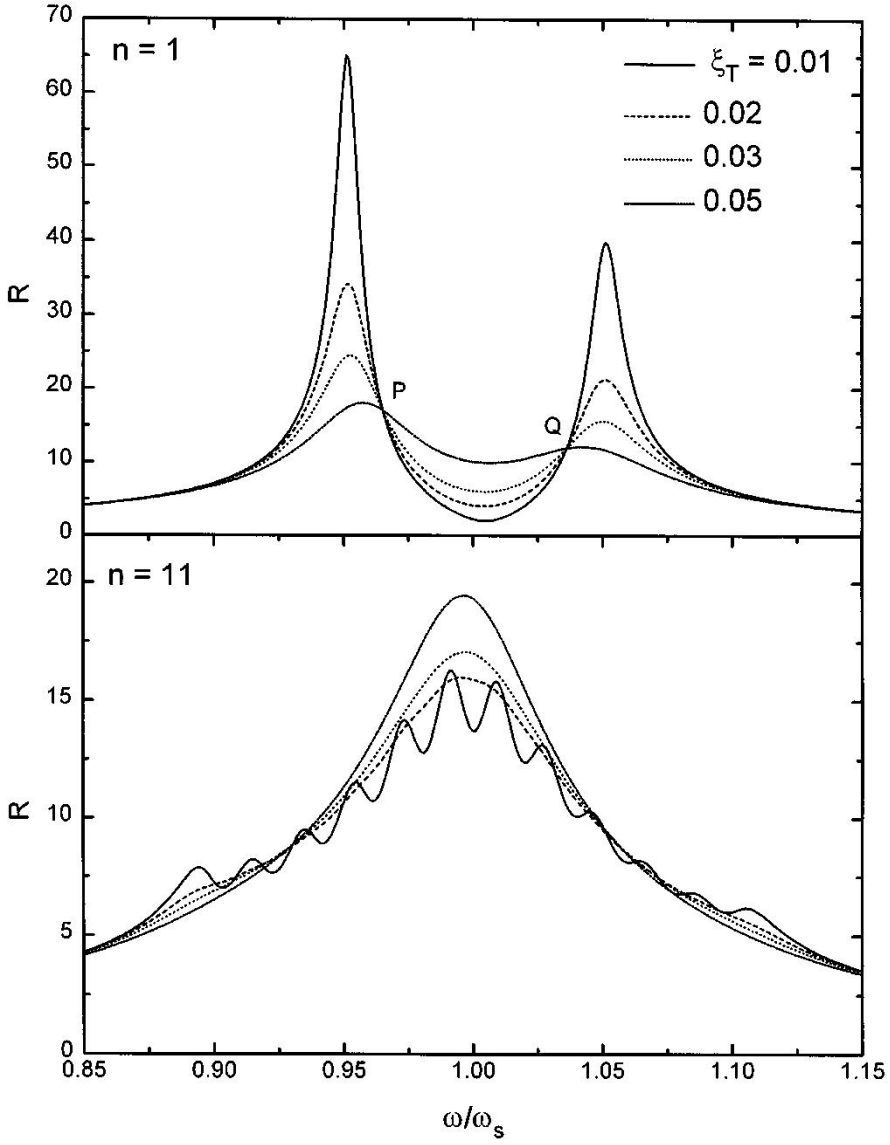

Figure 2.17.: Comparison of the response (R) of a single TMD versus $n = 11$ TMD, with various damping ratios (ξ_T). Retrieved from Jangid (1999)

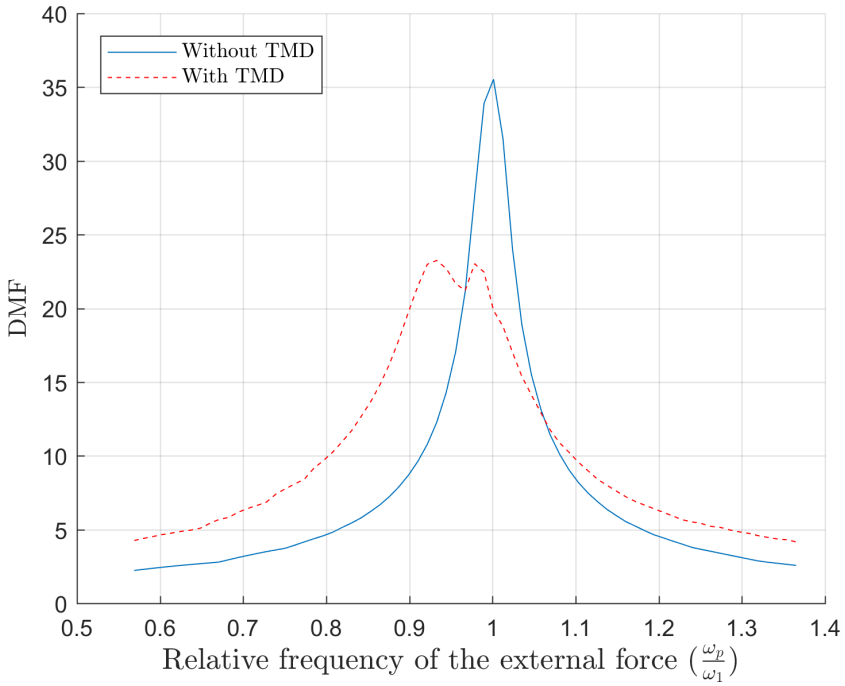

Figure 2.18.: Example of the vibration control a tuned mass damper provides

$$m_d\ddot{d}_d + c_d\dot{d}_d + k_d d_d = P(t) \tag{2.35}$$

m_d mass of the TMD

c_d damping of the TMD

k_d stiffness of the TMD

d_d displacement of the TMD

$\dot{d}_d$ velocity of the TMD

$\ddot{d}_d$ acceleration of the TMD

P force acting on the TMD

2.3.1. TMD design

Carefully choosing the design parameters of the TMD is of great importance: ill-tuned parameters can cause increased vibrations all along the frequency spectrum.

However, there is not an unequivocal tuning method that works for every TMD: the approach varies with the characteristics of the force that is exciting the system and with the constraints of the project. Several authors provide different approximated formulas or tables to calculate the parameters of the TMD. These parameters are:

$\overline{m} = \frac{m_d}{m_s}$ mass coefficient between TMD and structure, usually chosen between 1-10%

$\eta = \frac{\omega_d}{\omega_s}$ natural frequency coefficient between TMD and structure

ξ_d damping ratio of the TMD

Ultimately, the absolute mass, stiffness and damping values are needed to work with the equation of motion. The following relations will be used:

$$k_d = \omega_d^2 m_d$$
$$c_d = 2\xi_d \omega_d m_d$$

The design process of a TMD relies on the damping of the main structure. Tsai and Lin (1993) concludes that structures with high damping ratio values (ξ_s) take less advantage from having a TMD and, at the same time, require a higher damping ratio value (ξ_d) for the TMD.

Den Hartog (1956) proposed an analytic method of tuning by simplifying the optimization problem. Its hypotheses are:

→ The whole system is reduced to a 2-DOF system: one node for the structure and one node for the TMD.

→ The damping of the structure is neglected.

→ Consider the acting force as a purely sinusoidal of the form $P(t) = P_0 sin(\omega t)$ where P_0, ω are the maximum amplitude and the frequency of the force.

The equations of motion of this system can be written as:

$$\begin{aligned} m_s\ddot{d}_s + k_s d_s + k_d(d_s - d_d) &= P_0 sin(\omega t) \\ m_d\ddot{d}_d + k_d(d_d - d_s) + c_d(\dot{d}_d - \dot{d}_s) &= 0 \end{aligned} \tag{2.36}$$

m_s mass of the structure

k_s stiffness of the structure

d_s displacement of the structure

$\dot{d}_s$ velocity of the structure

$\ddot{d}_s$ acceleration of the structure

After performing some algebra on 2.36 and solving:

$$\frac{d_{s0}}{d_{st0}} = \sqrt{\frac{(2\xi_d\eta\phi)^2 + (\phi^2 - \eta^2)^2}{(2\xi_d\eta\phi)^2 (\phi^2 - 1 + \bar{m}\phi^2)^2 + [\bar{m}\eta^2\phi^2 - (\phi^2 - 1)(\phi^2 - \eta^2)]^2}} \tag{2.37}$$

Where $\phi = \frac{\omega_p}{\omega_s}$ is the forced frequency ratio, $d_{st0} = {}^{P_0}/_{k_s}$ was previously defined as the static displacement, and d_{s0} is the amplitude for the system's displacement (that is, the maximum value).

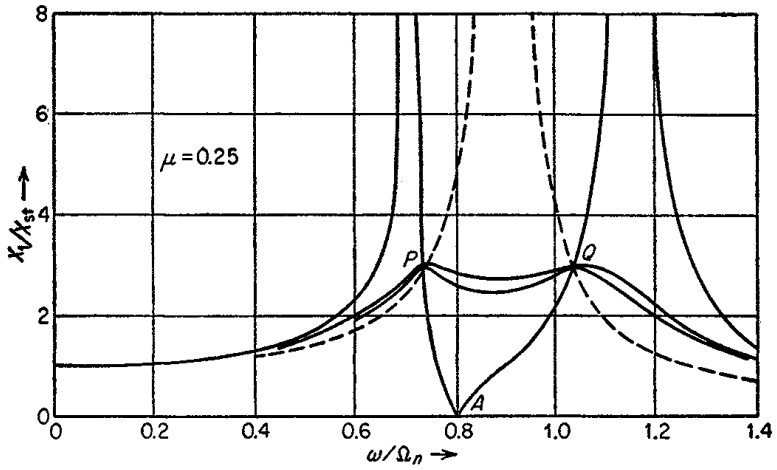

Figure 2.19.: Resonance curves for a system with $\bar{m} = 0.25$ and different TMD damping. Notice that points P and Q remain fixed. Retrieved from Den Hartog (1956)

If this equation is plotted, it can be seen that for any chosen value of the damping ratio of the TMD (ξ_d), the curves always pass through two fixed points P and Q (see figure 2.19).

By undergoing a long process of differentiation of equation 2.37, the following closed-form expressions can be obtained:

$$\xi_d = \sqrt{\frac{3\bar{m}}{8(1+\bar{m})^3}} \tag{2.38}$$

$$\omega_d = \frac{\omega_s}{1+\bar{m}} \tag{2.39}$$

These equations allow the calculation of the optimum TMD parameters. See figure 2.20 for a visualization of the optimum damping ratio as a function of $\bar{m}$.

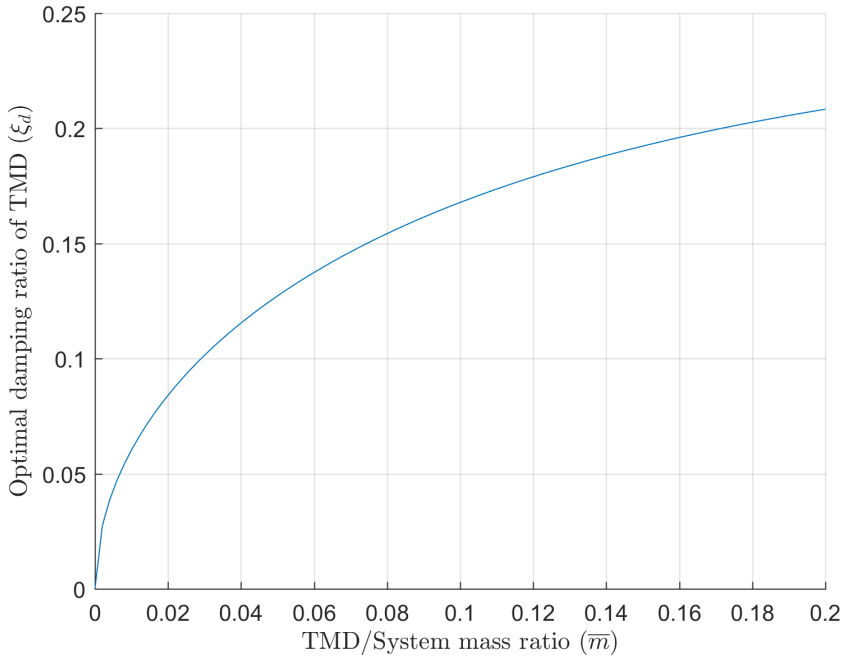

Figure 2.20.: Optimum TMD damping ratio for common TMD/System mass coefficients ($\bar{m}$)

Design procedure

Finally, the design procedure of a tuned mass damper is summed up by Soong and Costantinou (1994) in the following steps:

1. Identify the system's structural properties: natural frequency and its associated mass and damping.
2. Decide on a starting value for the mass coefficient $\bar{m}$.
3. Calculate the damping ratio and frequency of the tuned mass damper with equations 2.38 and 2.39.
4. Compute the maximum displacements for the tentative design. If they are too large, go back to step 2.
5. Design the mechanical system and the tuning system of the TMD.
6. Perform physical verification tests.

3. Non-linear model design

This chapter will go over the various phases of development of the non-linear dynamic model, from an explanation of the original physical scale model to the implementation of the Newmark method, along with the introduction of the elastoplastic friction analogy.

3.1. Original lumped mass tower model

The model built for this thesis is loosely based on the physical scale model that was designed in the department of structures to investigate tuned mass dampers. This choice was made so that the starting point of the testing builds upon a real case.

The tower's skeleton was a round steel bar of diameter $\phi = 42\,\text{mm}$ and height $H = 2073\,\text{mm}$, weighting a total of $m = 22.5\,\text{Kg}$. To simulate the extra masses of the nacelle, rotor and electronics, supplemental weights of $287.5\,\text{Kg}$ were distributed along the uppermost part of the tower.

The computer lumped mass model was comprised of 36 nodes with proportional weights. The stiffness of each segment was calculated by applying the properties of the material and the geometry. These are the used formulas:

$$h_i = \frac{H}{35}$$
$$m_i = \frac{\pi\phi^2}{4} h_i \rho_s + m_{p,i}$$
$$k_i = \frac{E_s \pi}{64} \phi^4$$

Where:

h_i height of each segment in relation to total tower height

m_i mass of each node

$m_{p,i}$ mass of the added weights

ρ_s steel density

k_i stiffness of each segment

E_s Young modulus of steel

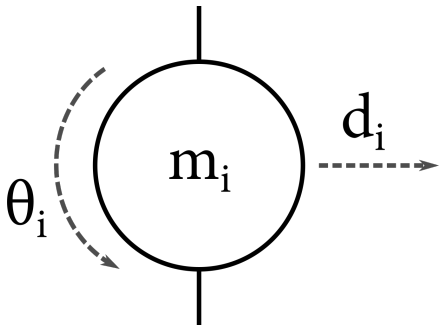

Figure 3.1.: Sketch of the displacement and rotation allowed for each tower node i

Each node is given two degrees of liberty for movement: one for the displacement on the horizontal axis, and the other for the rotation on the plane containing the structure. See figure 3.1 for clarification.

The mass and stiffness matrices can now be constructed. Each one will be of size 72×72 (36 nodes times 2-DOF), and will be built by following equation 2.1.

Damping is modeled using Rayleigh's method (equations 2.19 and 2.20) and the values of the damping ratio for the first two modes can be adjusted with the physical model.

After solving the eigenproblem, the first three fundamental frequencies are:

$$\begin{aligned} f_1 &= 0.879\,\mathrm{Hz} \\ f_2 &= 22.61\,\mathrm{Hz} \\ f_3 &= 58.32\,\mathrm{Hz} \end{aligned} \tag{3.1}$$

The corresponding modes for these frequencies are plotted in figure 3.2.

The TMD used in this tower was tuned with the following parameters:

$$\begin{aligned} m_d &= 26.3\,\mathrm{Kg} \\ k_d &= 1940\,\mathrm{N/m} \\ \xi_d &= 0.124 \\ c_d &= 42.25\,\mathrm{Kg/s} \end{aligned}$$

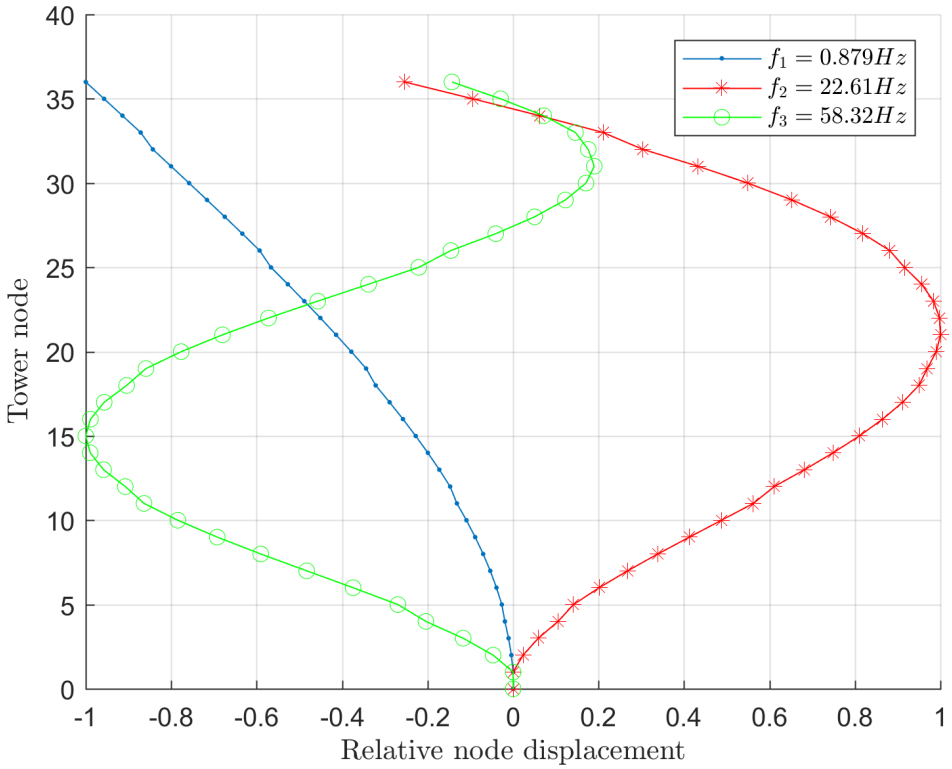

Figure 3.2.: First three modes of vibration for the physical tower model

3.2. Simplified two degrees-of-freedom model

The model that is used in the computations of this thesis is a 2-DOF where one node stands for the whole structure and the other node is the tuned mass damper. This simplification was made for the following reasons:

→ Speed of computations. Since the model will be non-linear and a great number of results have to be computed to study the behavior of the structure in response to modifications of each parameter, a sizable amount of time will be spent running simulations.

→ Structure and tuned mass dampers 2-DOF systems are a widely used method of damper optimization: it is in fact the one employed to obtain Den Hartog's classical tuning equations (2.38 and 2.39).

→ The 2-DOF system simplification is ill-advised when the structure has harmonic frequencies that are relatively close to the fundamental frequency. The reason behind this is that when the structure is reduced to a single node, only one resonant frequency can be represented. This is, however, not the case for the studied tower (see results 3.1).

→ Reducing the complexity of the system allows the conclusions to be have a broader significance, and not just fit an overly particular structure or case.

The simplified structure will share the fundamental node of the tower model ($f_1 = 0.879\,\text{Hz}$), so the following equation has to be satisfied at all times:

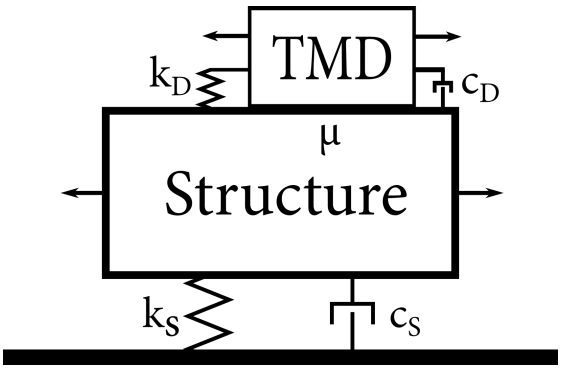

Figure 3.3.: Schematic representation of the 2-DOF model

Table 3.1.: Base values for the 2-DOF system

Variable	System	Tuned mass damper
Mass	256 Kg	22.54 Kg
Stiffness	7808.7 N/m	-
ξ	0.01	-
ω	5.525 1/s	-

$$\omega_s = \sqrt{k_s/m_s}$$

Where the subscript s indicates these are the structure's parameters. The angular frequency is fixed at $\omega_s = 2\pi f_1 = 5.525$ 1/s.

The TMD of reference will be optimized with Den Hartog's tuning equations. New tuning equations where the friction between the structure and the TMD is taken into account will be developed in the next chapter. The friction coefficient will become a new parameter of the tuned mass damper that needs to be optimized.

A schematic physical interpretation of the model can be seen in figure 3.3.

The equations of motion that govern the linear model are:

$$\begin{bmatrix} m_s & 0 \\ 0 & m_d \end{bmatrix} \begin{bmatrix} \ddot{d}_s \\ \ddot{d}_d \end{bmatrix} + \begin{bmatrix} c_s + c_d & -c_d \\ -c_d & c_d \end{bmatrix} \begin{bmatrix} \dot{d}_s \\ \dot{d}_d \end{bmatrix} + \begin{bmatrix} k_s + k_d & -k_d \\ -k_d & k_d \end{bmatrix} \begin{bmatrix} d_s \\ d_d \end{bmatrix} = \begin{bmatrix} P_0 \sin(\omega_p t) \\ 0 \end{bmatrix} \quad (3.2)$$

The chosen values for the simplified 2-DOF system are described in table 3.1.

In the following section, friction (and therefore, non-linearity) will be introduced, which will modify the equations of the model.

3.3. Elastoplasticity and sliding friction analogy

3.3.1. Perfect elastic and plastic behavior

Perfect elastic materials endure strains that are completely proportional to the resultant force acting upon them. They do not suffer any permanent deformations and, when the force recedes, they assume their initial form. They satisfy the relation:

$$\sigma = E\varepsilon \tag{3.3}$$

Where σ is the stress, ε is the strain (dimensionless), and E is Young's modulus, which mostly depends on the used material but it's also affected by temperature, conditions of the material, and so on. In elastic theory E is assumed constant. In a one-dimensional problem, equation 3.3 can also be represented as:

$$F_S = Kd$$

Which is equivalent to the stiffness of structural analysis (see subsection 2.1.1).

Elastoplastic materials (also known as *elastic-perfectly plastic*) have an initial elastic behavior, up until the stresses reach the *yield strength* that is characteristic of said material. After surpassing the yield point, the linear relation between stress and strain is lost and deformations become irreversible: when the acting force stops, the deformation that has occurred during plastic regime remains. See figure 3.4 for a real-world plastic behavior example and figure 3.5 for the idealized performance. Plasticity is a highly complex non-linear phenomenon that differs for different materials, but proper simplifications, such as fitting two different lines to describe the transition between elastic and plastic behavior, can be made for most cases.

3.3.2. Sliding friction

Sliding friction is the force that resists the movement between two solid objects that are in physical contact. Its maximum value is defined as:

$$F_\mu = \mu N$$

Where F_μ is the frictional force, μ is the *friction coefficient* and N is the normal force. The friction coefficient is highly independent of the mass, the relative velocity of the objects and the contact surface between them, so it is often treated as a constant that depends on the choice of materials.

In some cases, the friction coefficient is divided into the static (μ_s) and the kinetic ($\mu_k \leq \mu_s$). The static coefficient is used to calculate the required force to start movement, and the kinetic coefficient to calculate the value of friction force when the objects are undergoing relative movement.

Friction cannot surpass the force that it's counteracting. Taking the force R as the resultant acting over a resting body and F_μ the friction force that's opposing it, then:

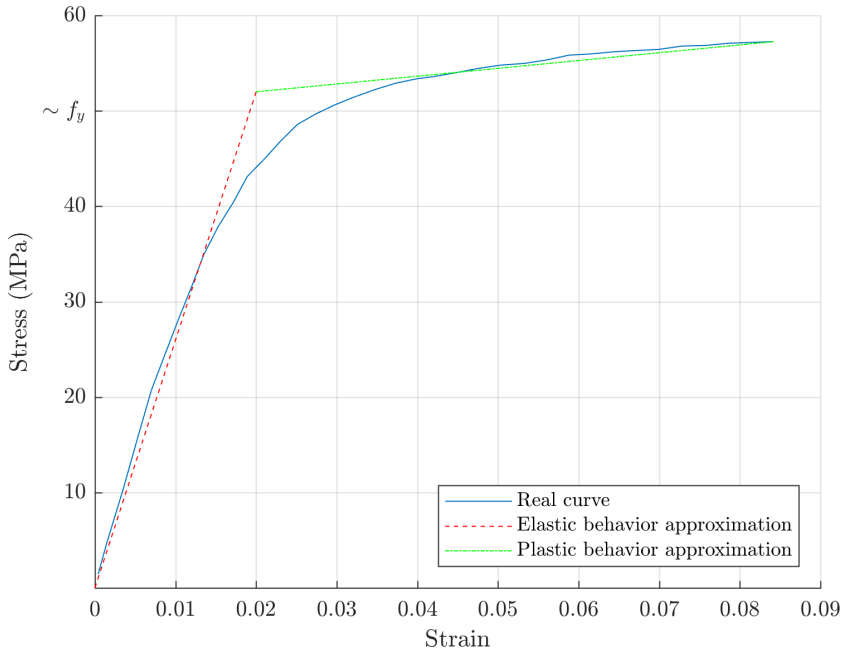

Figure 3.4.: Real strain-stress curve for rubber, along with linear approximations of the elastic and plastic regimes

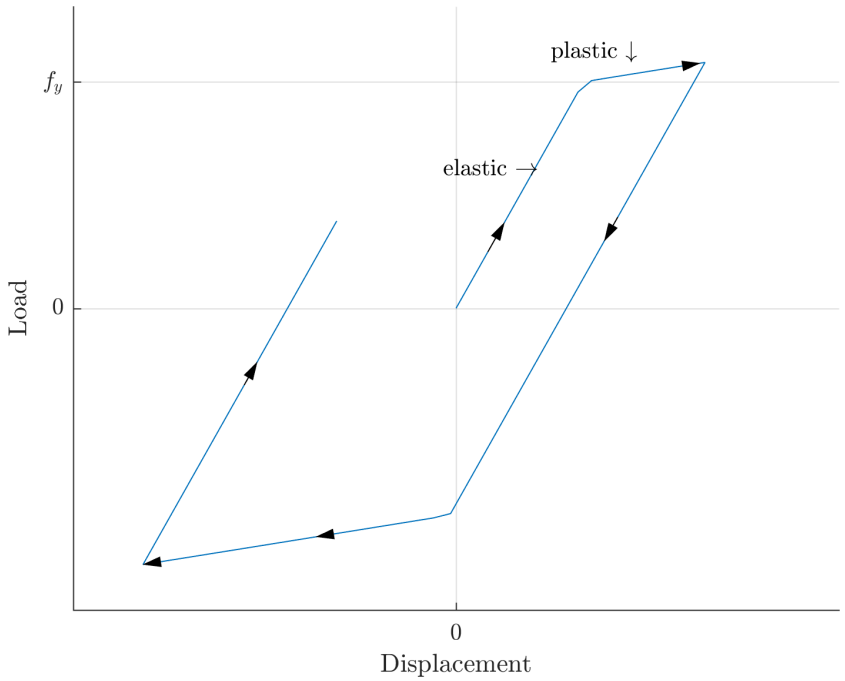

Figure 3.5.: Displacement-load plot of a perfect elastoplastic material under a cyclic load

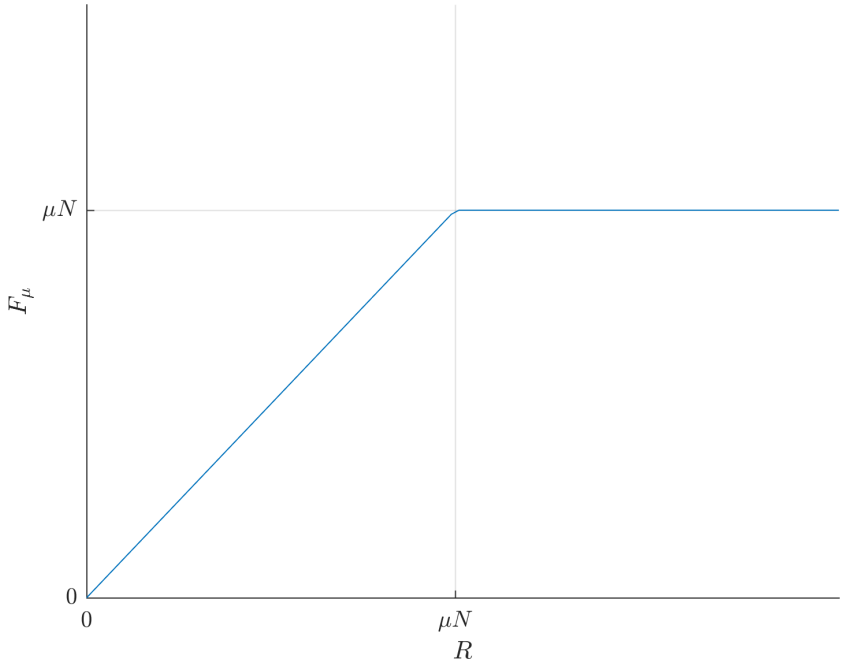

Figure 3.6.: Friction force F_μ scales with the resultant (R) until its maximum value is reached

$$F_\mu = \min\{R, \mu N\}$$

Which has been plotted in figure 3.6. Until $R > \mu N$, the resultant cannot overcome the frictional forces and the displacement of the body will be negligible.

Consider now that this body is the TMD of figure 3.3 and that the normal force is $N = m_d g$. The spring with constant k_d won't be able to exert any force until there is non-null relative displacement between the TMD and the structure ($F_S = k_d(d_d - d_s)$), and relative displacement will only change when the force of friction is exceeded ($F_S > \mu N$).

Conversely, if relative displacements and velocities are zero (TMD and structure move together), the resultant over the TMD is zero:

$$\begin{aligned} m_d\ddot{d}_d + c_d(\dot{d}_d - \dot{d}_s) + k_d(d_d - d_s) &= 0 \\ m_d\ddot{d}_d &= 0 \end{aligned}$$

This results in a non-linear behavior between the relative displacement and the value of the stiffness force, which is portrayed in figure 3.7. Notice how this model is extremely similar to the elastoplastic model discussed in the previous subsection (figures 3.4 and 3.5).

The element of figure 3.7 can be described as a perfectly elastoplastic spring with:

→ A high value of elastic stiffness k_e. Note that this value has to be sufficiently bounded to avoid convergence issues during the Newton-Raphson iteration.

→ A plastic stiffness that corresponds to the actual TMD stiffness $k_p = k_d$.

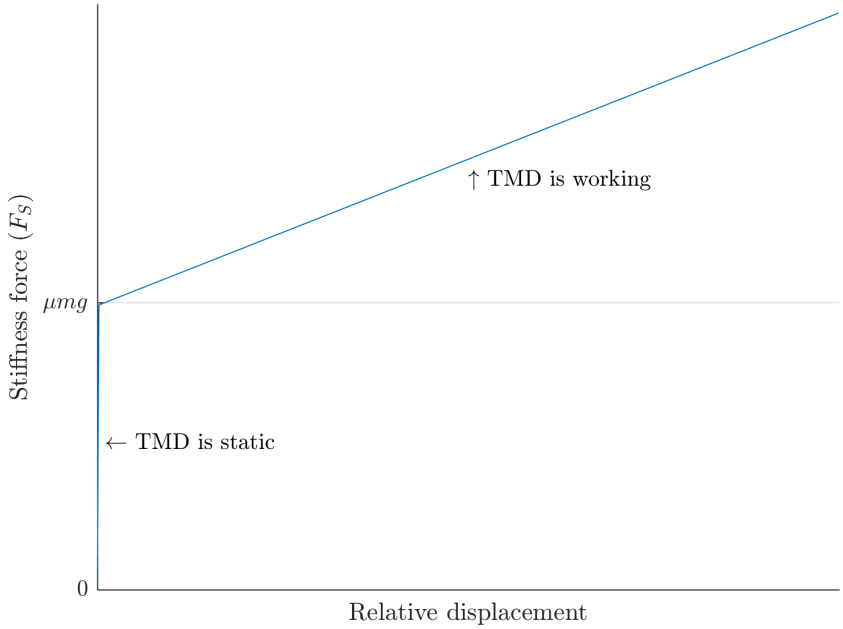

Figure 3.7.: Stiffness force of the TMD spring in function of the relative displacement between structure and TMD

→ A yield limit equal to the maximum value of frictional force $f_y = \mu mg$.

Another way of understanding the concept behind this analogy is picturing the superposition of a purely elastic behavior and a friction force response, as in the case of figure 3.8.

In the next section, the Newmark method described in algorithm 2.3 is adapted to work with non-linear systems, so that the friction-stiffness model just described can be used.

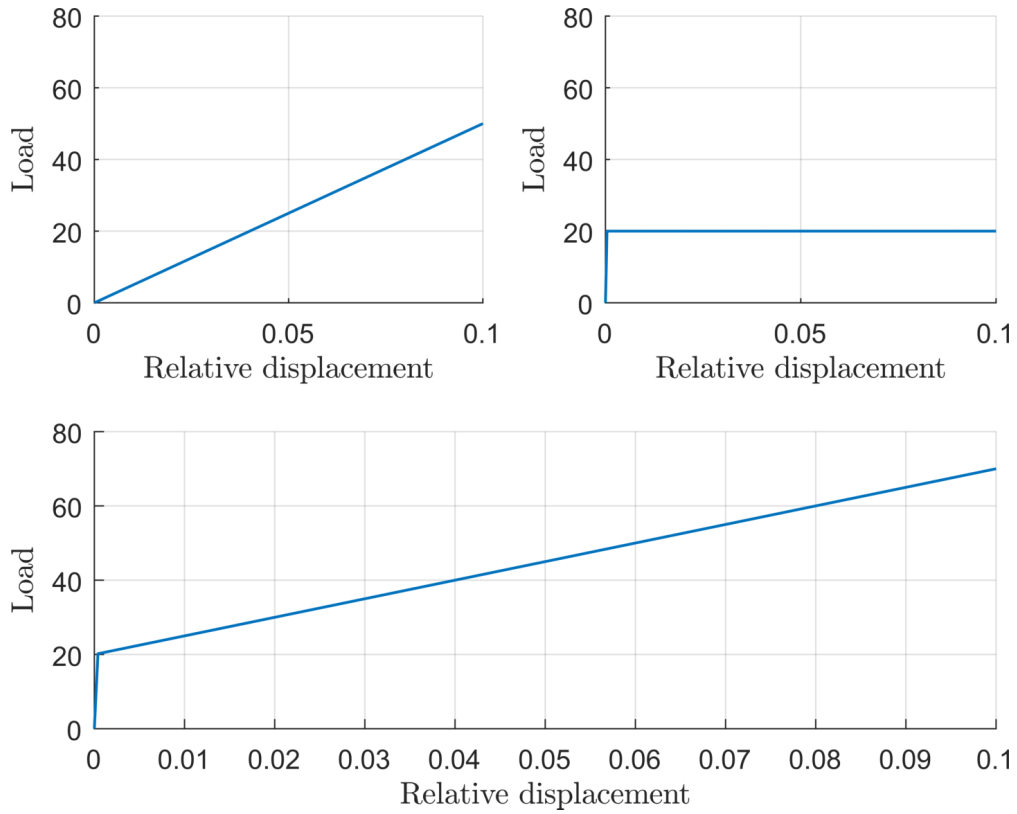

Figure 3.8.: Superposition (bottom) of the force applied to an elastic spring (top-left) and a mass with friction (top-right)

3.4. Non-linear Newmark method

If the equations of the linear Newmark method 2.33 and 2.34 are expressed in terms of increments, they can be written as:

$$\Delta \dot{d}_i = h\ddot{d}_i + \gamma h \Delta \ddot{d}_i \tag{3.4}$$

$$\Delta \ddot{d}_i = \Delta d_i - h\dot{d}_i - \frac{1}{2}h^2\ddot{d}_i - \beta h^2 \tag{3.5}$$

And the increment-based equation of motion with non-linear stiffness is:

$$\mathbf{M}\Delta \ddot{d}_i + \mathbf{C}\Delta \dot{d}_i + \Delta F_{S,i} = \Delta P_i \tag{3.6}$$

The incremental stiffness force can be rewritten as (Chopra (2001)):

$$\Delta F_{S,i} = \mathbf{K}_{sec,i}\Delta d_i$$

Where $\mathbf{K}_{sec,i}$ is the secant stiffness matrix for that increment. Over a small time step, the secant can be approximated to the tangent matrix:

$$\Delta F_{S,i} \approx \mathbf{K}_{t,i}\Delta d_i \tag{3.7}$$

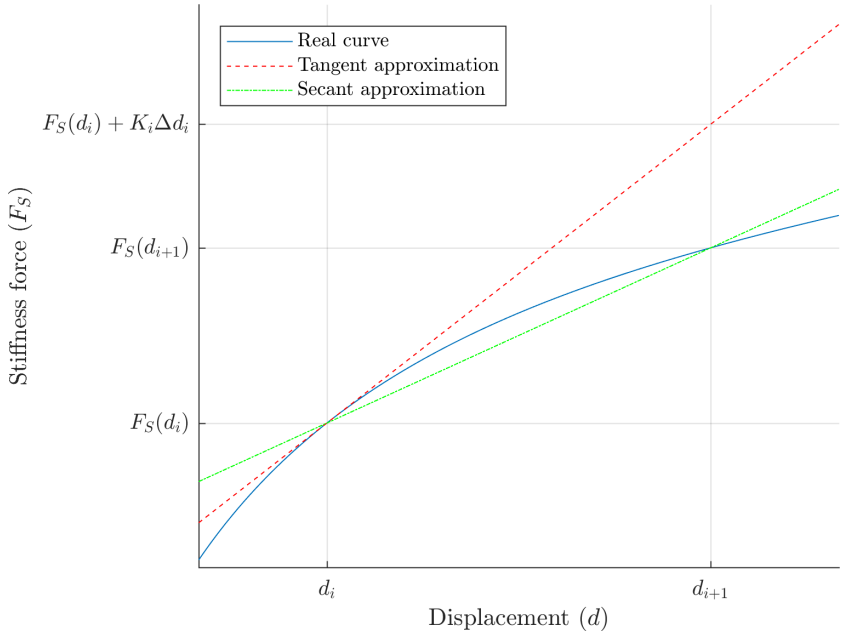

Figure 3.9.: Displacement versus stiffness force, the slope of the plot corresponds to the stiffness

See figure 3.9 for a visualization of the tangent and the secant stiffness. The nomenclature of the tangent matrix $\mathbf{K}_{t,i}$ will be simplified to $\mathbf{K}_i$ for convenience.

Adding equations 3.4, 3.5 and 3.7 to 3.6 and solving for Δd_i results in:

$$\left\{\mathbf{K}_i + \frac{\gamma}{h\beta}\mathbf{C} + \frac{1}{h^2\beta}\mathbf{M}\right\}\Delta d_i = \Delta P_i + \left\{\frac{\gamma}{\beta}\mathbf{C} + \frac{1}{h\beta}\mathbf{M}\right\}\dot{d}_i + \left\{h\left(\frac{\gamma}{2\beta} - 1\right)\mathbf{C} + \frac{1}{2\beta}\mathbf{M}\right\}\ddot{d}_i \tag{3.8}$$

$$\hat{\mathbf{K}}_i \Delta d_i = \Delta \hat{P}_i \tag{3.9}$$

Where:

$$\hat{\mathbf{K}}_i = \left\{\mathbf{K}_i + \frac{\gamma}{h\beta}\mathbf{C} + \frac{1}{h^2\beta}\mathbf{M}\right\}$$

$$\Delta \hat{P}_i = \Delta P_i + \left\{\frac{\gamma}{\beta}\mathbf{C} + \frac{1}{h\beta}\mathbf{M}\right\}\dot{d}_i + \left\{h\left(\frac{\gamma}{2\beta} - 1\right)\mathbf{C} + \frac{1}{2\beta}\mathbf{M}\right\}\ddot{d}_i$$

After Δd_i is known, the rest of increments can be computed:

$$\Delta \dot{d}_i = \frac{\gamma}{h\beta}\Delta d_i - \frac{\gamma}{\beta}\dot{d}_i + h\left(1 - \frac{\gamma}{2\beta}\right)\ddot{d}_i$$

$$\Delta \ddot{d}_i = \frac{1}{h^2\beta}\Delta d_i - \frac{1}{h\beta}\dot{d}_i - \frac{1}{2\beta}\ddot{d}_i$$

Moreover, additional iterations within each time step might be necessary in order to mini-

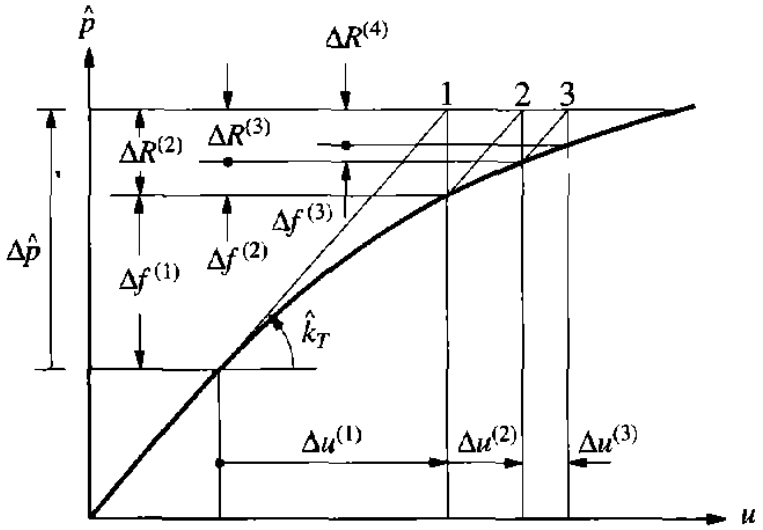

Figure 3.10.: Displacement versus $\Delta\hat{P}$ plot that shows the modified Newton-Raphson iteration process. Retrieved from Chopra (2001)

Algorithm 3.1 Modified Newton-Raphson algorithm

1. Obtain the following data from the current time step: $d_{i+1}^{(0)} = d_i,\ F_S^{(0)} = F_{S,i},\ \Delta R^{(1)} = \Delta\hat{P}_i,\ \hat{\mathbf{K}}_i$
2. For each iteration $j = 1,\ 2,\ 3,\ ...$
   a) Solve $\hat{\mathbf{K}}_i \Delta d^{(j)} = \Delta R^{(j)}$.
   b) Compute the force variation $\Delta F^{(j)} = F_S^{(j)} - F_S^{(j-1)} + (\hat{\mathbf{K}}_i - \mathbf{K}_i)\Delta d^{(j)}$.
   c) Compute the residual force $\Delta R^{(j+1)} = \Delta R^{(j)} - \Delta F^{(j)}$.
   d) Stop the iteration if the displacements reach the set tolerance: $\left\|\Delta d^{(j+1)}\right\| < \epsilon \left\|d_i\right\|$

mize the error introduced when the tangent stiffness matrix is used. This will be solved with the use of the modified Newton-Raphson iteration.

Modified Newton-Raphson

The non-linear relation between d and $\Delta\hat{P}$ can be seen in figure 3.10.

The modified Newton-Raphson method uses a tangent stiffness matrix that is computed at the beginning of each time step and iterates until ΔR or Δd reach a set tolerance. See algorithm 3.1 for a complete review of this process.

Finally, the method's constants that will be used throughout the thesis will be:

$$\gamma = 1/2,\ \beta = 1/4$$

Which guarantee unconditional stability and no added numeric damping.

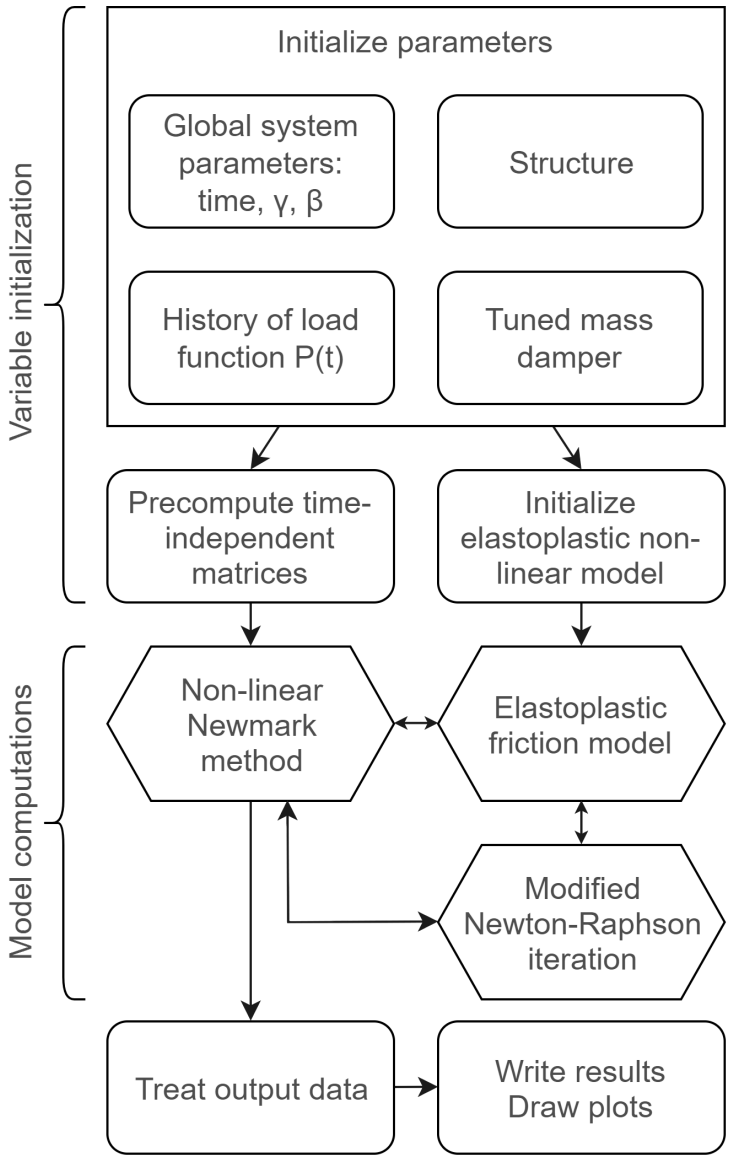

Figure 3.11.: Diagram of the MATLAB code used in the thesis

3.5. MATLAB code

A diagram with an overview of the written MATLAB code, which integrates everything that has been discussed in this chapter, can be seen in figure 3.11.

In order to check the reliability of the code, two textbook examples have been reproduced and compared to the theoretical results.

3.5.1. Verification 1: MDOF system

The first test case is taken from Chopra (2001), example 15.1. It is a linear 5-DOF system with no damping subjected to a static force for 2 seconds. The data of the book is transformed into SI units without any conversion for simplification's sake.

$$\mathbf{M} = \begin{bmatrix} m_0 & 0 & 0 & 0 & 0 \\ 0 & m_0 & 0 & 0 & 0 \\ 0 & 0 & m_0 & 0 & 0 \\ 0 & 0 & 0 & m_0 & 0 \\ 0 & 0 & 0 & 0 & \frac{m_0}{2} \end{bmatrix}, \; m_0 = 208.6\,\text{Kg}$$

$$\mathbf{K} = \begin{bmatrix} 596.0 & -376.6 & 151.1 & -37.8 & 6.3 \\ & 463.7 & -339.0 & 132.2 & -22.0 \\ & & 445.0 & -301.1 & 81.8 \\ & sym & & 312.6 & -115.4 \\ & & & & 50.9 \end{bmatrix} \text{kN/m}$$

$$P_i = \begin{bmatrix} 0 \\ 0 \\ 0 \\ 0 \\ 1000 \end{bmatrix} \text{N}$$

The effectiveness of the model will be evaluated with the relative error of the displacements:

$$e_{rel} = \frac{d_{model} - d_{book}}{d_{book}}$$

Since in the book the displacements are also computed with a numeric method, some errors are expected. The results of the analysis can be seen in figure 3.12.

3.5.2. Verification 2: SDOF elastoplastic system

The second case is taken from Paz (2012), example 7.1. It is a non-linear SDOF system where the stiffness behaves like that of a perfect elastoplastic. The data of the book is transformed into SI units without any conversion, for simplification's sake.

$$M = 0.2\,\text{Kg},\; \xi = 0.087,\; C = 0.2735\,\text{Kg/s}$$

$$K_e = 12.35\,\text{N/m},\; K_p = 0,\; f_y = 15\,\text{N}$$

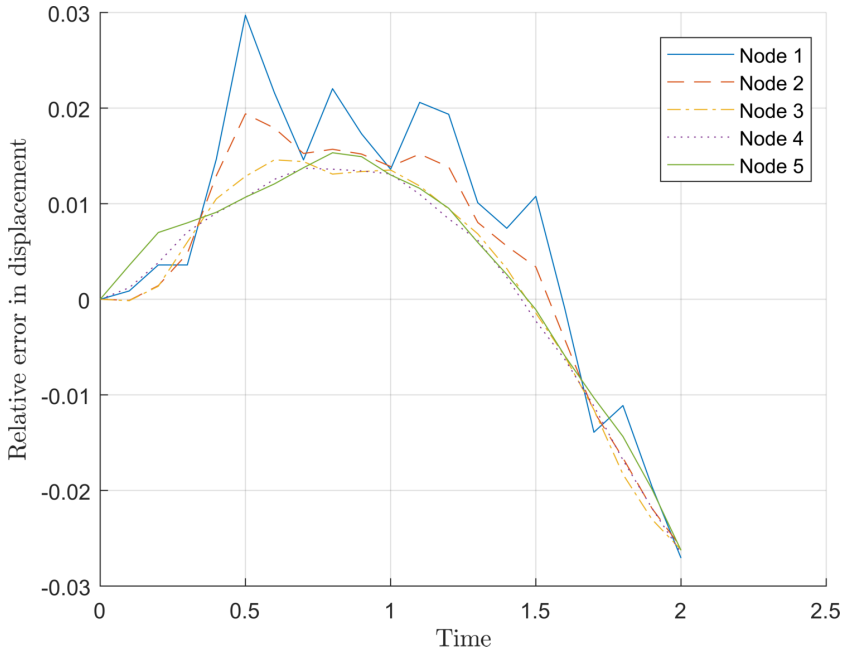

Figure 3.12.: Relative error over time of the MDOF system test case

The applied force is a non-linear load with the following discrete values:

$$P(0) = 0\,\mathrm{N},\ P(0.45\,\mathrm{s}) = 20\,\mathrm{N},\ P(1.1\,\mathrm{s}) = 0\,\mathrm{N}$$
$$P(1.2\,\mathrm{s}) = -10\,\mathrm{N},\ P(1.4\,\mathrm{s}) = 0\,\mathrm{N}$$

The comparison between displacements after running the model can be seen in figure 3.13.

3.5.3. Performance of the code

In order to speed up the execution of the code, some optimizations of the code were sought. These included preallocating as many variables as possible and eliminating most of the debugging checks that the scripts had, cutting back processing times around 54%. MATLAB's built-in tool for optimization "MATLAB Profiler" was used to this effect.

The final average time for the non-linear Newmark function (t_{nln}) is:

$$t_{nln} = \frac{n_{ts}}{2840}\,\mathrm{s}$$

Where n_{ts} is the number of time steps that are requested. In figure 3.14,a graph comparing the performance of the code before and after the optimizations can be seen.

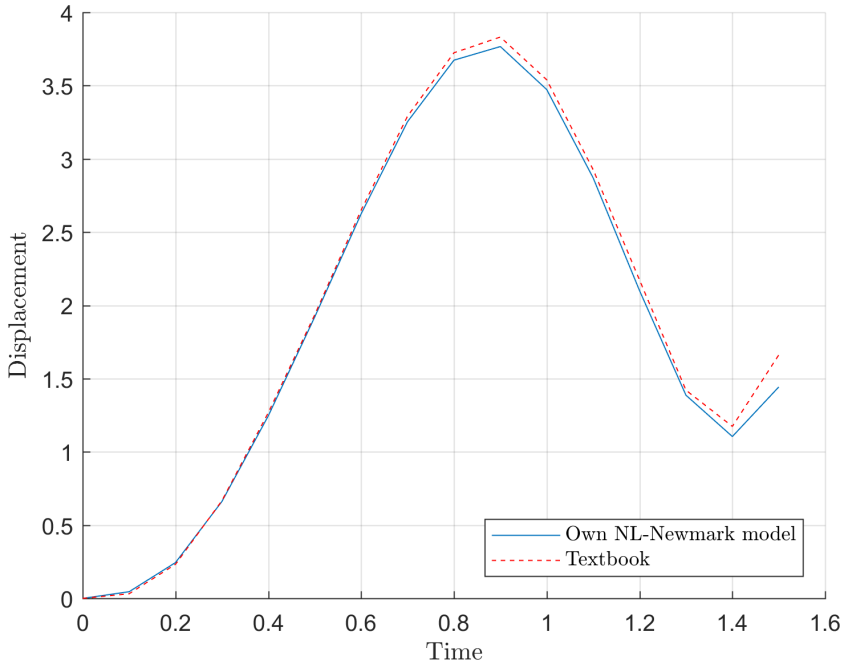

Figure 3.13.: Displacements over time of the SDOF system test case

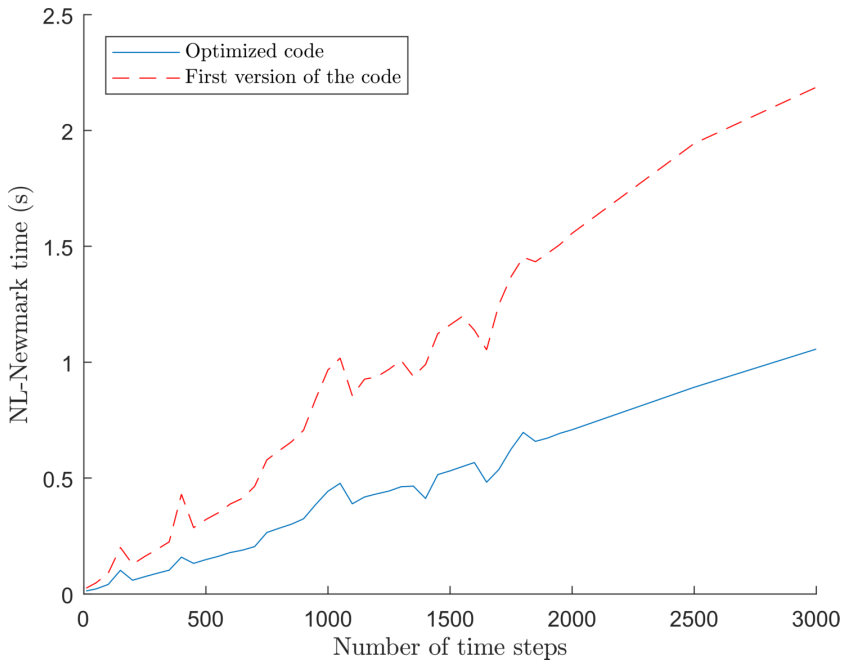

Figure 3.14.: Time spent on every call to the non-linear Newmark function, pre and post-optimization

4. Derivation of TMD optimization equations

As stated on subsection 3.3.2, the observed stiffness of a tuned mass damper under the effects of friction is not constant. Since Den Hartog's derivation of the optimization equations is based on a constant stiffness value, some way of obtaining better suited parameters can possibly be found.

First, two new parameters will be introduced. On the one hand, the design parameter d_{max} is defined as the TMD's maximum working displacement. Tuned mass dampers absorb a part of the energy of the main structure and transform it into displacements: d_{max} is the highest displacement in service conditions that the TMD is allowed to have in both directions.

On the other hand, μ is the friction coefficient between the TMD and the system. Friction depends on the used material but might be adjusted with lube oil or other methods.

Mixing these new parameters with the frictional behavior seen in figure 3.7, the theoretical plot of figure 4.1 can be drawn. Two different stiffness values can be set apart. The effective stiffness K_{eff} is the stiffness that the model uses, and it depends on the present relative displacement. The frictionless stiffness of the TMD K_d is a constant value, and it is equal to the effective stiffness when friction is neglected.

If the elastic portion of the displacement is not taken into account ($K_{elastic} \to \infty$), the effective stiffness can be represented as:

$$\begin{aligned} K_{eff} &= \frac{F_S(d_{max})}{d_{max}} \\ K_{eff} &= \frac{K_d d_{max} + \mu m_d g}{d_{max}} \\ K_{eff} &= K_d + \frac{\mu m_d g}{d_{max}} \end{aligned} \tag{4.1}$$

Or, inversely:

$$K_d = K_{eff} - \frac{\mu m_d g}{d_{max}} \tag{4.2}$$

Then, the effective stiffness represented in terms of the device's parameters is equal to:

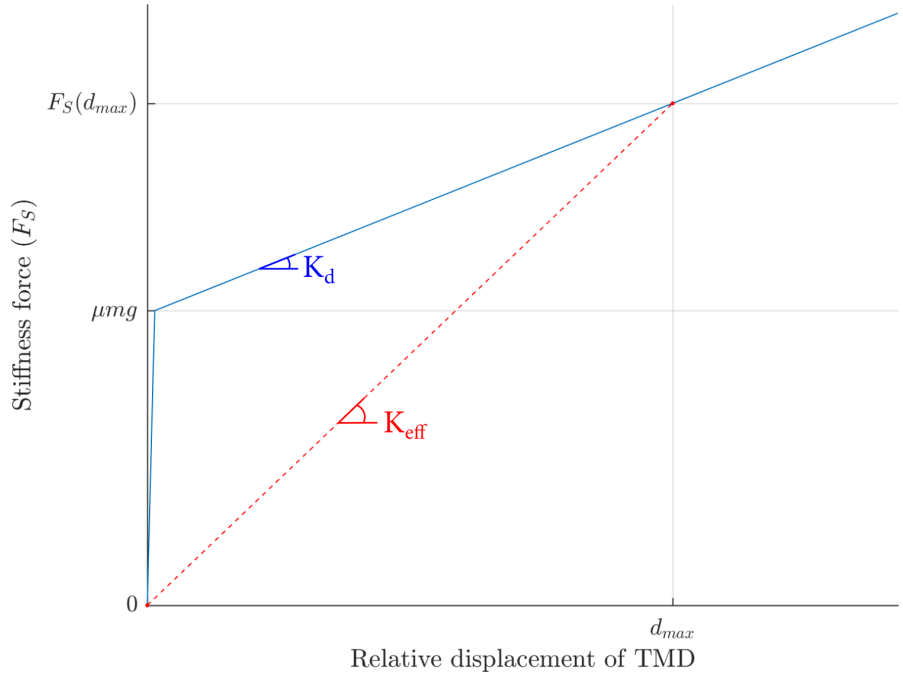

Figure 4.1.: Relative displacement versus stiffness force of TMD

$$\omega_{eff} = \omega_d \sqrt{1 + \frac{\mu m_d g}{K_d d_{max}}}$$
$$\omega_{eff} = \sqrt{\omega_d^2 + \frac{\mu g}{d_{max}}} \tag{4.3}$$

And:

$$\omega_d = \sqrt{\omega_{eff} - \frac{\mu g}{d_{max}}} \tag{4.4}$$

Den Hartog's tuning can only be applied when stiffness is constant. If the effective stiffness is put into the original equation (2.39), then:

$$\omega_{eff} = \omega_{sys} \frac{1}{1+\bar{m}}$$
$$\sqrt{\frac{K_{eff}}{m_d}} = \sqrt{\frac{K_s}{m_s}} \frac{1}{1+\bar{m}}$$
$$K_{eff} = K_s \frac{\bar{m}}{(1+\bar{m})^2}$$

And then, expressed in terms of the frictionless stiffness:

$$K_d = K_s \frac{\bar{m}}{(1+\bar{m})^2} - \frac{\mu m_d g}{d_{max}} \tag{4.5}$$

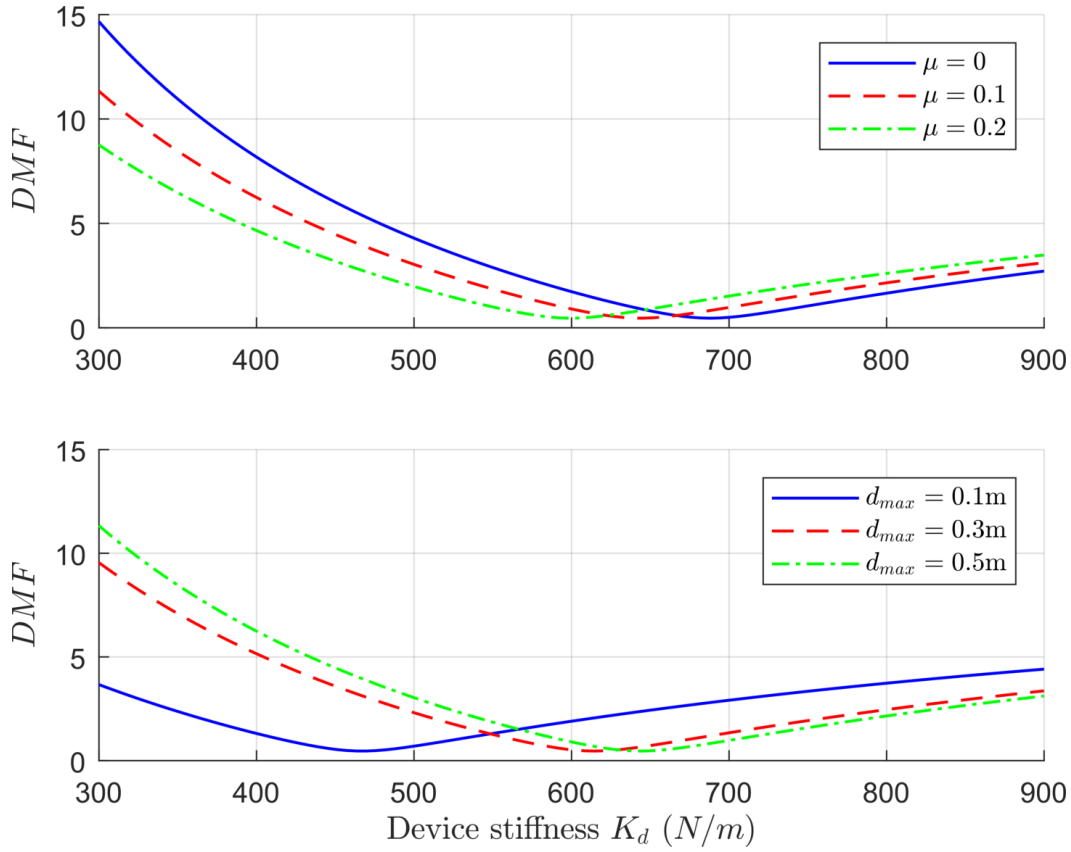

Figure 4.2.: Response of the system when changing the values for μ (top) and d_{max} (bottom) while fixing the other parameters, according to Den Hartog's equation

Note that the stiffness of the device has to be positive, so there is a minimum on the possible values of the parameter d_{max}:

$$K_s \frac{\bar{m}}{(1+\bar{m})^2} - \frac{\mu m_d g}{d_{max}} > 0$$
$$d_{max} > d_{min} = \frac{\mu m_d g}{K_s} \frac{(1+\bar{m})^2}{\bar{m}} = \frac{\mu g}{\omega_s^2} (1+\bar{m})^2 \tag{4.6}$$

Additionally, it is heavily advised for d_{max} to be chosen significantly higher than this limit. During the parametric study, further recommendations on the values of parameter d_{max} will be given.

Using the effective stiffness in Den Hartog's equation for the amplitude of the displacements (equation 2.37) leads to some results that can illustrate the impact of the new design variables d_{max} and μ: see figure 4.2.

Finally, another interesting concept to define is the residual displacement d_{res}. This is the displacement for which the spring force matches the friction force, and consequently the TMD stops moving. Developing in equation form:

$$K_d d_{res} = \mu m_d g$$
$$d_{res} = \frac{\mu m_d g}{K_d}$$

The implication of this is that d_{res} is the maximum possible displacement after the external forces stop and the system reaches equilibrium.
Note that the design value d_{max} should be larger than d_{res} for the TMD to have any noticeable effect.

Updated design procedure

In subsection 2.3.1 the design procedure using Den Hartog's equations was described. With the introduction of the effective frequency and stiffness, this procedure can be updated to the following steps:

1. Identify the system's structural properties: natural frequency and its associated mass and damping, as well as the friction coefficient between TMD and system.
2. Decide on a starting value for the mass coefficient $\bar{m}$ and for the maximum design displacement of the TMD d_{max}.
3. Calculate the optimal stiffness with the new equation 4.5, and the damping ratio with the classic equation 2.38.
4. Compute the maximum displacements for the tentative design. If they are too large, go back to step 2 and choose new design values.
5. Design the mechanical system and the tuning system of the TMD.
6. Perform physical verification tests.

5. Parametric study

Now that the specifics of the non-linear numeric model have been laid out and a new design equation has been derived, the parametric study that intends to investigate the impact of friction on the performance of tuned mass dampers can begin.

In the first place, the various parameters and the overall conditions of the experiments will be established, along with an explanation of how the performance will be evaluated. Then, each set of experiments will be detailed, reproduced, and then a few observations will be extracted.

5.1. Experiment design

The parametric study will be (except where noted otherwise) carried out with fixed properties for the main structure. Great focus will be placed onto the design variables and the amplitude of the exciting force. An overview of all the variables that control the system can be examined in table 5.1.

Table 5.1.: Summary of variables used throughout the parametric study

Global	Structure (main)	TMD	TMD design	Applied force
Time t	Mass m_s	Mass m_d	Mass ratio $\bar{m}$	Amplitude P_0
Time step h	Stiffness K_s	Stiffness K_d	Effective stiffness K_{eff}	Frequency ω_p
Newmark's β, γ	Damping ratio ξ_s	Damping ratio ξ_d	Max displacement d_{max}	
		Friction coefficient μ	Residual displacement d_{res}	

In each test, the structure is subjected to harmonic excitation by means of the sinusoidal force $P(t)$:

$$P(t) = P_0 \sin(\omega_s t)$$

This force is applied for 11 seconds, and then the system is allowed to vibrate freely for 11 seconds more.

The performance of a particular experiment is given by the already defined dynamic magnification factor (DMF). Applied to the model of the thesis, the DMF of the main structure can be expressed as:

$$DMF = \frac{\max\{|d_s|\}}{P_0/K_s}$$

Lower values represent better-performing systems.

Another interesting indicator is the DMF of the tuned mass damper. It will be used in some instances to have an idea of how much energy the TMD is taking away from the main structure.

$$DMF_{tmd} = \frac{\max\{|d_t - d_s|\}}{P_0/K_d}$$

The parametric study will have a *factorial design*, that is, two or three parameters will be defined with multiple discrete values, and the results will reflect every possible combination of these values.

The graphic method to present the results will be the 2-D plot:

→ The performance indicator of the sytem (the DMF) will be plotted in the y-axis.

→ The first tested parameter will be plotted in the x-axis.

→ The second tested parameter will be plotted by means of colored lines, each corresponding to a disctinct discrete value.

→ The optional third parameter will be conveyed by presenting a plot for each distinct discrete value.

5.2. Effects of friction and non-optimal tuning parameters

The first set of tests that will be performed have the objective of finding out what is the impact of friction on a system where the TMD parameters have been obtained with the classic Den Hartog procedure. The displacements on these tests are expected to be greater than those obtained with a TMD optimized with the new, updated procedure.

Therefore, according to Den Hartog's equations (2.38 and 2.39), the optimal parameters are:

$$\xi_d = 0.1600$$
$$K_d = 580.8\,\mathrm{N/m}$$

Friction coefficient and force amplitude

The goal of the first batch of tests is to have an overview of the interaction between friction and force amplitude, using the classic Den Hartog optimization.

The values for the damping ratio and stiffness of the TMD are, therefore:

$$\xi_d = 0.1600$$
$$K_d = 580.8\,\mathrm{N/m}$$

An array of values of P_0 ranging between 30 N and 1000 N are plotted on the x-axis. Five different friction coefficients (including a frictionless case) are represented with differing line colors.

This results in a total of 65 different cases with their associated DMF values.

The representation can be seen in figure 5.1.

The plot at the top corresponds to the DMF of the main structure

Some observations:

→ In the cases where friction is present (real world scenario), the performance of the TMD increases when the applied force is higher.

→ The TMD is not *activated* (the force of friction is not surpassed) for some combinations of high friction coefficient and low force amplitude. In these cases, the tuned mass damper acts like an extra mass attached to the system.

→ The performance of the frictionless device is superior to the ones with friction, but the benefit decreases as the magnitude of the applied force is increased. For some of the lower friction coefficient values, the achieved performance is almost identical to that of the frictionless case.

→ The DMF of the TMD when friction is present is much lower (about half) than that of the frictionless case.

Friction coefficient and TMD stiffness

The goal of this set of tests is to have a better idea on the role of TMD stiffness in the tuning process.

The amplitude of the applied force is fixed to $P_0 = 200$ N. Different values of TMD stiffness ranging from $300\,\mathrm{N/m}$ to $1000\,\mathrm{N/m}$ are plotted on the x-axis. Five values of friction coefficient (including a frictionless case) are represented with differing lines colors.

The results are plotted in figure 5.2.

In this case, the following observations can be made:

→ A low stiffness value is very detrimental to the performance of the frictionless case, but it's slightly beneficial for the lower friction coefficient values.

→ The frictionless case performs better than every other case with friction.

→ TMD DMF increases with higher values of stiffness, in the non-null friction cases.

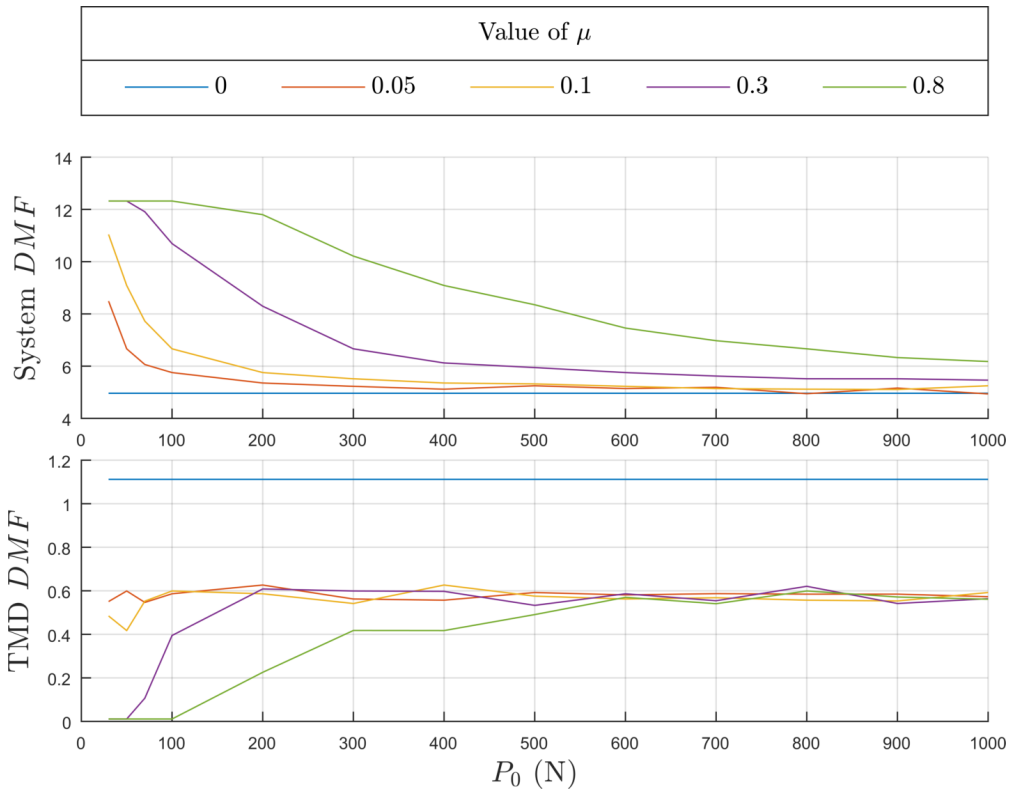

Figure 5.1.: DMF of the system and TMD for different μ and P_0 values

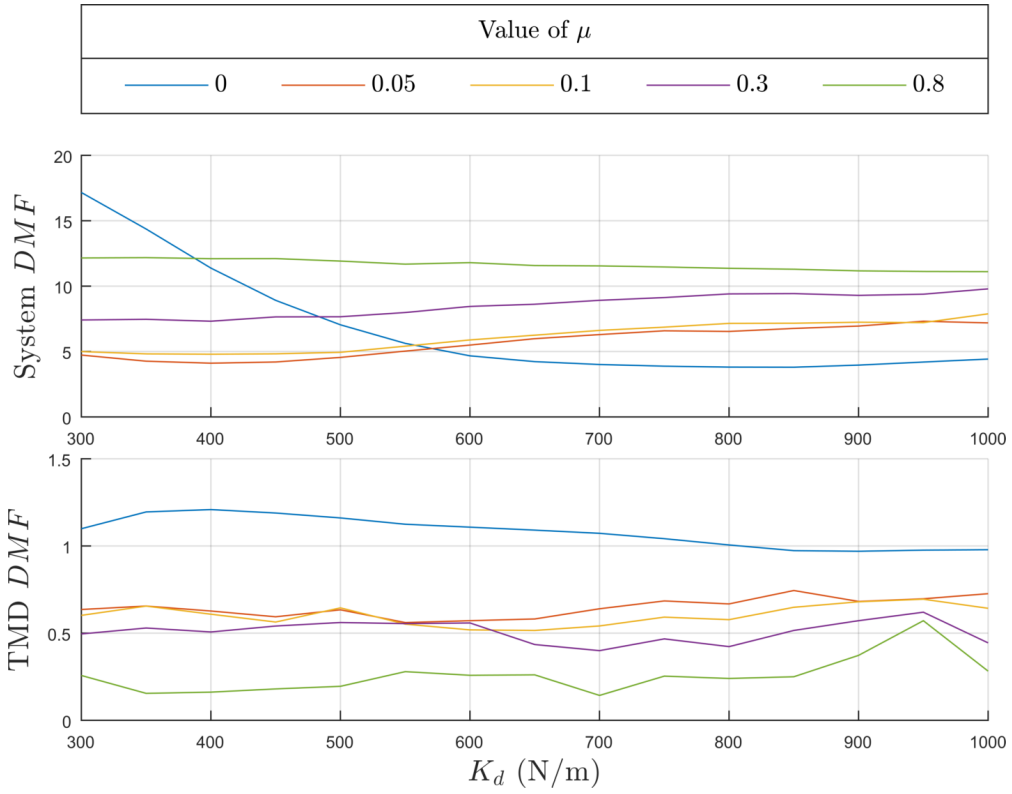

Figure 5.2.: System response to different friction coefficients and TMD stiffness, with $P_0 = 200\,\mathrm{N}$

This set of tests is then reproduced with a higher force amplitude of $P_0 = 1000\,\mathrm{N}$, while keeping every other characteristic exactly the same.

Results are in figure 5.3.

For the first time, a TMD with friction performs better than a frictionless one. The optimal stiffness for these cases is around the 400-450$\mathrm{N/m}$ range.

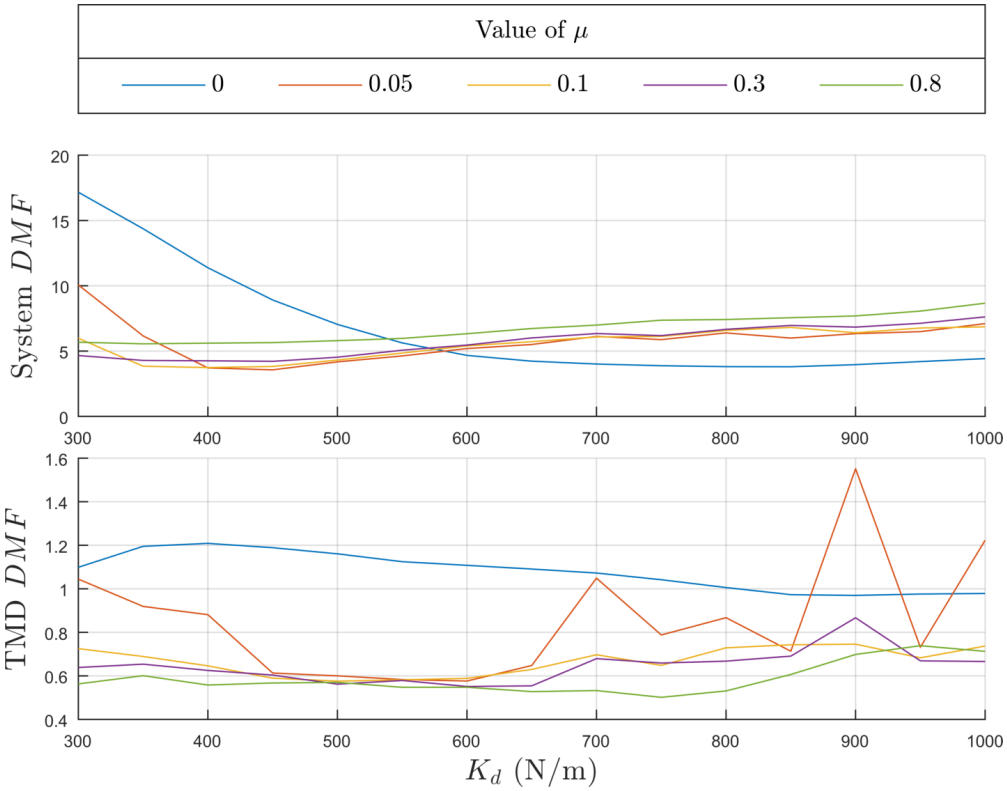

Figure 5.3.: System response to different friction coefficients and TMD stiffness, with $P_0 = 1000\,\mathrm{N}$

5.3. Performance of new tuning procedure versus the classic Den Hartog's equations

The next step is verifying whether the new tuning equations (4.5 and 4.6) achieve a better performance with respect to the Den Hartog equations or not.

Force amplitude and friction coefficient

Two sets of tests are prepared: the first set of tests will have a constant TMD stiffness, obtained with Den Hartog's procedure:

$$K_d = 580.8\,\mathrm{N/m}$$

The second set of tests will have a varying TMD stiffness that will be determined with equation 4.5:

$$K_d = K_s \frac{\bar{m}}{(1+\bar{m})^2} - \frac{\mu m_d g}{d_{max}}$$

The value of d_{max} is fixed at $0.5\,\mathrm{m}$.

For both sets, a range of force amplitudes between $30\,\mathrm{N}$ and $1000\,\mathrm{N}$ is plotted on the x-axis. Four different values of the friction coefficient are represented with varying line colors.

The results can be seen in figure 5.4. The following observations can be made:

→ The performance of the new equations is superior for every friction coefficient value:
  - For $\mu = 0.1$ the average reduction of the DMF is 7.1%.
  - For $\mu = 0.3$ the average reduction of the DMF is 11.4%.
  - For $\mu = 0.5$ the average reduction of the DMF is 8.7%.
  - For $\mu = 0.7$ the average reduction of the DMF is 4.9%.

→ The increase of performance is usually superior when higher force amplitudes are applied. Focusing now only on the tests where the force amplitude is between $500\,\mathrm{N}$ and $1000\,\mathrm{N}$:
  - For $\mu = 0.1$ the average reduction of the DMF is 9.6%.
  - For $\mu = 0.3$ the average reduction of the DMF is 20.3%.
  - For $\mu = 0.5$ the average reduction of the DMF is 15.0%.
  - For $\mu = 0.7$ the average reduction of the DMF is 7.4%.

→ The best performance for this test set is achieved when the coefficient of friction is $\mu = 0.3$ and the forces are $P_0 > 650\,\mathrm{N}$: the DMF gets as low as 4.26. This is the first clear indication that friction in tuned mass dampers can be beneficial in some cases.

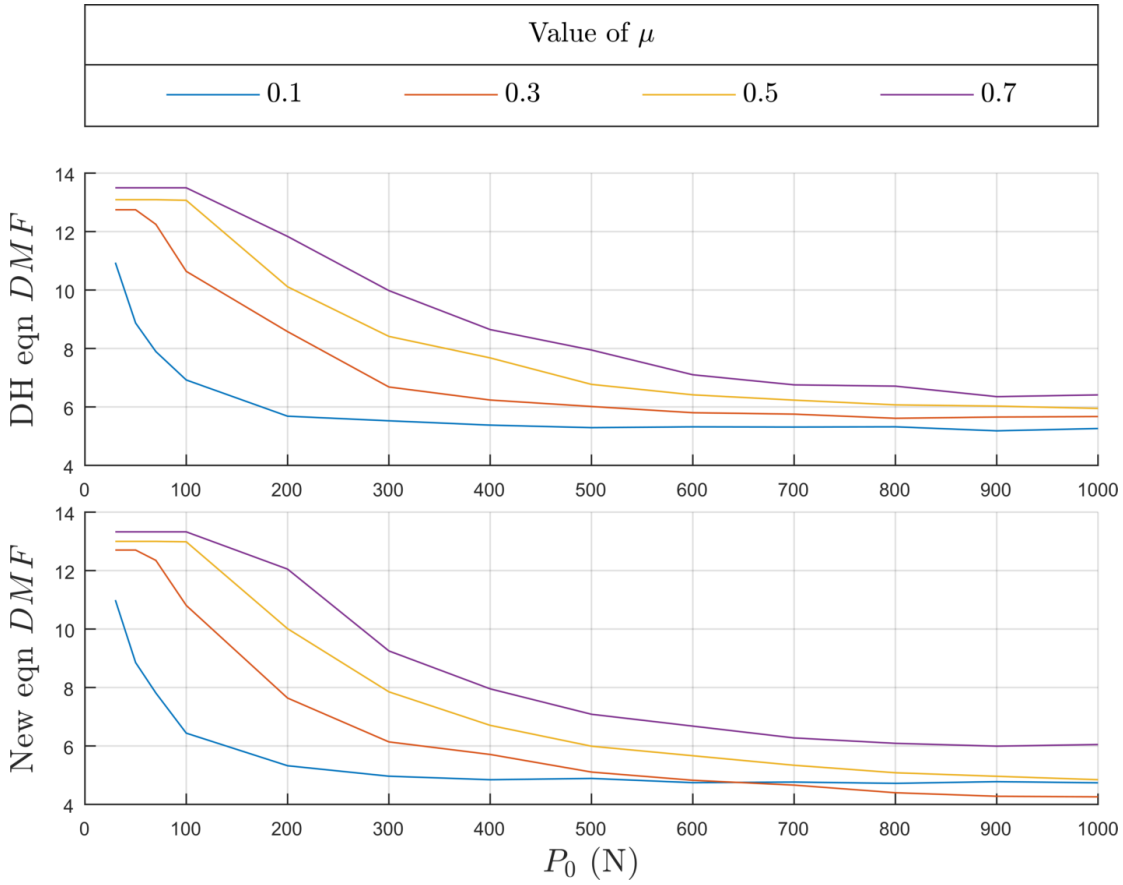

Figure 5.4.: DMF when Den Hartog's optimization is applied (top) versus the new optimization presented in this thesis (bottom)

5.4. Impact of the design parameters

It has now been established that the new optimization method delivers better performance in almost every tested case. From now on, the stiffness of the TMD in every test will be tuned according to the new method.

The objective of the following tests is having an overview of the impact that the design parameters have on the performance of the system.

Maximum TMD displacement and mass ratio

In this set of tests the force amplitude is fixed at $P_0 = 800\,\text{N}$.

Different values of d_{max} within the range 0.2-$1\,\text{m}$ are plotted in the x-axis. Three values of the mass ratio $\bar{m}$ are represented with different line colors:

→ Mass ratio $\bar{m} = 0.03$, for which the mass of the TMD is $m_d = 7.68\,\text{Kg}$.

→ Mass ratio $\bar{m} = 0.07$, for which the mass of the TMD is $m_d = 17.92\,\text{Kg}$.

→ Mass ratio $\bar{m} = 0.10$, for which the mass of the TMD is $m_d = 25.60\,\text{Kg}$.

Finally, three friction coefficient values (frictionless $\mu = 0$, low $\mu = 0.2$, medium $\mu = 0.5$ and high $\mu = 0.8$) are conveyed in three different plots. A total of 90 tests are carried out due to the combinations of values.

Note that the parameter d_{max} has to verify the lower bound of equation 4.6 ($d_{max} > d_{min}$) at all times in order to avoid negative stiffness: this is why in some of the plots several of the lower d_{max} values are not present.

The results can be seen in figure 5.5.

The following remarks are made:

→ As expected, increasing the mass of the TMD allows lower DMF values.

→ The importance of properly tuning the d_{max} parameter is higher for lower $\bar{m}$ values.

→ The optimum value of d_{max} is close to the lower bound of the parameter.

→ The value of $\bar{m}$ does not seem to have a great effect on where the optimum of d_{max} is located.

→ Conversely, the value of μ does have a great effect on where the optimum of d_{max} is located.

Maximum TMD displacement and friction coefficient

In this set of experiments, the mass of the TMD is fixed at $m_d = 22.5\,\text{Kg}$.

Different values for the maximum displacement of the TMD in the range of 0.1-$1\,\text{m}$ are plotted on the x-axis. Four values of the friction coefficient are represented by means of colored lines, with a the frictionless case as the baseline.

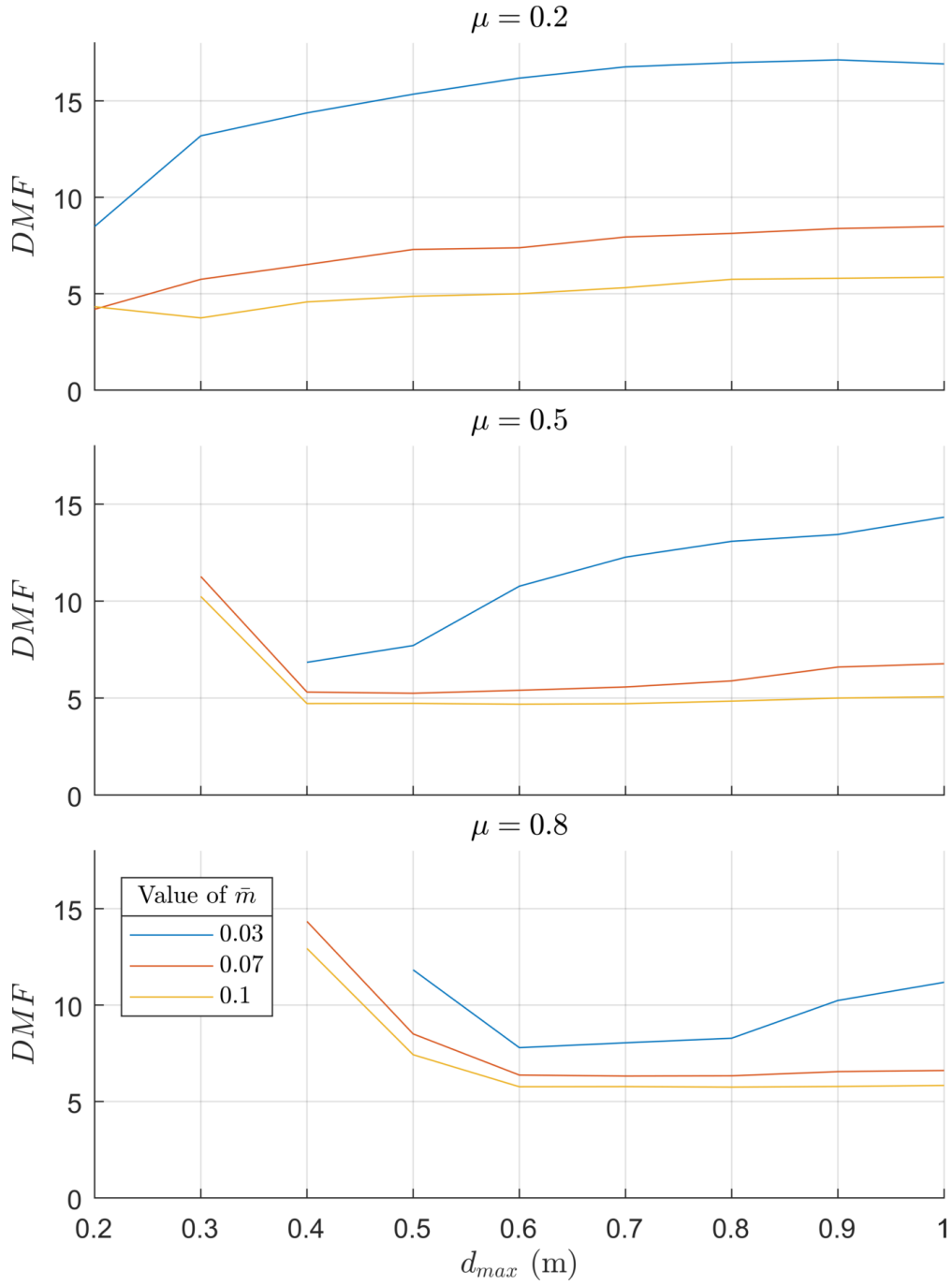

Figure 5.5.: Response of a system to different friction μ values and design parameters d_{max} and $\bar{m}$

Finally, three values of applied force amplitude ($P_0 = 500, 1000$ and 1500 N) are represented in three different plots, which represents a total of 120 experiments.

The results are available in figure 5.6. Some observations:

→ For higher amplitudes of force, low friction has a worse performance than medium and high friction. In particular, for $P_0 = 1500$ N a friction coefficient of $\mu = 0.5$ performs 26% better than $\mu = 0.2$.

→ The performance of low friction isn't impacted much by the increase of applied force. Only about 3% from $P_0 = 500$ N to $P_0 = 1500$ N.

Force amplitude and maximum TMD displacement

In this set of experiments, several values of the force amplitude in the range of 100-1500 N are plotted in the x-axis. Three different values of the maximum TMD displacement are represented by means of different colored lines.

Three different friction values are also divided into three plots, for a total of 135 parametric combinations. The results can be seen in figure 5.7. Some observations:

→ Medium friction and $d_{max} = 0.3$ m results in poor performance, very possibly due to its proximity to the $d_{min} = 0.190$ m lower bound. In the high friction case, $d_{min} = 0.304$ m and therefore it has not been plotted.

→ Friction clearly becomes beneficial on the higher tested values of P_0.

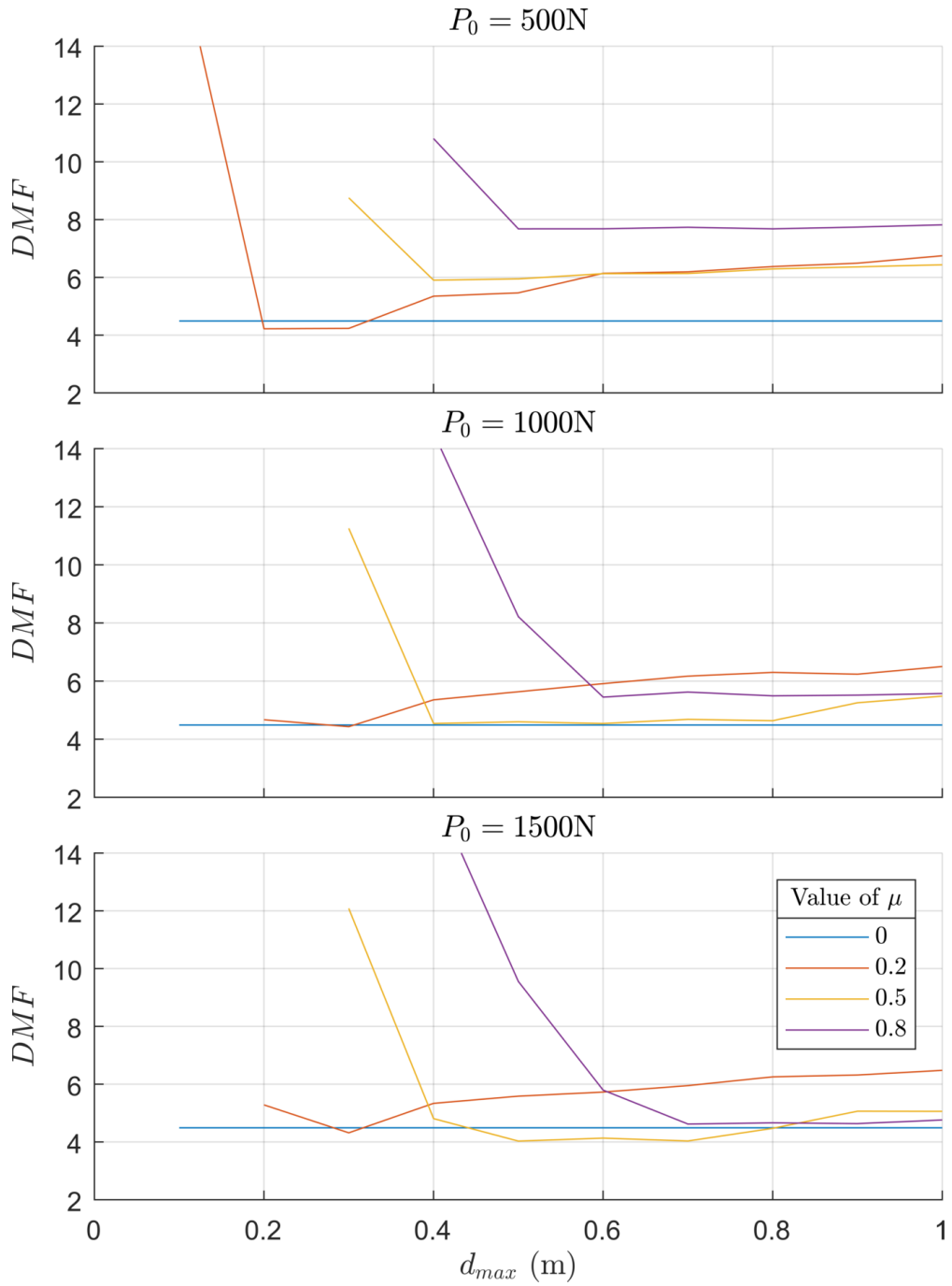

Figure 5.6.: Response of the system versus different P_0, d_{max} and μ values

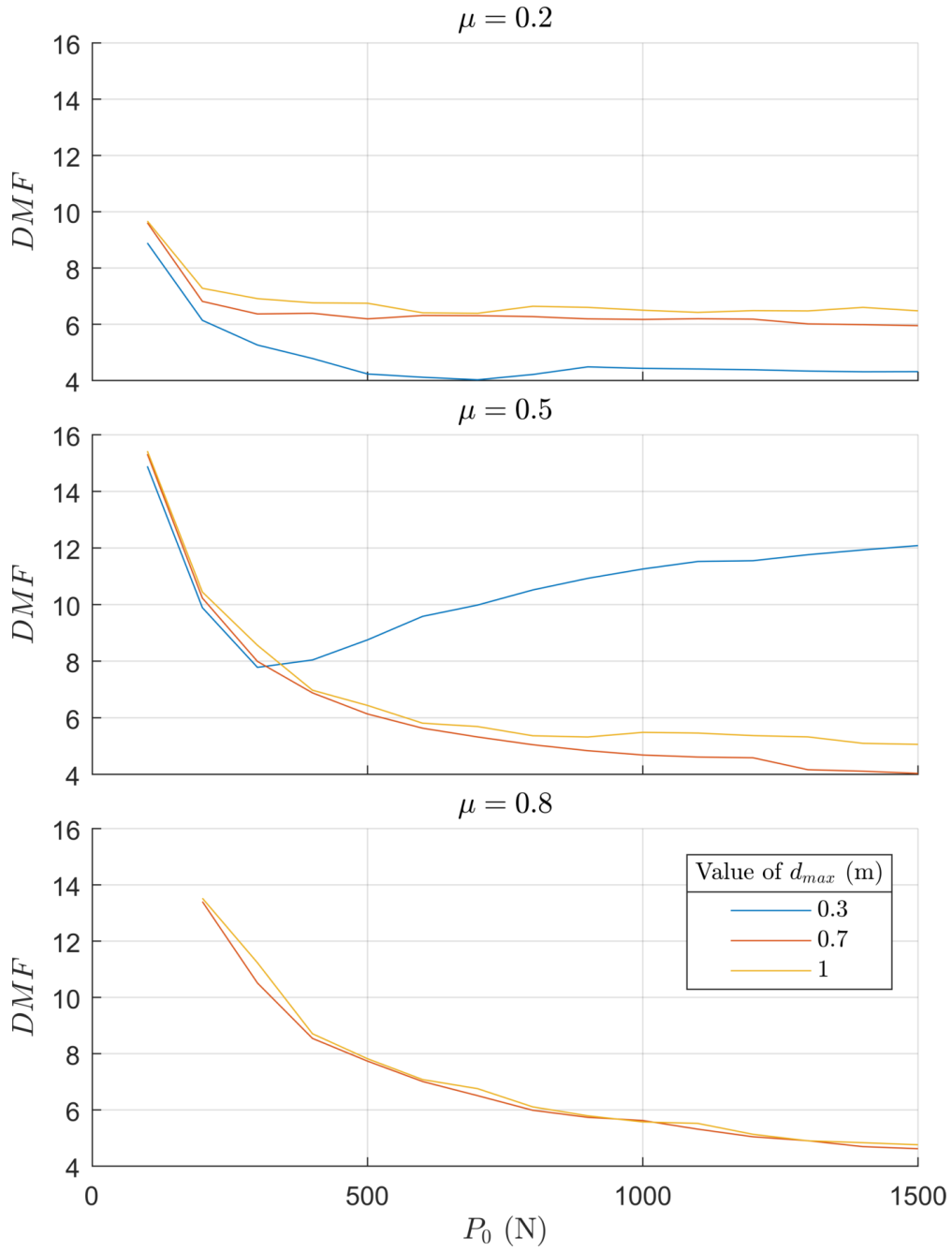

Figure 5.7.: Response of the system to different μ, P_0 and d_{max} values

5.5. The δ-ratio

As it has been experienced in a couple of tests (such as those carried out in figures 5.6 and 5.7), the behavior of the TMD becomes erratic when d_{max} approaches its lower bound d_{min}. In order to further investigate the d_{max} parameter, the following ratio is defined:

$$\delta = \frac{d_{min}}{d_{max}} < 1$$
$$\delta = \frac{\frac{\mu g}{\omega_s^2}\left(1+\bar{m}\right)^2}{d_{max}} \tag{5.1}$$

As δ approaches $\delta = 1$, the performance of the tuned mass damper is expected to plummet.

A new set of tests is prepared where several δ values ranging from 0.05 to 0.80 are plotted in the x-axis. Four different values of the friction coefficient are represented by means of colored lines. Three different force amplitudes are tested in three plots, for a total of 120 combinations.

The results are available in figure 5.8.

Some observations:

→ The performance of the TMD generally starts declining after $\delta = 0.5$.

→ Lower friction has higher performance peaks but is more sensible to changes in δ.

→ The overall best-performing values of δ appear to be in the 0.2-0.5 range (equivalent to d_{max} being 2 to 5 times bigger than d_{min}).

DMF averaging

In order to find the optimum value of δ for the TMD of the studied structure, several cases are averaged within the following range:

→ Coefficient of friction between 0.2 and 0.8.

→ Force amplitude between 500 N and 1500 N.

The averages of the DMF are aggregated on the y-axis and the δ-ratio is plotted on the x-axis.

The resulting plot can be seen in figure 5.9. The best-performing value is $\delta = 0.33$, for which the average DMF is 4.9.

It is then concluded that $d_{max} = \frac{9.8 \cdot 22.5}{580.76}\mu = 1.139\mu$ m would be the most beneficial maximum TMD displacement for the studied case.

In order to find the sensibility of the δ-ratio to the properties of the structure, its mass m_s is increased and new tests are carried out. In figure 5.10 the mass has been set to $m_s = 500$ Kg while maintaining the original mass of the TMD. In figure 5.11 the mass has also been set to $m_s = 500$ Kg, but the mass ratio $\bar{m}$ has been preserved ($m_d = 43.95$ Kg).

The optimum for the δ-ratio shifts upwards with a higher structure mass. When the tuned mass damper is scaled accordingly, the response curve flattens. Based on these results, values between $\delta = 0.30$ and $\delta = 0.45$ seem like a good first approximation for the delta parameter.

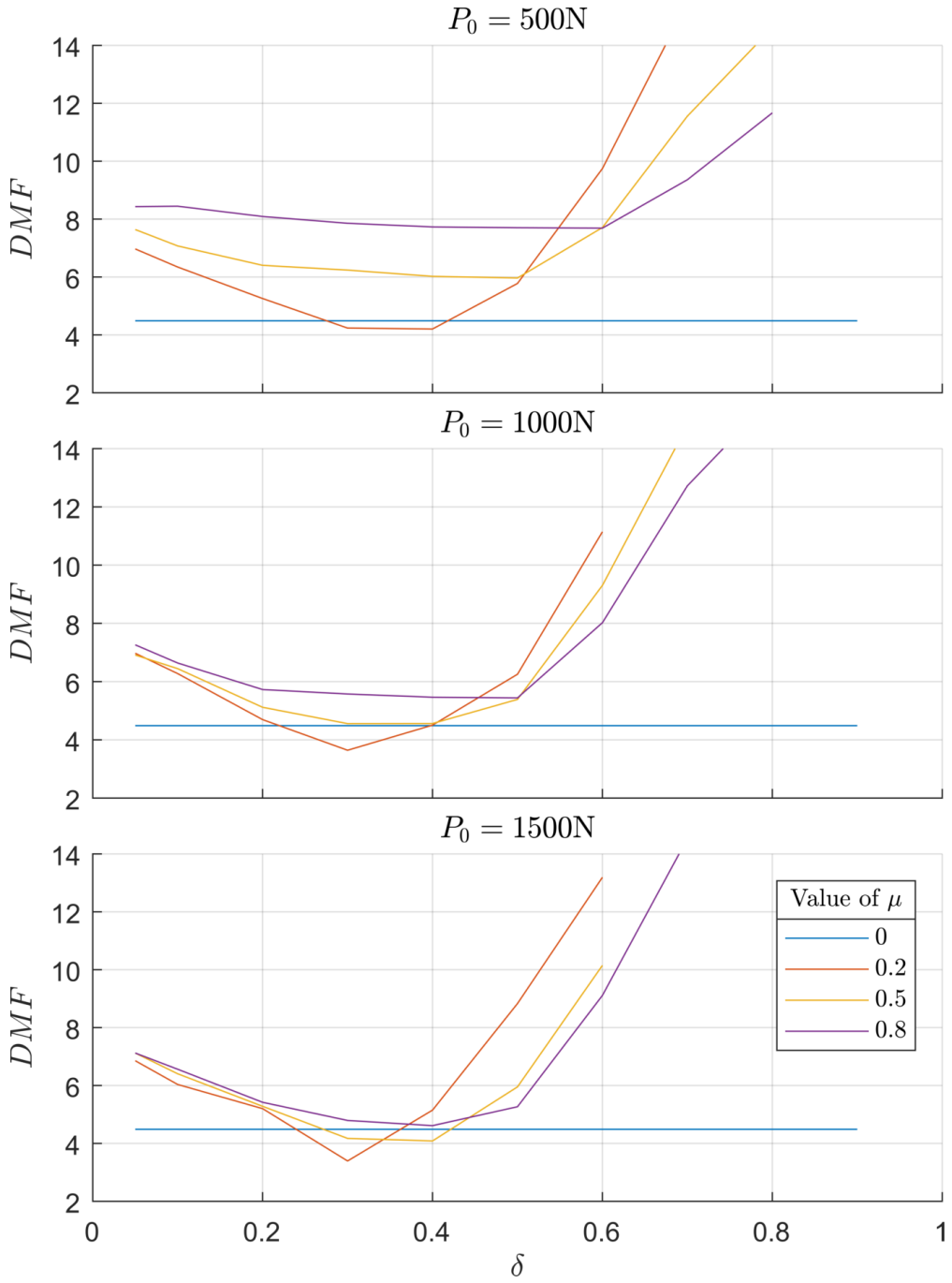

Figure 5.8.: Response of the system to P_0, μ and the newly defined δ ratio

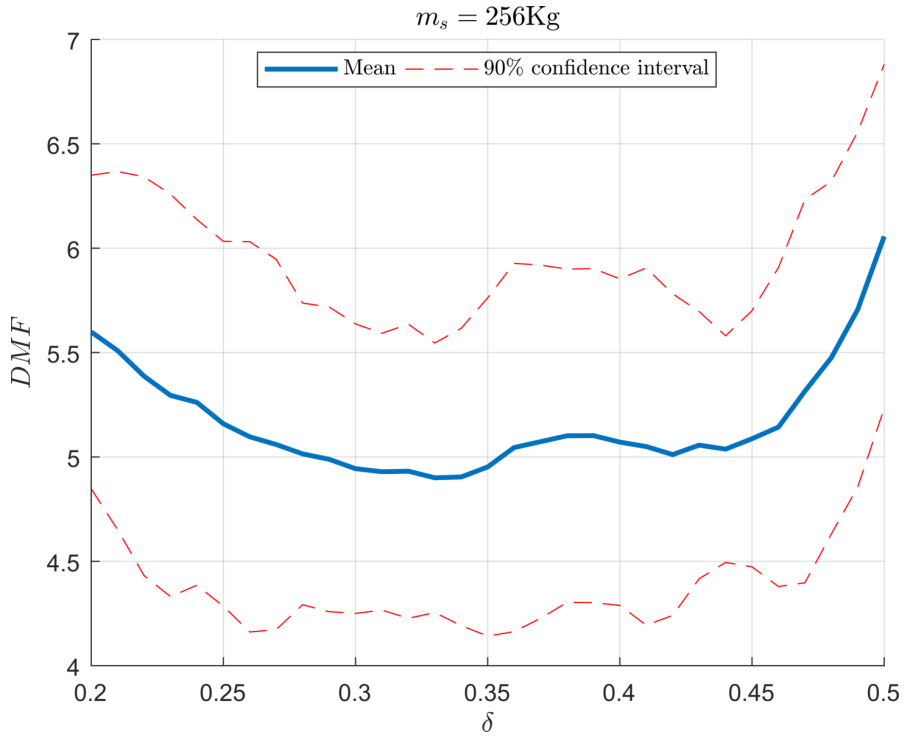

Figure 5.9.: Averaging of the DMF for several μ and P_0 values

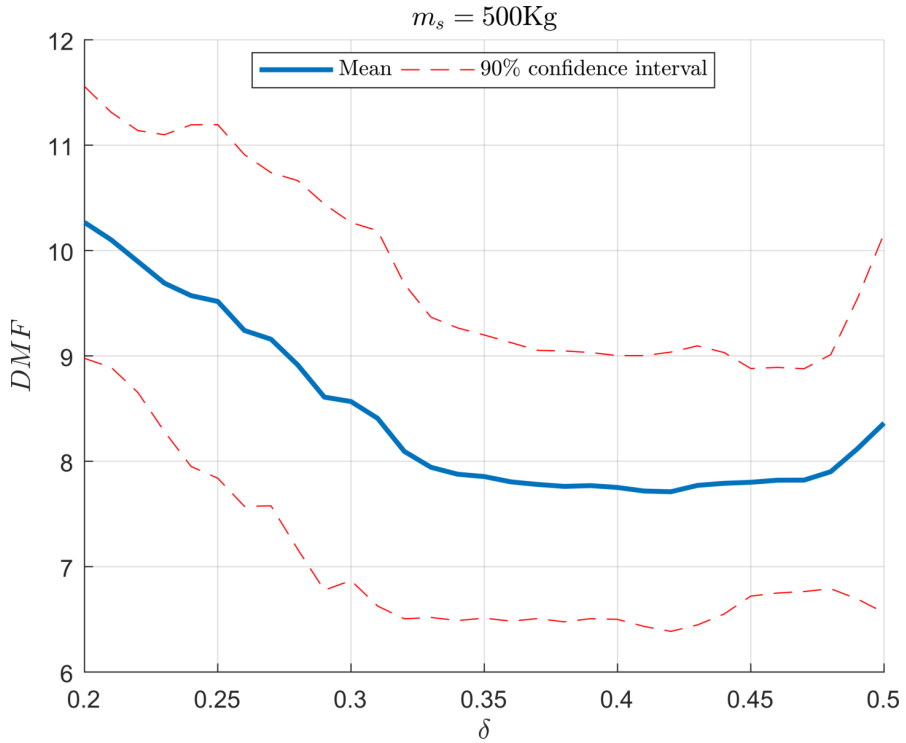

Figure 5.10.: Averaging of the DMF for $m_s = 500\,\mathrm{Kg}$

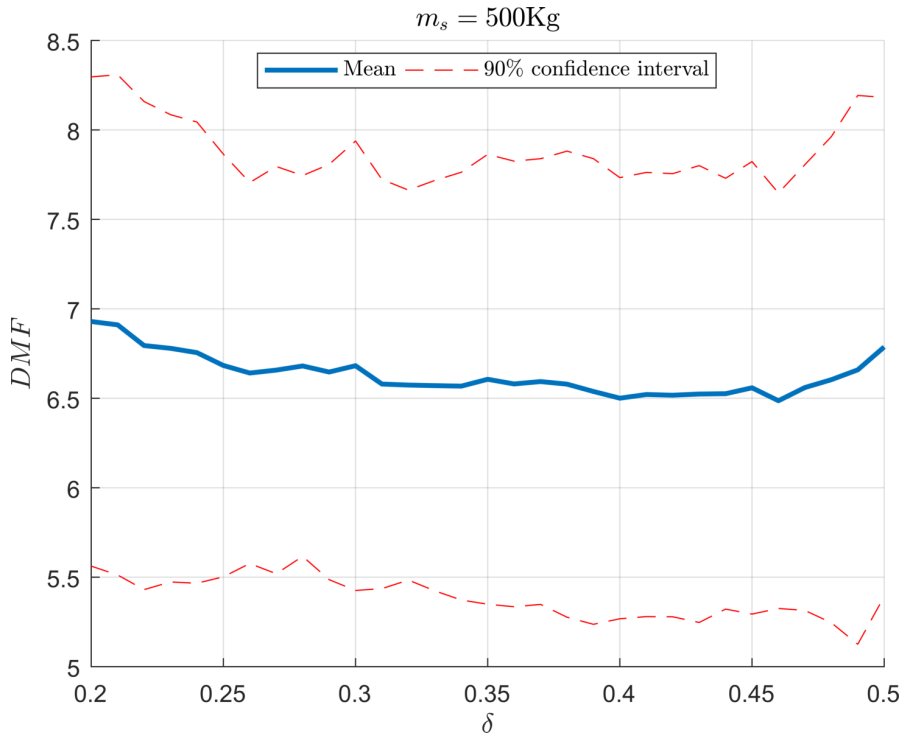

Figure 5.11.: Averaging of the DMF for $m_s = 500$ Kg while maintaining the original mass ratio $\bar{m} = 0.088$

6. Conclusion

In the introduction of this thesis, various objectives were laid out: to have a basic understanding of the impact of friction on the operation of tuned mass dampers, to develop rules that improved the optimization of these devices and to check their validity with a series of tests. This was carried out with the help of a numerical model coded in MATLAB.

To build this model, an assortment of literature was researched, starting with the basic dynamic and vibrational theory of classic books, and then building up to a deep understanding of the equations of motion that would eventually be used. Several important parameters and concepts were also introduced and explained, such as the dynamic magnification factor, the natural frequency, modes, and so on. Then, a couple of the most used numerical methods in dynamic analysis were tackled, with a special focus on the Newmark method. Finally, tuned mass dampers were researched and the analytical approach to tuning of Den Hartog was explained.

At this point, the progressive building of the model was detailed, including an explanation of the 2-DOF system used, the non-linear version of the Newmark method including the modified Newton-Raphson iteration, and the friction model analogy. Frictional forces were designed so that they could be included in the definition of stiffness, and therefore take advantage of the properties of the Newmark method.

At the same time, the improvement of the classic design methodology was developed. The concepts of frictionless stiffness and effective stiffness were introduced, as well as their frequency counterparts. By introducing the frictional model into the classical design, an equation was derived that permits a new approximate of the TMD stiffness parameter. This equation depends on the friction coefficient and on a new design parameter called the "maximum displacement" of the TMD, which were never part of the original optimization process. Finally, a lower bound of the maximum displacement parameter was also found.

Subsequently, the methodology of the experiments was explained, along with a complete array of the relevant variables, and the outputs of these experiments. Each experiment was introduced, reproduced and then some observations were made. The main conclusions extracted from the parametric study were:

→ The presence of friction causes for a minimum value of excitation force to be needed so that the TMD enters operation.

→ Friction causes the TMD to have reduced performance when handling lower excitation forces.

→ Friction reduces the displacements suffered by the TMD (meaning less kinetic energy) but provides dissipation in the form of heat.

→ The optimal TMD stiffness when accounting friction is lower than when friction is not accounted for.

→ The new design steps that were developed in this thesis proved to deliver better performances (in the form of lower DMF values).

→ The performance of devices with friction (tuned according to the new method) for applied force values on the high-end can surpass the performance of frictionless devices.

→ The mass ratio of TMD and system does not significantly affect the optimum value of the maximum displacement design parameter.

→ The friction coefficient does have a big impact on the optimum value of maximum displacement. As friction increases, so does the optimum maximum displacement.

→ As the applied force amplitude increases, the optimum value of friction also increases. This indicates that more energy can be dissipated through friction.

Finally, the concept of the δ-ratio was introduced. The δ-ratio is a quotient between the minimum displacement (lower boundary) and the maximum displacement (design parameter) of the TMD that has a value less than one. Some testing was also performed on this new parameter:

→ The optimal δ-ratio was largely unaffected by variations of the mass ratio.

→ The optimal δ-ratio was slightly affected the changes in the friction coefficient, but only in cases with low applied force values.

→ The optimal δ-ratio increases when the system's mass is increased.

The most important conclusion of the parametric test is that the new optimization method proved successful in ensuring a better performance of the TMD. However, great importance has to be placed in the choosing of the maximum displacement parameter (d_{max}). The concept of δ-ratio was introduced so that an approximate range of optimal values for d_{max} could be found. The author considers a δ-ratio of 0.35-0.40 to be a good initial guess to find the best performance. This means that the maximum displacement should be chosen between $d_{max} = 2.5d_{min}$ and $d_{max} = 2.85d_{min}$.

The author believes that, since friction is an unavoidable in real-life situations, the developed methods in this thesis have proven to be useful in the pre-dimensioning of tuned mass dampers for structures with an outstanding fundamental frequency.

Some of the limitations of this thesis were due to a lack of computation power: with better computing the factorial testing could have been more ambitious. More conclusions could have been developed if numerous discrete values of every variable were tested simultaneously. A more numerical and exact approach to finding the relations between them might have been found.

On the other hand, further testing of this theory with more complex structural models would also be interesting, in order to check if all the conclusions of this thesis still stand when faced with external resources.

Further improvements would also include the realization of a complete energy analysis of the impact of friction on the TMD and the structure.

Bibliography

Abubakar, I. and B. Farid (2013). *Generalized Den Hartog tuned mass damper system for control of vibrations in structures.* WIT Press London.

Adams, V. and A. Askenazi (1999). *Building better products with finite element analysis.* Cengage Learning.

Barbat, A. H. and J. M. Canet (1994). *Estructuras sometidas a acciones sísmicas: cálculo por ordenador.* Centro Internacional de Métodos Numéricos en Ingeniería.

Bathe, K.-J. and E. L. Wilson (1976). *Numerical methods in finite element analysis*, Volume 197. Prentice-Hall Englewood Cliffs, NJ.

Beranek, L. L. and I. L. Ver (1992). Noise and vibration control engineering-principles and applications. *Noise and vibration control engineering-Principles and applications John Wiley & Sons, Inc., 814 p.*.

Biggs, J. M. (1964). *Introduction to structural dynamics.* McGraw-Hill College.

Breton, S.-P. and G. Moe (2009). Status, plans and technologies for offshore wind turbines in europe and north america. *Renewable Energy 34*(3).

Chopra, A. K. (2001). *Dynamics of structures: theory and applications to earthquake engineering.* Prentice-Hall.

Den Hartog, J. (1956). *Vibrations.* McGraw-Hill Book Company, Inc., New York.

Espejo Marín, C. (2004). Energía eólica en españa. *Investigaciones Geográficas (Esp)* (35).

Géradin, M. and D. J. Rixen (2014). *Mechanical vibrations: theory and application to structural dynamics.* John Wiley & Sons.

Global Wind Energy Council (2017). Global wind report 2016. *Brussels, Belgium.*

Jangid, R. (1999). Optimum multiple tuned mass dampers for base-excited undamped system. *Earthquake engineering & structural dynamics 28*(9).

Jonkman, J. and D. Matha (2011). Dynamics of offshore floating wind turbines—analysis of three concepts. *Wind Energy 14*(4), 557–569.

Kelvin, W. T. B. and P. G. Tait (1867). *Treatise on natural philosophy*, Volume 1. Claredon Press.

Kost, C., J. N. Mayer, J. Thomsen, N. Hartmann, C. Senkpiel, S. Philipps, S. Nold, S. Lude, N. Saad, and T. Schlegl (2013). Levelized cost of electricity renewable energy technologies. *Fraunhofer Institute for Solar Energy Systems ISE*.

Krohn, S. (2009). *The economics of wind energy*. EWEA.

Newmark, N. M. (1959). A method of computation for structural dynamics. *Journal of the engineering mechanics division* (3).

Paz, M. (2012). *Structural dynamics: theory and computation*. Springer Science & Business Media.

Persson, B. (2013). *Sliding friction: physical principles and applications*. Springer Science & Business Media.

Soong, T. T. and M. C. Costantinou (1994). *Passive and active structural vibration control in civil engineering*. Springer.

Sovacool, B. K. (2009). Contextualizing avian mortality: A preliminary appraisal of bird and bat fatalities from wind, fossil-fuel, and nuclear electricity. *Energy Policy 37*(6).

Symans, M., F. Charney, A. Whittaker, M. Constantinou, C. Kircher, M. Johnson, and R. McNamara (2008). Energy dissipation systems for seismic applications: current practice and recent developments. *Journal of structural engineering* (1).

Tsai, H.-C. and G.-C. Lin (1993). Optimum tuned-mass dampers for minimizing steady-state response of support-excited and damped systems. *Earthquake engineering & structural dynamics* (11).

Whittaker, E. T., G. Robinson, et al. (1924). *The calculus of observations*, Volume 8. Blackie London.

Wilson, E. (1998). *Three dimensional static and dynamic analysis of structures: a physical approach with emphasis on earthquake engineering*. Computers and Structures Inc.

Wiser, R., K. Jenni, J. Seel, E. Baker, M. Hand, E. Lantz, and A. Smith (2016). Expert elicitation survey on future wind energy costs. *Nature Energy 1*.

Zareian, F. and R. A. Medina (2010). A practical method for proper modeling of structural damping in inelastic plane structural systems. *Computers & structures* (1).

List of Algorithms

List of Figures

List of Tables

Index

Annexes

A. Extended test results

In this annex, the raw numbers of the tests presented in chapter 5 on page 56 are exposed in tables.

Reminder: the dynamic magnification factor is computed with the following formula:

$$DMF = \frac{\max\{|d(t)|\}}{d_{st0}}$$

Where:

$$d_{st0} = \frac{P_0}{K_s}$$

Table A.1.: DMF values corresponding to figure 5.1 on page 59

P_0 (N) \ μ	0.00	0.05	0.10	0.30	0.80
30	4.96	8.49	11.04	12.32	12.32
50	4.96	6.66	9.09	12.32	12.32
70	4.96	6.06	7.72	11.91	12.32
100	4.96	5.75	6.66	10.69	12.32
200	4.96	5.35	5.75	8.29	11.80
300	4.96	5.23	5.52	6.66	10.21
400	4.96	5.12	5.35	6.12	9.09
500	4.96	5.25	5.32	5.95	8.35
600	4.96	5.14	5.23	5.75	7.46
700	4.96	5.19	5.14	5.62	6.97
800	4.96	4.94	5.12	5.52	6.66
900	4.96	5.16	5.11	5.52	6.33
1000	4.96	4.94	5.25	5.46	6.18

Table A.2.: DMF values corresponding to figure 5.2 on page 59

K_d (N/m) \ μ	0.00	0.05	0.10	0.30	0.80
300	17.16	4.73	5.00	7.41	12.15
350	14.37	4.26	4.82	7.46	12.18
400	11.38	4.11	4.79	7.32	12.10
450	8.91	4.20	4.82	7.65	12.11
500	7.04	4.55	4.94	7.66	11.92
550	5.63	5.03	5.41	7.98	11.68
600	4.67	5.49	5.89	8.45	11.80
650	4.23	5.98	6.25	8.62	11.58
700	4.01	6.30	6.62	8.91	11.55
750	3.88	6.59	6.87	9.13	11.47
800	3.81	6.54	7.15	9.41	11.36
850	3.80	6.77	7.16	9.43	11.29
900	3.96	6.95	7.24	9.29	11.17
950	4.20	7.32	7.21	9.38	11.12
1000	4.42	7.19	7.88	9.79	11.11

Table A.3.: DMF values corresponding to figure 5.3 on page 61

K_d (N/m) \ μ	0.00	0.05	0.10	0.30	0.80
300	17.16	10.06	5.98	4.66	5.68
350	14.37	6.16	3.84	4.29	5.56
400	11.38	3.71	3.74	4.26	5.61
450	8.91	3.57	3.82	4.22	5.65
500	7.04	4.17	4.31	4.53	5.80
550	5.63	4.63	4.85	5.07	5.97
600	4.67	5.19	5.40	5.46	6.33
650	4.23	5.51	5.72	6.01	6.73
700	4.01	6.12	6.08	6.34	6.99
750	3.88	5.88	6.13	6.19	7.36
800	3.81	6.39	6.58	6.67	7.42
850	3.80	6.00	6.81	6.96	7.56
900	3.96	6.34	6.40	6.84	7.69
950	4.20	6.49	6.77	7.13	8.06
1000	4.42	7.10	6.86	7.62	8.67
850	3.80	6.77	7.16	9.43	11.29
900	3.96	6.95	7.24	9.29	11.17
950	4.20	7.32	7.21	9.38	11.12
1000	4.42	7.19	7.88	9.79	11.11

Table A.4.: DMF values corresponding to figure 5.4 on page 63

	Den Hartog				New equations			
P_0 (N) \ μ	0.10	0.30	0.50	0.70	0.10	0.30	0.50	0.70
30	10.99	12.70	13.00	13.33	10.94	12.75	13.09	13.50
50	8.85	12.70	13.00	13.33	8.87	12.75	13.09	13.50
70	7.81	12.35	13.00	13.33	7.89	12.25	13.09	13.50
100	6.44	10.81	12.99	13.33	6.92	10.64	13.07	13.50
200	5.32	7.64	10.01	12.05	5.68	8.58	10.11	11.83
300	4.97	6.14	7.85	9.25	5.53	6.68	8.41	9.98
400	4.84	5.71	6.70	7.95	5.38	6.24	7.68	8.65
500	4.89	5.11	5.99	7.08	5.29	6.01	6.77	7.95
600	4.74	4.83	5.67	6.68	5.32	5.80	6.41	7.10
700	4.76	4.66	5.34	6.27	5.31	5.75	6.23	6.76
800	4.72	4.40	5.08	6.09	5.32	5.61	6.07	6.71
900	4.78	4.28	4.96	5.99	5.18	5.65	6.03	6.35
1000	4.74	4.26	4.85	6.05	5.26	5.67	5.95	6.41

Table A.5.: DMF values corresponding to figure 5.5 on page 65

	$\mu = 0.2$			$\mu = 0.5$			$\mu = 0.8$		
d_{max} (m) \ $\bar{m}$	0.03	0.07	0.10	0.03	0.07	0.10	0.03	0.07	0.10
0.20	8.48	4.19	4.33						
0.30	13.19	5.75	3.74	13.93	11.27	10.24			
0.40	14.38	6.51	4.57	6.84	5.31	4.72	18.46	14.34	12.94
0.50	15.35	7.29	4.87	7.71	5.25	4.72	11.83	8.50	7.43
0.60	16.18	7.38	5.00	10.77	5.40	4.68	7.79	6.37	5.77
0.70	16.76	7.94	5.31	12.26	5.57	4.71	8.04	6.32	5.77
0.80	16.98	8.13	5.75	13.08	5.89	4.84	8.28	6.33	5.74
0.90	17.13	8.38	5.80	13.43	6.60	5.00	10.24	6.55	5.78
1.00	16.92	8.49	5.86	14.33	6.77	5.07	11.18	6.61	5.83

Table A.6.: DMF values corresponding to figure 5.6 on page 67

	$P_0 = 500\,\mathrm{N}$			$P_0 = 1000\,\mathrm{N}$			$P_0 = 1500\,\mathrm{N}$		
μ / d_{max} (m)	0.2	0.5	0.8	0.2	0.5	0.8	0.2	0.5	0.8
0.10	17.19								
0.20	4.22			4.67			5.28		
0.30	4.23	8.75		4.43	11.26		4.32	12.08	
0.40	5.35	5.90	10.80	5.36	4.54		5.34	4.81	
0.50	5.46	5.95	7.68	5.63	4.60	8.22	5.58	4.03	9.56
0.60	6.14	6.13	7.68	5.91	4.54	5.45	5.73	4.13	5.79
0.70	6.19	6.13	7.73	6.17	4.68	5.62	5.95	4.03	4.62
0.80	6.37	6.29	7.68	6.30	4.64	5.49	6.25	4.47	4.66
0.90	6.49	6.36	7.74	6.24	5.25	5.52	6.32	5.06	4.63
1.00	6.75	6.43	7.82	6.50	5.48	5.57	6.48	5.06	4.76

Table A.7.: DMF values corresponding to figure 5.7 on page 68

	$\mu = 0.2$			$\mu = 0.5$			$\mu = 0.8$	
d_{max} (m) / P_0 (N)	0.3	0.7	1.0	0.3	0.7	1.0	0.7	1.0
100	8.89	9.61	9.67				16.24	16.24
200	6.14	6.81	7.28	9.89	10.23	10.44	13.40	13.52
300	5.26	6.37	6.91	7.78	7.99	8.56	10.51	11.23
400	4.78	6.39	6.76	8.04	6.88	6.97	8.54	8.71
500	4.23	6.19	6.75	8.75	6.13	6.43	7.73	7.82
600	4.12	6.31	6.41	9.58	5.63	5.81	7.01	7.08
700	4.03	6.30	6.39	9.98	5.32	5.69	6.51	6.75
800	4.21	6.27	6.64	10.51	5.05	5.36	5.99	6.11
900	4.49	6.19	6.60	10.93	4.84	5.32	5.74	5.79
1000	4.43	6.17	6.50	11.26	4.68	5.48	5.62	5.57
1100	4.41	6.20	6.42	11.52	4.61	5.46	5.32	5.52
1200	4.38	6.18	6.48	11.55	4.59	5.37	5.05	5.13
1300	4.34	6.01	6.47	11.76	4.16	5.32	4.90	4.90
1400	4.31	5.99	6.60	11.93	4.11	5.10	4.69	4.83
1500	4.32	5.95	6.48	12.08	4.03	5.06	4.62	4.76

Table A.8.: DMF values corresponding to figure 5.8 on page 70

	$P_0 = 500\,\mathrm{N}$			$P_0 = 1000\,\mathrm{N}$			$P_0 = 1500\,\mathrm{N}$		
δ \ μ	0.2	0.5	0.8	0.2	0.5	0.8	0.2	0.5	0.8
0.05	6.97	7.64	8.43	6.97	6.91	7.26	6.86	7.12	7.12
0.10	6.34	7.07	8.45	6.27	6.44	6.64	6.04	6.41	6.56
0.20	5.26	6.40	8.09	4.69	5.12	5.73	5.20	5.28	5.42
0.30	4.24	6.24	7.86	3.64	4.56	5.57	3.39	4.17	4.79
0.40	4.20	6.02	7.73	4.50	4.56	5.46	5.15	4.09	4.61
0.50	5.78	5.97	7.70	6.25	5.39	5.44	8.83	5.95	5.27
0.60	9.75	7.71	7.69	11.14	9.30	8.02	13.19	10.15	9.11
0.70	15.49	11.56	9.36		14.80	12.72			14.53
0.80		14.60	11.67			15.76			

B. Wind power

B.1. A brief history

Wind power is one of the oldest energy sources that humanity has taken advantage of. The first sailing ships of the world that we know of existed as far back as 5000 BC in the area that occupies the current Kuwait. By 1000 BC, windmills were used to pump seawater in China. During the XIIIth century, windmills were extensively used in northwestern Europe to grind flour.

Electricity was discovered in the 1820s, and the first electric windmill would be built in 1887 by Scottish engineer James Blyth. These power sources remained uncommon until the 1930s, when technological advances made them an attractive option for farms and other buildings that had a difficult access to the very young electric grid. In 1931, a 32-meter high horizontal axis wind turbine built in the Crimean peninsula, was the first to achieve a capacity of 100kW.

Interest in wind power rose again during World War II, since diesel fuel prices reached astronomical highs. Russia, Germany and Denmark started investing heavily in very ambitious wind projects, most of which wouldn't see the light of day. In 1941 the Smith-Putnam wind turbine was invented, which featured a capacity of 1250kW.

After World War II fossil fuels became cheap again, and wind power wouldn't get attention until the energy crisis of 1973, when crude oil prices more than doubled due to the embargo perpetrated by OPEC. During the late 1970s wind turbine research was heavily subsidized, and big industrial companies started building prototypes which attained capacities (figure B.1) that are still impressive by today's standards, but had incredibly low durability.

In the 1990s, turbine research focus shifted to achieving the highest possible energy outcome without sacrificing useful life. Wind farms bloomed all over the developed world, and eventually they started becoming competitive with traditional energy.

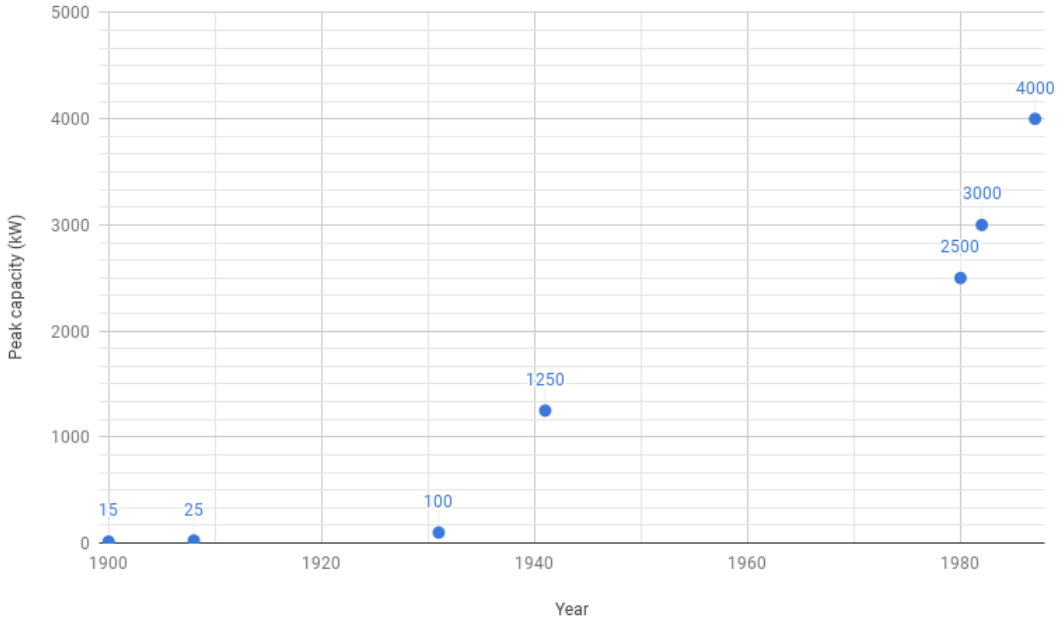

Figure B.1.: History of peak wind turbine capacity through the XXth century

B.2. The present

Nowadays, wind power has become the most promising renewable energy source, with some estimates placing its onshore LCOE[1] in the same range as that of coal and natural gas (figure B.2). Offshore wind power is still not a competitor to fossil fuels, but the technology is young and its costs are dropping rapidly.

Spain's involvement with wind power started in January 1993, when the first sizable (total of 30MW output) wind farms were inaugurated in Tarifa. Since then, its significance has steadily grown and, as of 2017, wind power amounts to 20% (figure B.3) of the total energy produced in Spain. This number surpasses the projections EWEA[2] proposed in the early 1990s, which calculated that wind power would reach 10% of total power production in 2025. Spain's production of wind power over time can be seen in figure B.4.

In the international scene, Spain is currently one of the biggest investors in wind power. If we rank every country by wind power capacity (see table B.1), Spain places at the fifth position as of 2016, with a grand total of 23074MW installed. In Europe, Spain is only surpassed by Germany (50018MW). Denmark is another big investor in wind power, in relation to its size. Denmark covers 38% of its power consumption through wind (29% onshore and 9% offshore) and produces 921.4W per person (figure B.5).

The Global Wind Energy Council expects Europe to grow its wind power output by 45% in five years.

The biggest challenges of wind power are:

[1] Levelized Cost of Electricity
[2] European Wind Energy Association, known as WindEurope since 2016

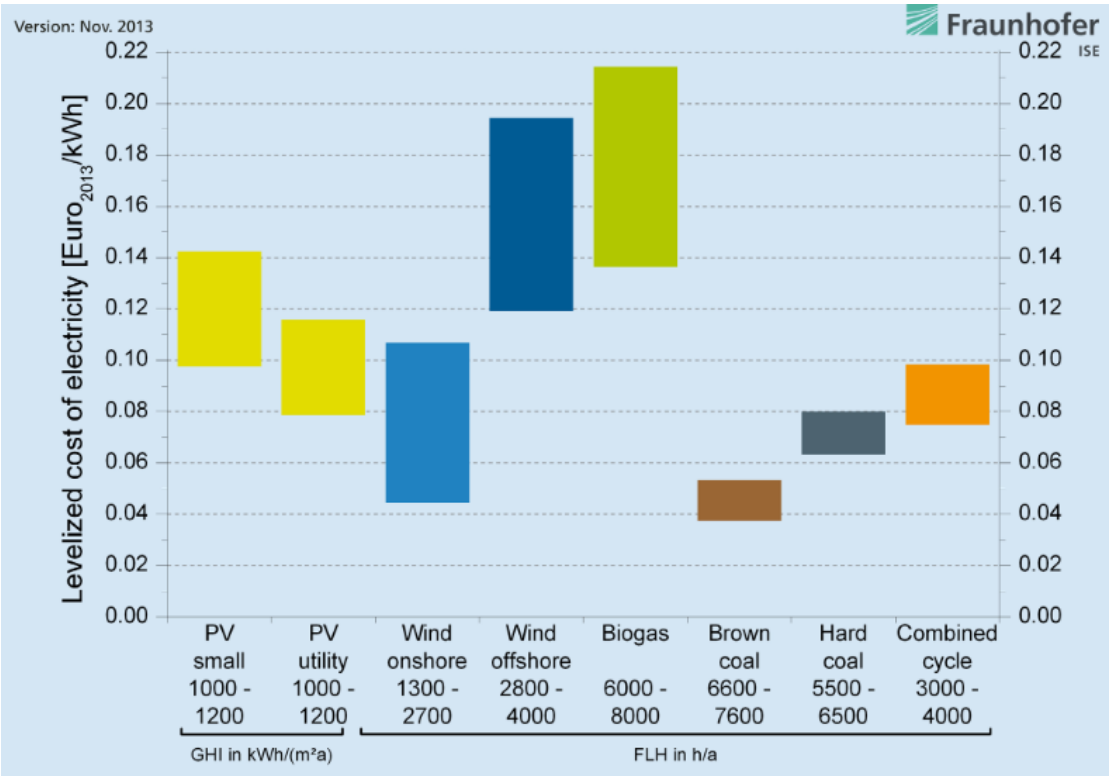

Figure B.2.: Estimated LCOE for various energy sources. Retrieved from "Levelized cost of electricity renewable energy technologies" by Kost, Mayer et al.

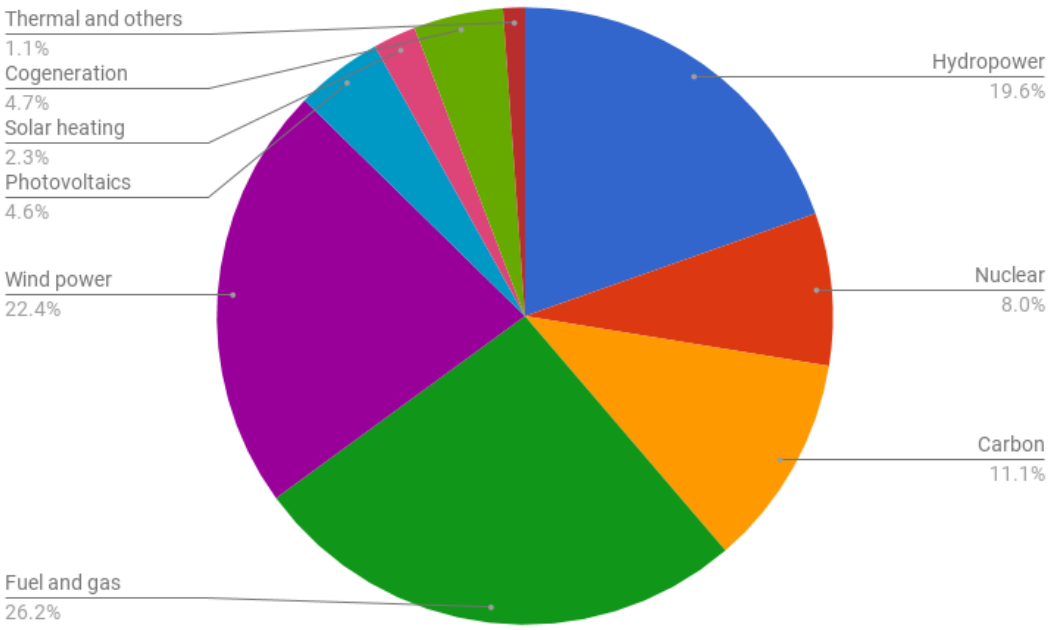

Figure B.3.: Power production in Spain by source in January 2017. Adapted from "Libro de la Energía en España 2015" by Subdirección General de Planificación Energética y Seguimiento

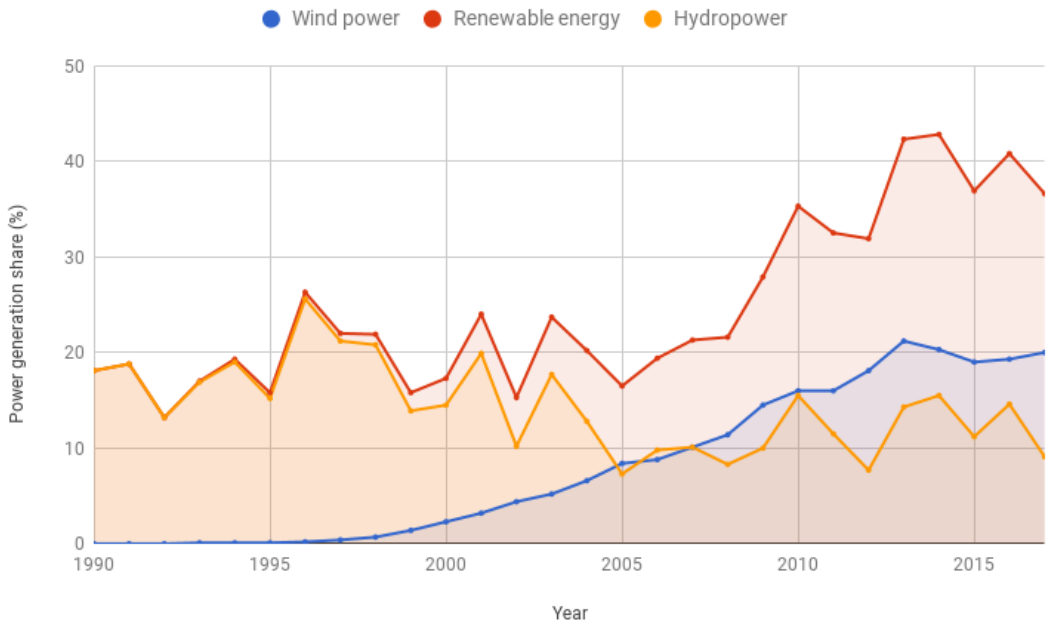

Figure B.4.: Evolution of wind power produced in Spain in relation to both all renewable sources and all sources total, between 1990-2017. Adapted from "Estadísticas Eléctricas Anuales" by Subdirección General de Planificación Energética y Seguimiento

Table B.1.: Wind power capacity for the top 10 countries in 2016. Adapted from "Global Wind Report 2016" by GWEC

Country	Capacity (MW)	Population	Capacity per capita (W/person)
PR China	168732	1,373,541,278	122.84
USA	82184	323,995,528	253.66
Germany	50018	82,890,792	603.40
India	28700	1,266,883,598	22.65
Spain	23074	46,563,476	497.10
UK	14543	64,430,428	223.30
France	12066	66,836,154	180.10
Canada	11900	35,362,905	336.51
Brazil	10740	205,823,665	52.18
Italy	9257	62,007,540	152.80

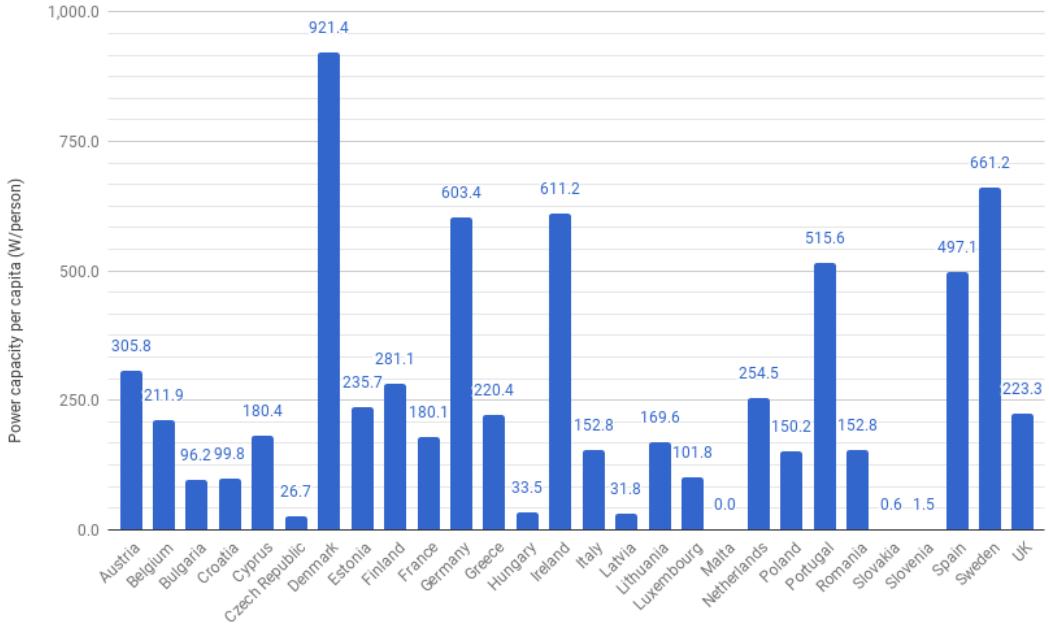

Figure B.5.: Wind power capacity per capita for EU countries at the end of 2016. Adapted from "WindEurope Annual Statistics 2016" by WindEurope

→ The necessity of fast, perpetual wind currents in order to achieve a reliable output of energy.

→ The high cost of the initial investment, including wind turbines and foundations.

→ The loss of energy that usually occurs due to the distance between wind farms and cities.

→ Noise and visual pollution that contribute to the "not in my backyard" effect.

→ The danger they pose to birds, although the ecological damage that fossil fuels cause per GWh is estimated to be far greater (Sovacool (2009)).

One way to increase the capacity of wind turbines is to increase the size of the turbine itself, since wind power intercepted by the turbine increases in proportion to approximately the square of the rotor diameter. Installation and maintenance costs do not scale as much with turbine size, so the optimum is as big as the material and the transport conditions allow. Modern onshore turbines have a diameter around the 80-100 meters range, and offshore turbines are significantly larger at 90-120 meters. These are expected to increase in the next 15 years to 135 meters and 190 meters respectively (Wiser et al. (2016)), which implies that nominal capacity could grow as much as 160%.

The upfront investment to commission a single onshore wind tower is averaged by Krohn (2009) to 1,230,000€ per MW of capacity, of which 75.6% covers the turbine costs, 8.9% for the grid connection, 6.5% for the foundation, 3.9% for the land rent and the rest is spent on financial costs, road transport and so on. For offshore wind farms the initial investment can be as high as 2,700,000€/MW.

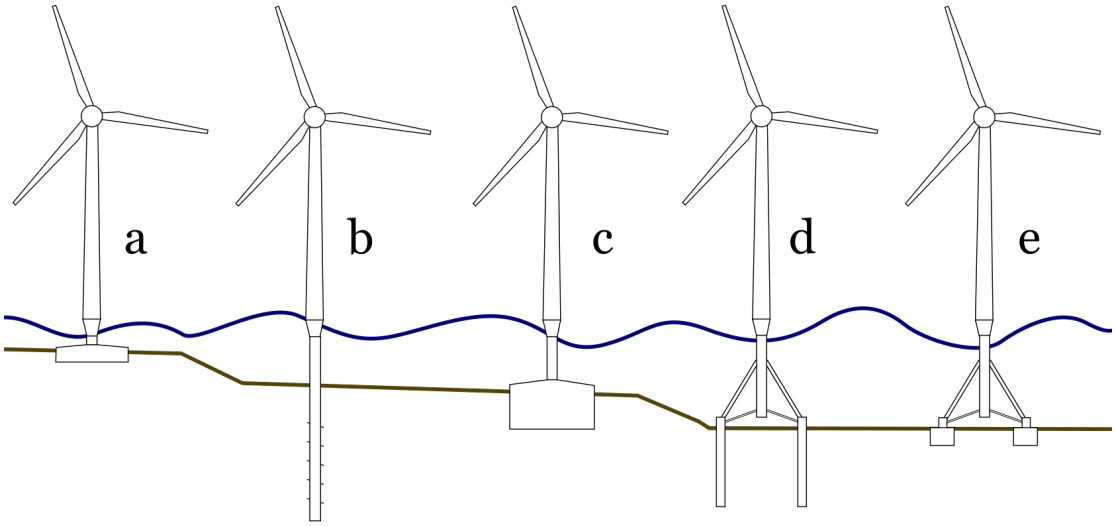

Figure B.6.: Types of offshore wind tower foundations. Adapted from Breton and Moe (2009)

B.3. Offshore wind power

The first offshore wind farm of the world, Vindeby Offshore Wind Farm, was built in the south east waters of Denmark in 1991, had an initial cost of 10,000,000 euros, and is being decommissioned in 2017. The 11 turbines were installed between 1.5-3 kilometers from the coastline and had a nominal export capacity of 5MW.

Rødsand II, a modern danish offshore wind farm completed in 2010, is placed at 9 kilometers from the coastline and has 90 turbines for a total of 207MW capacity.

The way a wind farm's efficiency is measured is the capacity factor, which puts the produced energy for a singular time period over the installed capacity of the farm. Vindeby had a capacity factor of 21.7% over its lifetime, while Rødsand II and more recent farms achieve factors of 43% and more, according to data from the Danish Energy Agency.

Offshore wind turbines have to overcome the challenge of staying balanced among a wide array of forces caused by wind, weather, waves, water currents and soil dynamics. This makes them an even bigger investment than their onshore counterparts, even when we take into account the fact that going offshore means higher average wind speeds.

The various types of foundations for offshore wind towers in shallow waters are portrayed in figure B.6.

A gravity-based foundation (a) that is very similar to the conventional wind tower foundation, where a big concrete or steel block is placed in contact with the seabed. The single pile based solution (b) that relies on friction forces with the submerged soil. Foundation (c) is a watertight support that suctions the seabed and is easier to construct. Foundation (d) is a variation of (b) that features a number of piles, and is projected to withstand deeper waters. Similarly, (e) is based on model (c) and uses a couple of suction piles in order to keep the tower in place.

Today, the number of offshore farms worldwide already surpasses 1500 with a joint capacity of 14,400MW, which could power up 7,200,000 average US households.

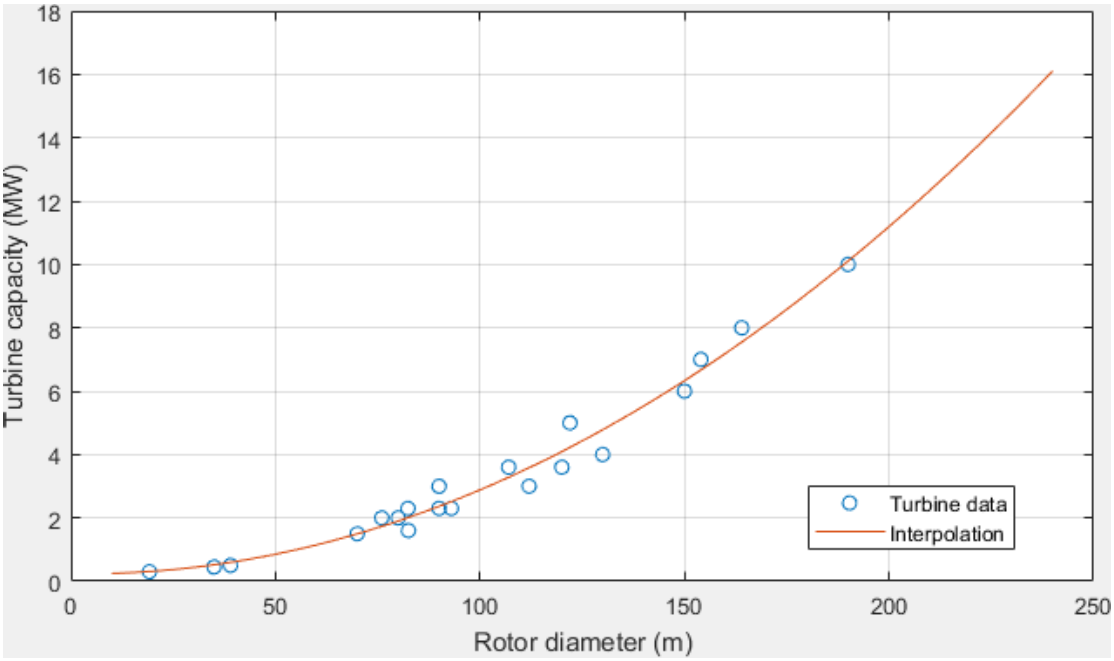

Figure B.7.: Rotor diameter vs Capacity chart based on offshore turbines. Data provided by "4C Offshore"

The scatter plot in figure B.7 shows the relation between nominal capacity and rotor diameter with an interpolation based on 20 different offshore turbines. The fitted polynomial ($R^2 = 0.976$) is:

$$y = 2.83 \cdot 10^{-4}x^2 - 0.0019x + 0.24$$

B.3.1. Floating offshore turbines

Development on floating wind turbines started in the 1990s, but it wasn't until 2008 that the first full-sized prototype was tested in the south-east waters of Italy. The cost of commissioning offshore wind farms is bound to be much superior to the cost of commissioning onshore wind farms due to the complexity of the floating structure and the higher distance to the electric grid.

The first floating wind farm of the world, Hywind Scotland, is set to be completed by the end of 2017. It will mostly stand as a proof-of-concept for future floating wind farms, since it will only feature 5 turbines with a total of 30MW of capacity. Each rotor has a diameter of 154m and a hub height of 100m, which can be seen in comparison with other offshore turbines in figure B.8.

There are three basic models to be followed in floating structure design. They differ on the main principle by which they achieve stability:

TLP Large submerged mass moored to the sea floor. Stability is achieved by excess buoyancy.

Spar buoy Thin, long cylinder that achieves stability by using ballast and reaching deep

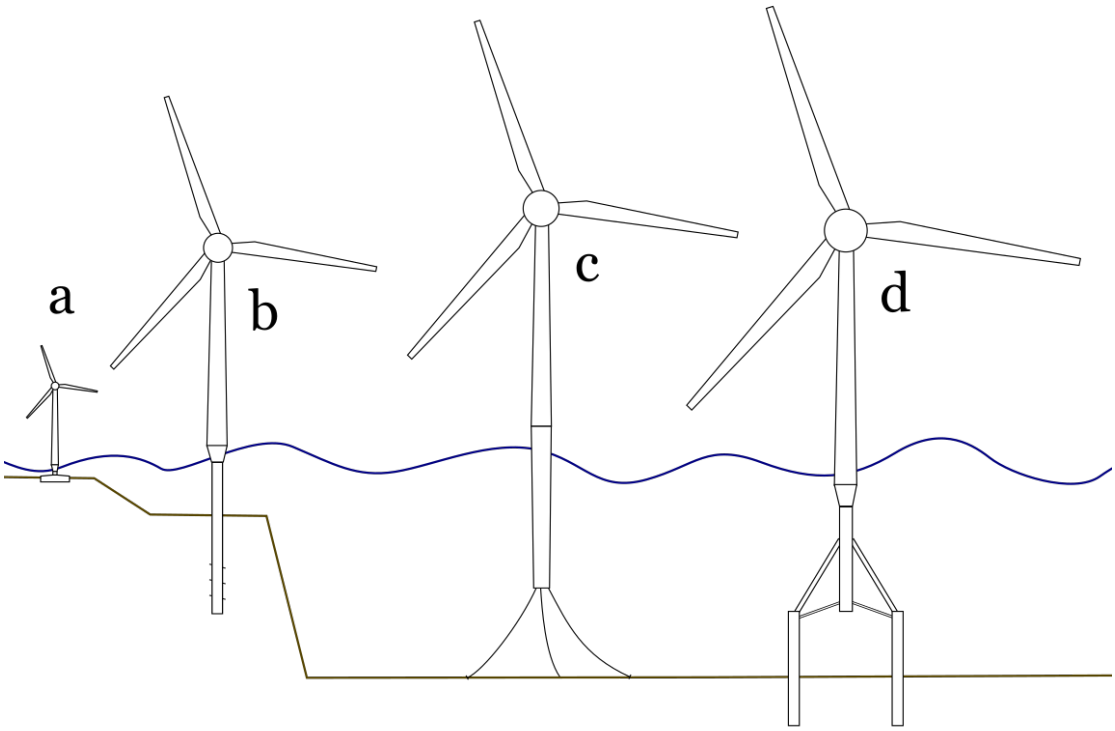

Figure B.8.: Comparison of offshore wind turbine sizes: (a) Decommissioned Vindeby farm (Denmark), (b) Sandbank (Germany), (c) Hywind Scotland (UK), (d) Projected 2030 turbine size

Table B.2.: Advantages and disadvantages of floating platforms for offshore wind turbines. Adapted from Jonkman and Matha (2011)

Basic design	TLP	Spar buoy	Barge
Stability principle	Mooring	Ballast	Buoyancy
Wave sensitivity	0	+	-
Natural frequency	+	0	-
Turbine weight	0	-	+
Construction	-	-	+
Maintenance	+	0	-

depths.

Barge Platform with a thin vertical axis and moored from the exterior corners. Stability is achieved by its large surface and a shallow draft.

In table B.2, these platforms are compared in relation to different technological challenges, pointing out if they are at an advantage (+), disadvantage (-) or are neutral (0).
These systems can be combined in order to obtain hybrid solutions, like the semi-submersible. Based on the barge and the spar buoy designs, the semi-submersible has a large surface as well as considerable thickness and the addition of ballast.